CALIFORNIA STATE UNIVERSITY, NORTHRIDGE

STRAIN LOCALIZATION IN QUARTZOFELDSPATHIC MYLONITES: A MICROSTRUCTURAL AND ELECTRON BACKSCATTER DIFFRACTION (EBSD) STUDY OF THE SOUTH MOUNTAINS CORE COMPLEX, ARIZONA

A thesis submitted in partial fulfillment of the requirements

For the degree of Master of Science in Geology

By

Rebecca Michelle Greenberg

August 2010

The thesis of Rebecca Michelle Greenberg is approved:

J. Douglas Yule, Ph.D.	Date
Richard Heermance, Ph.D.	Date
Elena A. Miranda, Ph.D., Chair	Date

California State University, Northridge

ACKNOWLEDGEMENTS

There are many people to whom I owe thanks and without whom I would not have been able to complete this thesis. First and foremost, I owe a great deal of gratitude to my advisor, Elena Miranda. Thank you for your never-ending patience, your inspiration and excitement, and for always making the time. Most importantly, I would like to thank you for showing me how to be a strong, successful woman in the field of science.

I would like to thank the CSUN Geology Department and the CSUN A.S. Accounting and Financial Services Office for financial assistance towards fieldwork and EBSD acquisition. Thank you to Gareth Seward at UCSB and Behzad Bavarian at CSUN for the great amount of time they spend helping me to begin the EBSD acquisition process. Thanks to Scott Sitzman at Oxford Instruments for his invaluable troubleshooting assistance. Thanks to Steve Reynolds and Frances Cooper for their insight in the field and help collecting samples. I would also like to thank my committee members Doug Yule and Dick Heermance for their valuable insights.

Finally, I would like to thank my family and friends for all of their love and support. Thank you Dani Morgan, Kristan Griffith, Jodi Stone, and Nicholas DeMarais for your unconditional, lasting friendship. I cannot express how much you all mean to me. Thanks to Aaron Hebeler for the countless coffee runs. Thanks Steve for all the texts and phone calls, and for being an amazing brother. Thanks Lauren for the fro yo, dinners, and being my best friend. And most importantly, thank you Mom and Dad for everything. I love you both so much and could not have accomplished this without knowing you were behind me every step of the way.

TABLE OF CONTENTS

LIST OF TABLES

LIST OF FIGURES

ABSTRACT

STRAIN LOCALIZATION IN GRANODIORITE MYLONITES: A MICROSTRUCTURAL AND ELECTRON BACKSCATTER DIFFRACTION (EBSD) STUDY OF THE SOUTH MOUNTAINS CORE COMPLEX, ARIZONA

By

Rebecca Michelle Greenberg

Master of Science in Geology

The evaluation of strain localization in detachment fault shear zones is essential to the study of continental core complex development and permits insight into continental crust rheology during extension. A microstructural and EBSD study of the naturally deformed Tertiary South Mountains granodiorite and granite mylonitic shear zone rocks was conducted to determine the deformation mechanisms that promote strain localization during metamorphic core complex development. It was hypothesized that the strength of quartz strongly influences strain localization in the naturally deformed granodiorite mylonites and granite mylonites.

Microstructural observation of quartz grains reveals the presence of elongate 'ribbon grains' with subgrain development along the rims of these grains, and irregular and sinuous sutured grain boundaries; these microstructures are interpreted as evidence of Regimes 2 and 3 dynamic recrystallization. In contrast, the plagioclase feldspar and potassium feldspar crystals are microfractured with limited development of bulging grain boundaries on the rims of the feldspar grains; this is interpreted as evidence of Regime 1

dynamic recrystallization. Pole figures of quartz EBSD data from granodiorite mylonites exhibit c-axis maxima that are interpreted as evidence of lattice preferred orientation. The locations of the maxima are indicative of rhomb <a> slip and prism <a> slip.

Based on the interpreted slip systems, it is inferred that deformation occurred at moderate temperatures of 500-650°C. Based on the microstructural evidence for crystal plasticity and the interpreted lattice preferred orientation, it is suggested that quartz deforms by dislocation creep. In contrast, microstructural observations of the feldspar grains indicate limited crystal plasticity, suggesting that feldspar was more rheologically competent during this period of fabric development, and deformed dominantly by microfracturing. The results of this microstructural and EBSD study on naturally deformed shear zone rocks will be used to help evaluate strain localization and the rheology of continental crust during the development of metamorphic core complexes in zones of continental extension along low-angle detachment faults.

CHAPTER 1: INTRODUCTION

GEOLOGIC AND TECTONIC HISTORY

Basin and Range Province

The Basin and Range Province is one of the best-studied examples of continental extension in the world. Most notably, there is a well known stratigraphic and structural record within the Basin and Range Province documenting western North America's transition from a convergent plate boundary with associated compressional deformational styles to a transform plate boundary accommodating two different styles of extension. The middle Tertiary extensional development of metamorphic core complexes in the North American Cordillera can be divided into two zones: the northern core complexes associated with the Nevada hinterland and the southeastern California and Arizona core complexes in the Basin and Range Province (e.g., Coney, 1980).

The Basin and Range Province is unique not only because of the rate at which extension occurred, but because the metamorphic core complexes in the Basin and Range Province are not associated with Mesozoic compression (e.g., Coney, 1980). This makes an evaluation of strain localization and the strength of continental crust during the development of metamorphic core complexes less fraught with error. In the southern Basin and Range Province, the southeastern California and Arizona metamorphic core complexes rapidly developed in approximately 1.5 million years (e.g. Reynolds et al., 1986).

The South Mountains, south of Phoenix, Arizona, are host to a Miocene metamorphic core complex (e.g., Reynolds, 1985; Reynolds et al., 1986). Prior geologic mapping indicates the development of the Tertiary metamorphic core complex is the only

deformational episode in the South Mountains since the Precambrian (e.g. Reynolds, 1985; Reynolds et al., 1986). In addition, the evidence of contemporaneous brittle and ductile deformation along the South Mountains detachment fault and the Tertiary age of the footwall mylonites enables one to evaluate strain localization in the continental crust of metamorphic core complexes, and to gain insight into the strength of continental crust in core complexes. A field study of strain localization in the Tertiary South Mountains granodiorite mylonites can help lead to greater insight into the deformation mechanisms and conditions that promote strain localization in continental detachment fault systems. The results of this study will contribute to knowledge of naturally deformed shear zone rocks that can be used to evaluate continental core complex development and continental crust rheology during extension.

The Basin and Range Province refers to a region of the North American tectonic plate that extends east of the Sierra Nevada and west of the Colorado Plateau, as well as south of the Snake River down into northwestern Mexico (Figure 1.1; e.g., Coney, 1987; Wernicke et al., 1988; Wells and Hillhouse, 1989; Niemi et al., 2001). Although geographically defined as a single region, the present-day Basin and Range Province developed during two distinct episodes of crustal extension (e.g., Coney, 1987), resulting in two very different structural styles of deformation.

The first episode of east-west extension occurred ~30-20 Ma in the middle Tertiary at the end of the Laramide Orogeny (e.g., Coney, 1987). This post-compressional northeast-trending extension along low-angle normal faults, accompanied by ignimbrite eruptions, led to widespread development of 'metamorphic core complex' structures in the North American Cordillera (e.g., Coney, 1987). The second extensional

period took place in the late Tertiary and is characterized by 'horst and graben' normal fault structures. This latter episode occurred as a result of west-northwest crustal extension (Niemi et al., 2001) in two extensional domains (Wernicke et al., 1988). Since the late Tertiary, the region has accommodated ~250 km of total extension (e.g., Wernicke et al., 1988; Niemi et al., 2001).

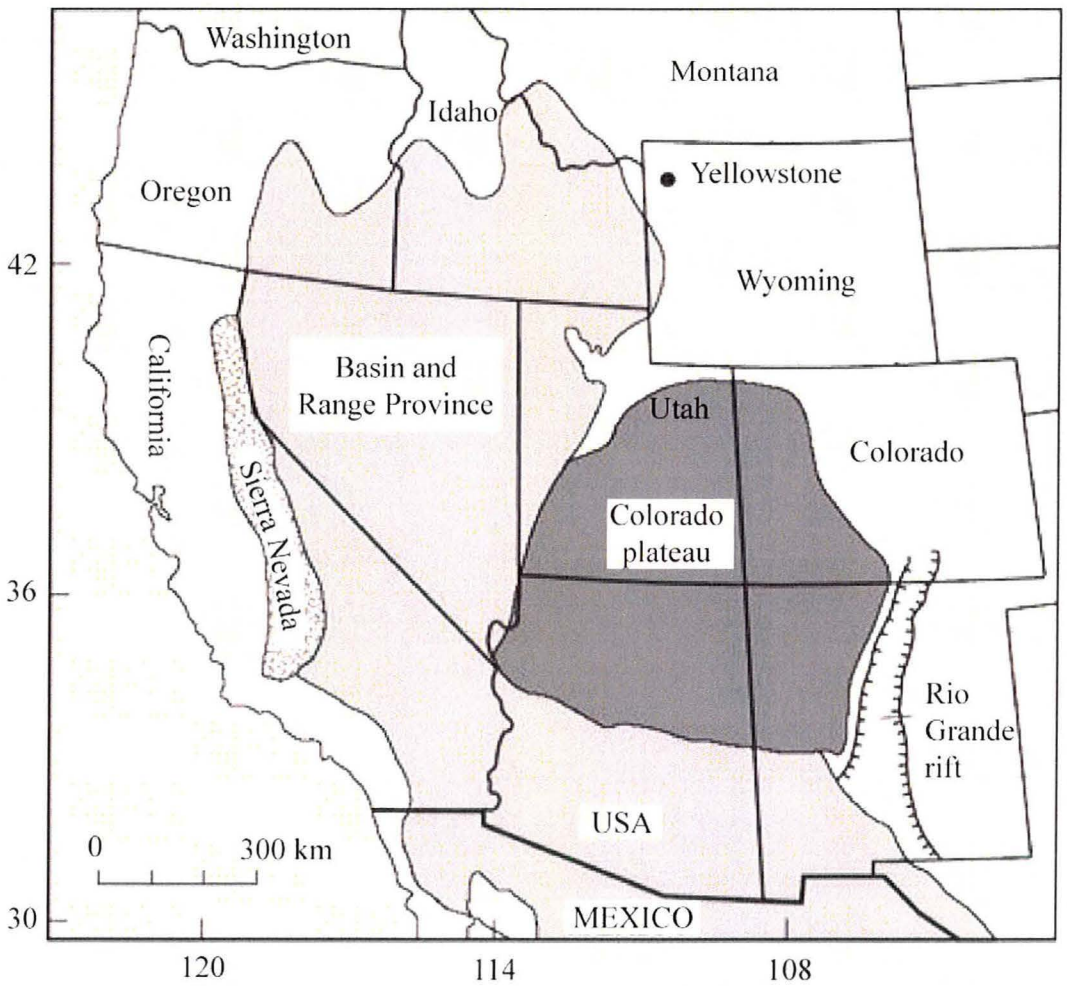

Figure 1.1 Map showing the geographic extent of the Basin and Range Province in the United States. Modified from Parsons (1995).

Geologic History of the Basin and Range Province

Mesozoic Compression

The North American Cordillera extends from Canada south into Mexico, and laterally extends from the Coast Ranges on the western margin of North America to the Front Range of the Rocky Mountains in Colorado, Wyoming, and Montana (Figure 1.2). Two Mesozoic compressional styles can be found within the North American Cordillera. An overview of Mesozoic compression is important to a study of the development of the Basin and Range Province because Basin and Range extensional structures are superimposed on earlier Mesozoic compressive structures related to the Sevier and Laramide orogenies (Figure 1.2). Both the Sevier and Laramide Orogenies resulted in over-thickening of the continental crust, which later helped to promote Tertiary extension in the Basin and Range Province.

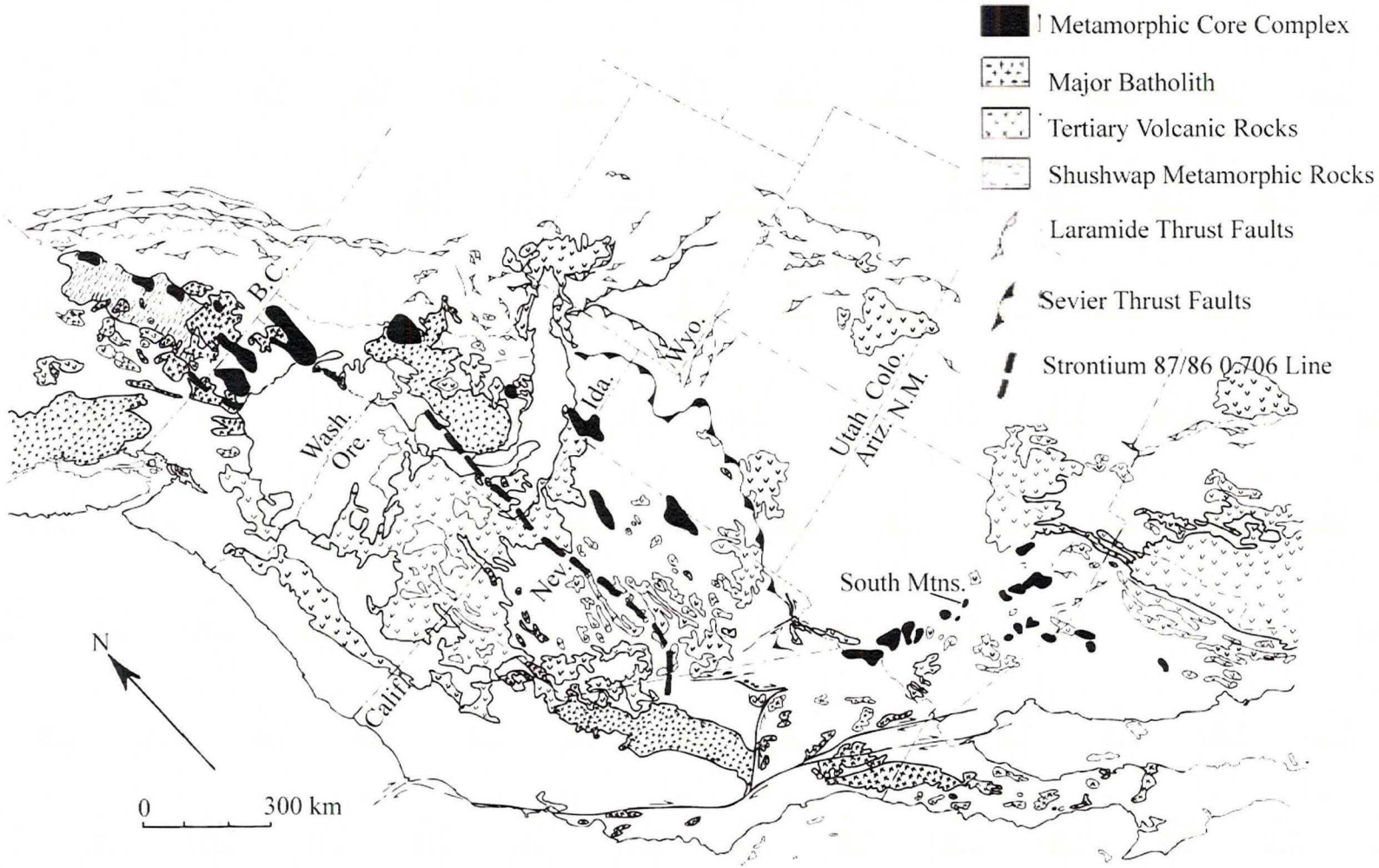

Figure 1.2 Map showing the geographic extent of the North American Cordillera, as well as the areas affected by the Laramide and Sevier Orogenies. Figure after Coney (1980).

Sevier-style deformation refers to thin-skinned tectonism within the back-arc basin. "Thin-skinned tectonics" implies that within the Sevier fold-and-thrust belt only the supracrustal rocks are affected and the crystalline basement is not deformed by the ramp-flat geometry along low-angle thrust faults (Figure 1.3b). These "fold-and-thrust belts" were developed in the back-arc region. The back-arc region developed within the overriding North American plate during subduction of the Farallon plate. The Sevier Orogeny began between ~140 Ma in the northern part of the North American Cordillera and ~50 Ma in the southern part of the Cordillera presumably due to the moderate dip angle of the subducting Farallon plate beneath the North American plate (Figure 1.3a; e.g., Coney, 1987). The over-thickened continental crust of the Sevier back-arc thrust belt and associated Sevier-style deformation is exposed in the northern portion of the Basin and Range Province from Canada south into Nevada; it is best exposed in Utah (Figure 1.2).

Laramide-style deformation occurred between ~80 Ma in the northern part of the North American Cordillera and ~30 Ma in the southern portion of the Cordillera (e.g., Coney, 1987). This expression of "thick-skinned tectonics" is defined by high-angle reverse faults within the arc in which both the supracrustal rocks and the crystalline basement are involved in the faulting (Figure 1.4b). The change in deformation style is interpreted to be due to a decrease in the subduction angle of the Farallon plate beneath the North American plate. The progressively lower dip angle of subduction led to the development of over-thickened continental crust in the actual arc itself (Figure 1.4a; e.g., Coney, 1987). In contrast to the Sevier Orogeny, the Laramide Orogeny affected a much larger area spatially, with evidence of high-angle reverse faulting found in Canada,

Montana, Wyoming, South Dakota, Nevada, Arizona, Colorado, and Mexico (Figure 1.2). The Laramide Orogeny thus affected the entire nascent Basin and Range Province.

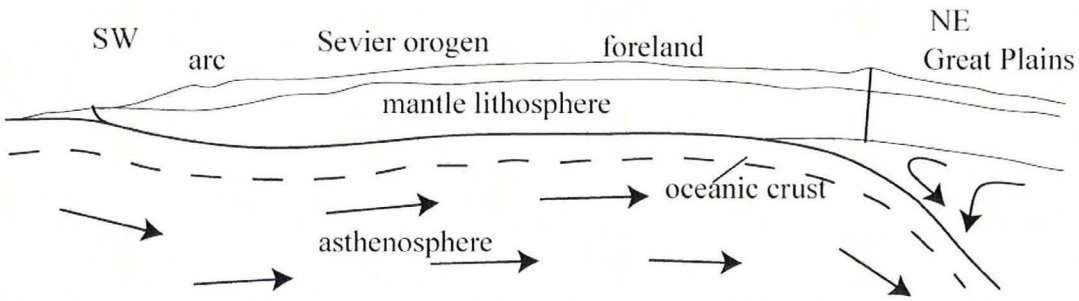

Figure 1.3 Schematic cross section from SW to NE across the western continental margin, Sevier orogen, Rocky Mountain foreland, and Great Plains during the late Cretaceous-early Tertiary episode of horizontal subduction of the Farallon plate. Inland volcanism was produced at a hingeline where the slab bent down and allowed water-rich metasediments on top of oceanic crust to contact hot asthenosphere. Figure 1 from Bird (1984).

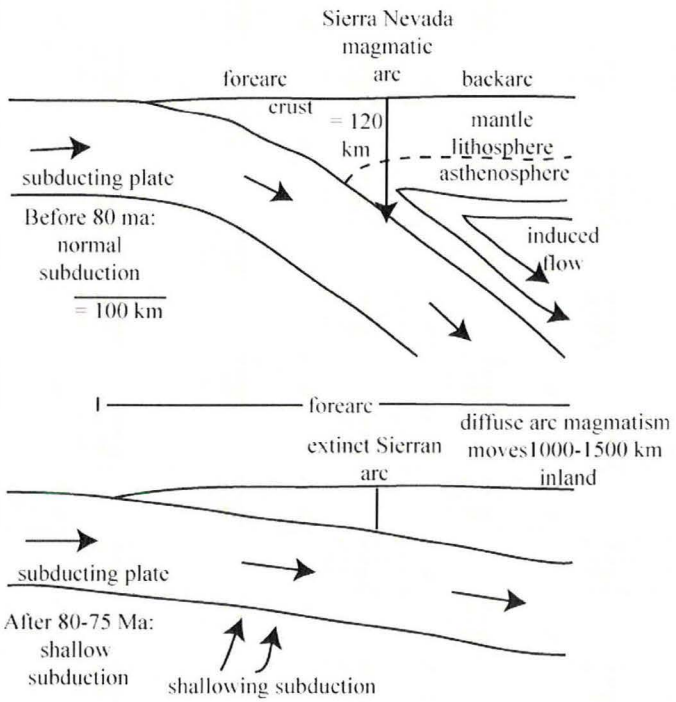

Figure 1.4 Schematic cross sections of the California subduction zone illustrating the proposed shallowing of subduction at the start of the Laramide orogeny. Figure 2 from Dumitry (1990).

Cenozoic Extension

The present-day Basin and Range Province developed during two distinct episodes of Tertiary crustal extension following the Mesozoic compressive episodes (e.g., Coney, 1987), resulting in two very different structural styles of deformation. The first episode of east-west extension occurred in the middle Tertiary at the end of the Laramide Orogeny ~30-20 Ma (e.g., Coney, 1987). This post-compressional northeast-trending extension along low-angle normal faults, accompanied by ignimbrite eruptions, led to widespread development of 'metamorphic core complex' structures in the North American Cordillera ~30-20 Ma (e.g., Coney, 1987).

The second extensional period took place in the late Tertiary and is characterized by 'horst and graben' high-angle (~60°) normal fault structures. This latter episode occurred as a result of west-northwest crustal extension (e.g., Niemi et al., 2001). While it is commonly accepted that the Basin and Range Province developed in part due to two periods of continental extension, there remains debate as to the driving tectonic processes behind its formation (e.g., Atwater, 1970; Coney and Reynolds, 1977; Dickinson and Snyder, 1979; Coney, 1980; Dewey, 1980; Wernicke, 1981; Coney, 1987; Severinghaus and Atwater, 1990). Despite this debate, both extensional episodes can be related to a change in the interaction of the Pacific and North American plates.

Episode 1: Early to Middle Tertiary

Extension during the Middle Tertiary is characterized by the development of 'metamorphic core complex' structures and associated low-angle normal faults. The slab roll-back and slab gap hypotheses are the two primary hypotheses used to explain the plate tectonic setting and the first period of extension that began with the conclusion of

the Laramide Orogeny in the beginning of the Tertiary ~65 Ma (e.g., Atwater, 1970; Dickinson and Snyder, 1979; Dickinson, 1981; Coney, 1987). During the first period of extension beginning in the Early Tertiary, the Farallon plate was obliquely subducted beneath the western margin of the North American plate (Figure 1.5; e.g., Atwater, 1970; Coney, 1980; Coney, 1987; Severinghaus and Atwater, 1990). In the Middle Tertiary (~30 – 20 Ma), once the Farallon plate was completely subducted, the East Pacific Rise came into contact with the North American plate at present-day Baja California and began to subduct beneath it (Figure 1.5; e.g., Atwater, 1970; Coney, 1980; Coney, 1987). With subduction of the Farallon plate complete by ~25 Ma, the northwest moving Pacific Plate came into contact with the west-moving North American plate, beginning to change what was previously a convergent plate boundary into a transform one (Figure 1.5; e.g., Atwater, 1970; Coney, 1980; Coney, 1987).

The slab roll-back hypothesis states that at the end of the Laramide Orogeny in the beginning of the Tertiary, the previously flat-dipping subducting Laramide slab experienced a significant increase in dip angle and began to roll back toward the western margin of the North American tectonic plate (e.g., Coney and Reynolds, 1977; Dickinson and Snyder, 1979; Coney, 1980; Dewey, 1980; Coney, 1987). The decrease in compressive stresses on the western margin of the North American plate allowed energy stored in the over-thickened continental crust of the arc complex to thermally relax and dissipate laterally in an east-west direction, resulting in crustal extension (e.g., Coney, 1987; DeCelles, 2004).

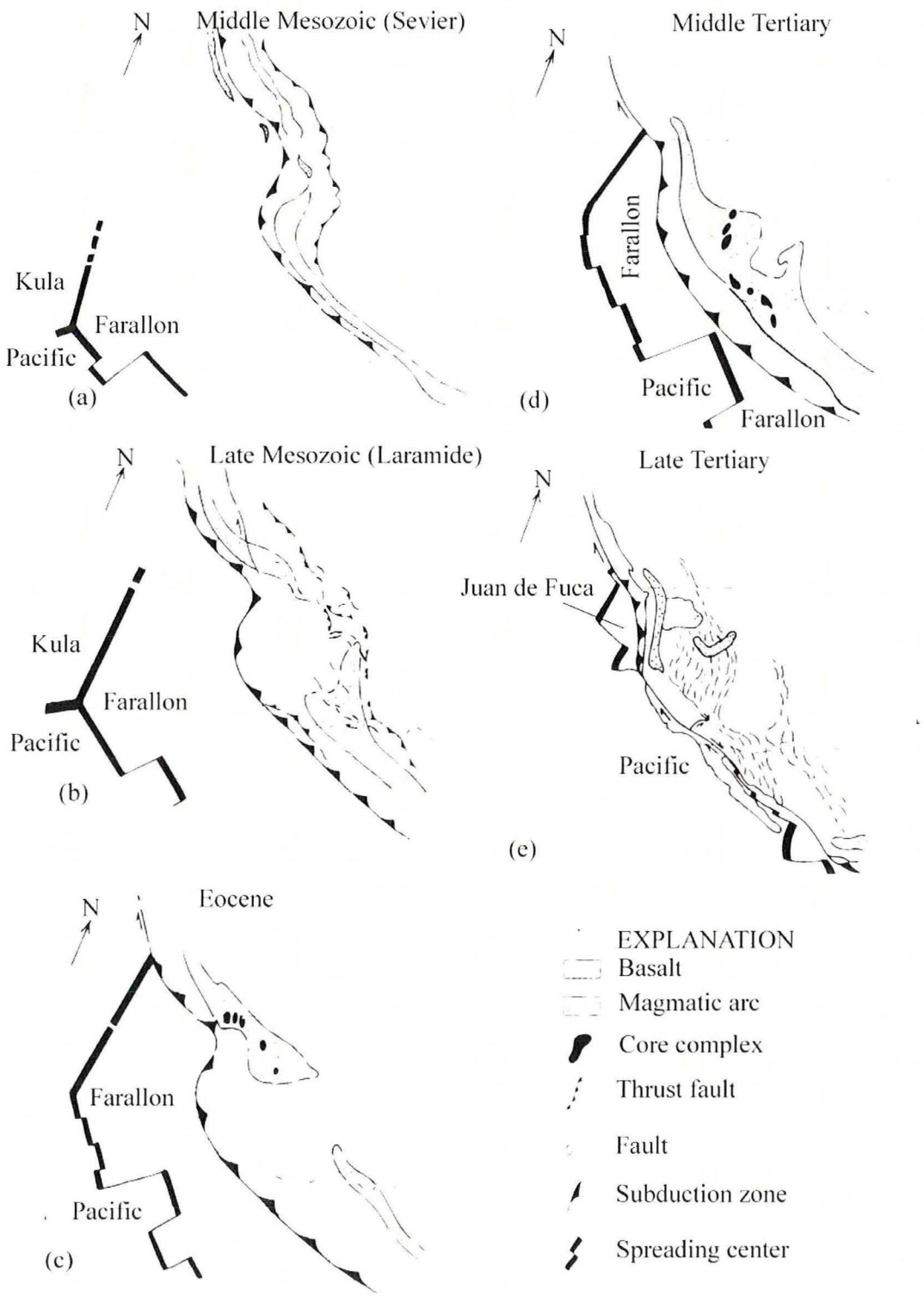

Figure 1.5 Plate tectonic arrangements throughout Tertiary extension. Modified after Coney (1980).

As a result of the thermal relaxation associated with slab roll-back, granitic crustal melts formed, initiating the ignimbrite flare-up (e.g., Coney, 1987). The ignimbrite flare-up migrated west, following the retreating Laramide slab (e.g., Coney and Reynolds, 1977; Coney, 1987). The massive heating of the lithosphere associated with the ignimbrite flare-up caused thinning of the crust, thus leading to extension.

The slab gap hypothesis (Figure 1.6), suggests that as the convergent plate boundary started to become a transform plate boundary (e.g., Atwater, 1970; Dickinson and Snyder, 1979), the triple junction where the East Pacific Rise came into contact with the North American plate began to migrate northwest. The subducting Farallon plate fell away, thus creating a gap where the subducting slab used to be (Figure 1.6; e.g., Dickinson and Snyder, 1979; Coney, 1980; Coney, 1987). This gap was located beneath the southern Basin and Range Province (e.g., Dickinson and Snyder, 1979; Coney, 1980; Coney, 1987). Upwelling mantle filled the gap, heating and thinning the lithosphere, and causing extension in the overriding plate (e.g., Dickinson and Snyder, 1979; Coney, 1987). Coincident with early to middle Tertiary extension is the 'ignimbrite flare-up' (e.g., Coney, 1987). The 'ignimbrite flare-up' of increased igneous activity occurred at the end of the Laramide Orogeny due to retreat of the Farallon plate associated with the transition from compressional to extensional tectonics (e.g., Coney, 1987). The subsequent increase in magmatic activity associated with the ignimbrite flare-up migrated southwest from Idaho to Arizona, also contributing to mid-Tertiary extension (e.g., Coney and Reynolds, 1977; Dickinson, 1981; Coney, 1987). This episode of mid-Tertiary extension happened over a protracted period of time in the North American

Cordillera, beginning in the Eocene in southern Idaho, and eventually extending down into the southern region of the province in the Oligocene-Miocene (Figure 1.5; e.g., Coney, 1980; Coney, 1987).

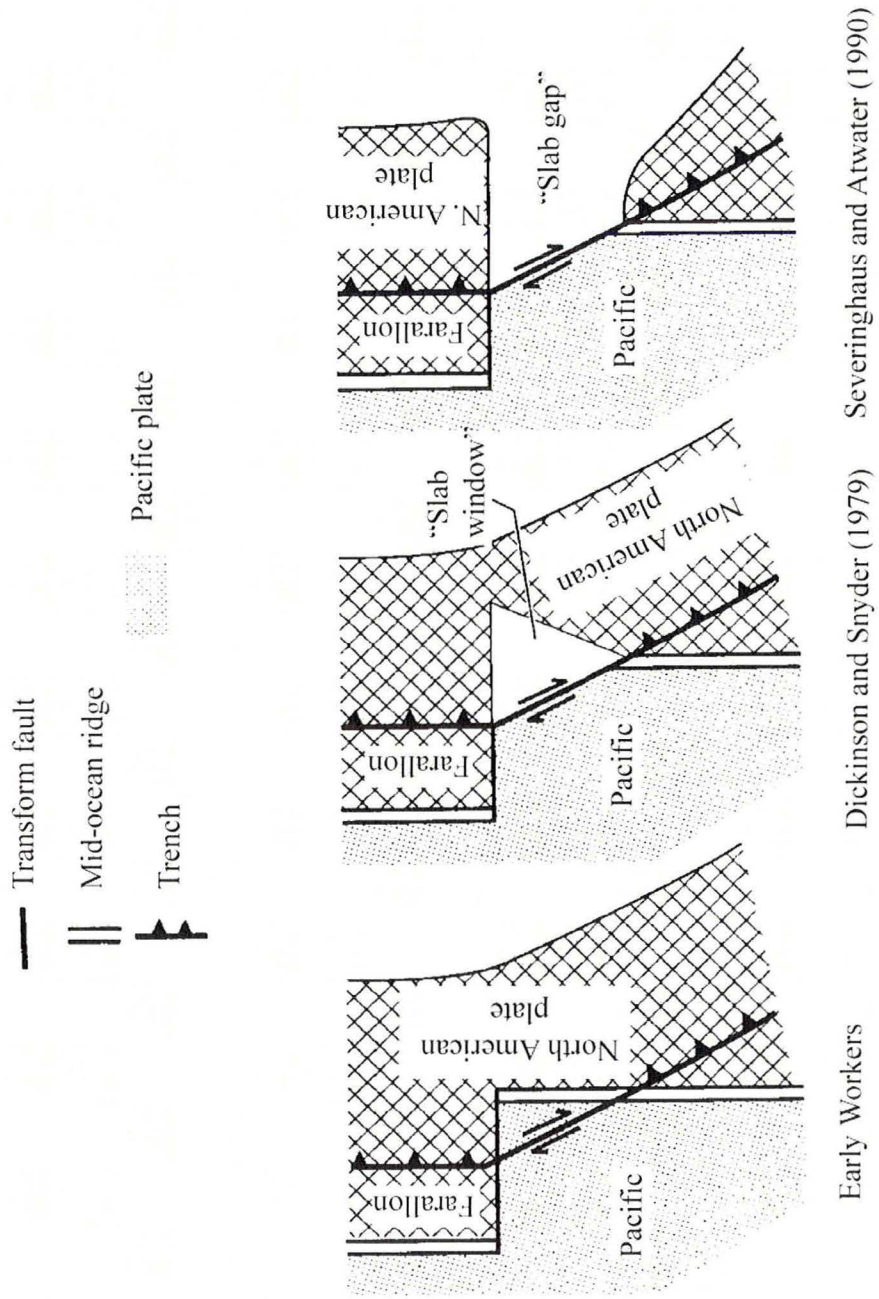

Figure 1.6 Hypotheses concerning plate interactions in the early to middle Tertiary. Figure 1 from Severinghaus and Atwater (1990).

Episode 2: Middle to Late Tertiary

Throughout the middle Tertiary, the continued subduction of the East Pacific Rise beneath the continental North American plate resulted in the increased lengthening of the proto-San Andreas fault while the Pacific plate continued to move northwestward along its plate boundary with the North American plate (Figure 1.5; e.g., Atwater, 1970; Coney, 1980; Coney, 1987). Lengthening of the outboard proto-San Andreas transform fault boundary occurred due to the northwestward migration of the triple junction away from Baja California, which resulted in the slab gap growing (Figure 1.6; e.g., Atwater, 1970; Coney, 1987; Severinghaus and Atwater, 1990). The expanding slab gap is represented on the surface by the development of high-angle normal faults.

At ~6 Ma the outboard transform plate margin shifted from the Pacific Ocean inboard to the North American continent, transferring Baja California and southern California from the North American to the Pacific tectonic plate, thus initiating the modern San Andreas fault system (e.g., Atwater, 1970; Coney, 1987; Severinghaus and Atwater, 1990). Right-lateral motion along the Pacific-North American transform plate boundary continued, as did northwest-southeast directed Basin and Range extension. Results of the changed boundary include clockwise rotation of the Western Transverse Ranges in southern California (e.g., Luyendyk, 1991; Crouch and Suppe, 1993; Atwater, 1998), and continued horst and graben style extension in the Basin and Range Province. In contrast to the mid-Tertiary extension characterized by the development of metamorphic core complexes along low-angle normal faults, late Tertiary extension is characterized by the development of 'horst and graben' structures bounded by high-angle normal faults.

Structural Styles Associated with Extension

Two styles of normal faulting are observed in the Basin and Range Province: the 'metamorphic core complex' and 'horst and graben' structures. Less common is the 'metamorphic core complex' structure, which emphasizes the role of low-angle ($\leq 30°$ dip) normal faults in denuding crustal rocks. According to Coney (1980), a metamorphic core complex is defined as an uplifted dome composed of metamorphic and plutonic rocks; the uplifted dome is overlain by a low-angle detachment fault and brittlely deformed hanging wall rocks (Figure 1.7).

Initially considered to be features of low-angle thrust faults associated with Sevier-style deformation (e.g., Misch, 1960), the metamorphic core complexes are found along the length of the North American Cordillera (Figure 1.2; e.g., Coney, 1979; Coney, 1980; Armstrong, 1982; Coney, 1987). The metamorphic core complexes are older in the north and younger in the south, possibly reflecting the retreat-to-the-southwest of the Farallon plate (e.g., Coney, 1980; Armstrong, 1982; Coney, 1987). Two domains of metamorphic core complexes exist in the North American Cordillera: one associated with the Nevada hinterland region to the north and the other in the Arizona-Sonora region to the south (e.g., Coney, 1980; Coney, 1987). The difference between the two domains is that while both formed due to retreat of the Farallon slab, the metamorphic core complexes located in the Nevada hinterland region developed in a time period overlapping with Laramide deformation; the Arizona-Sonora metamorphic core complexes did not develop until after Laramide deformation ceased.

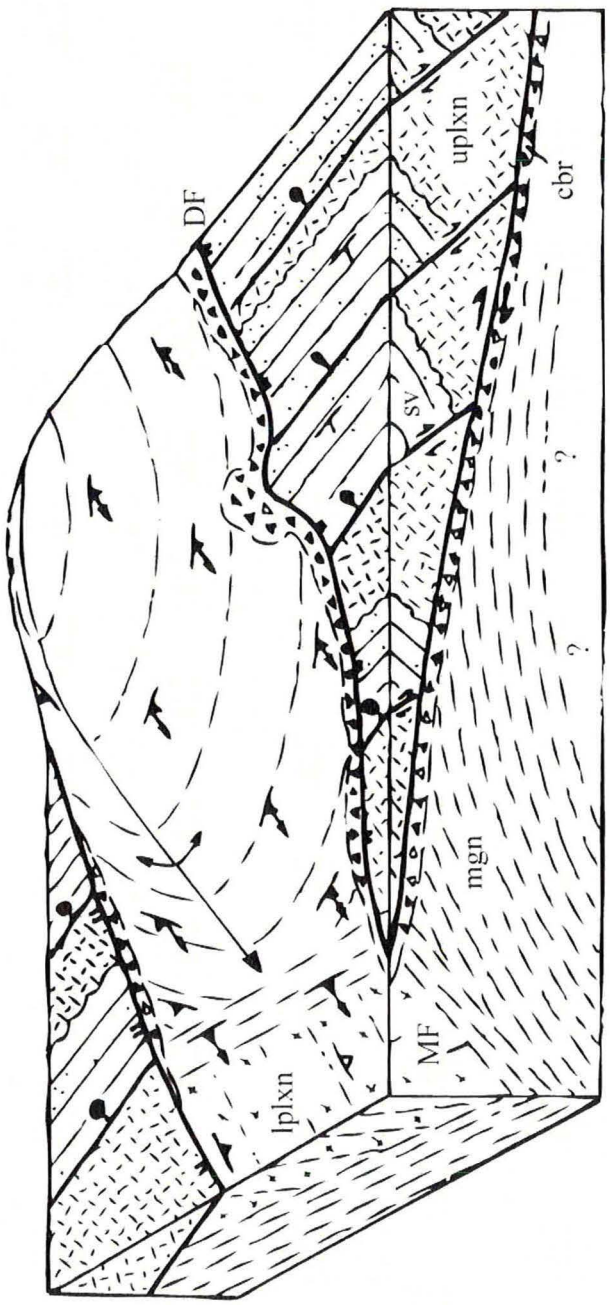

Figure 1.7 Diagrammatic representation of general geologic relations of metamorphic core complexes. Structural features designated by symbols: DF = detachment fault; MF = mylonitic front. Rock units: lpxln = lower plate crystalline rocks; mgn = undifferentiated mylonitic gneisses;cbr = chloritic breccias; uplxn = upper plate crystalline rocks; sv = Miocene sedimentary and volcanic rocks. Modified from Davis and Lister (1988).

Based on previous field studies (e.g., Coney, 1980; Davis, 1980; Rehrig and Reynolds, 1980; Reynolds, 1985; Coney, 1987; Lister and Davis, 1989), there are several common structures, lithologies, and textures indicative of metamorphic core complexes

(Figure 1.7). Structures associated with metamorphic core complexes include: (1) a domed footwall, (2) a low-angle (less than 30°) fault surface, (3) an elongate outcrop pattern in the direction of extension, and (4) corrugated fault surfaces with corrugations parallel to slip direction. Indicative lithologies and textures of extension along low-angle normal faults are: (1) metamorphic or plutonic footwall rocks that may show evidence of ductile deformation; (2) a down-temperature deformation history of the footwall rocks, which indicates the cooling and denudation of lower crustal rocks and thus, extension; (3) a brittlely deformed hanging wall; and (4) a sharp detachment fault surface polished with slickensides and usually underlain by fault gouge (e.g., Coney, 1980; Davis, 1980; Rehrig and Reynolds, 1980; Reynolds, 1985; Davis et al., 1986; Reynolds et al., 1986; Coney, 1987; Lister and Davis, 1989).

Northern Cordillera vs. Southern Cordillera

As mentioned previously, the Sevier Orogeny and the Laramide Orogeny occurred during the Mesozoic. The Sevier Orogeny affected the northern and central portions of the North American Cordillera, and its deformational effects did not extend into southern Arizona and northern Mexico. Thus, only the northern portion of the metamorphic core complexes, especially those in Utah and the Nevada hinterland (e.g., Cooper and Platt, 2008), show evidence of Sevier-style deformation. In contrast, the Laramide Orogeny had a larger spatial distribution and its effects reached further south into southern Arizona and northern Mexico (Figure 1.2).

In the northern and central portions of the North American Cordillera, Sevier and Laramide-style deformation overlaps in both space and time (Figure 1.2), adding a further layer of structural complexity to this region. Additionally, the thrust-related low-angle

mylonites associated with the Sevier Orogeny were initially confused with the normal fault-related mylonites associated with the metamorphic core complexes (e.g., Misch, 1960; Armstrong, 1968; Price and Mountjoy, 1970). Combined with development of the metamorphic core complexes in the mid-Tertiary, the overlapping Mesozoic deformational styles make it difficult to ascertain the individual effects of the Laramide and Sevier orogenies, as well as the development of the metamorphic core complex structures (e.g., Coney, 1980).

Southeastern-California and Arizona Core Complexes and Their Significance

Geologic mapping was conducted in the Catalina-Rincon, Harcuvar, Whipple-Buckskin-Rawhide Mountains, and the South Mountains metamorphic core complexes of southeastern-California and Arizona (e.g., Banks, 1980; Davis et al., 1980; Rehrig and Reynolds, 1980; Reynolds and Rehrig, 1980; Reynolds, 1985; Bykerk-Kauffman and Janecke, 1987). The results of these previous geologic studies indicate that Laramide-style deformation definitely preceded the development of the southeastern-California and Arizona metamorphic core complexes (e.g., Coney, 1980; Reynolds and Rehrig, 1980; Reynolds et al., 1986). The Tertiary metamorphic core complexes located in southeastern California and Arizona are especially significant because in addition to definitely forming after the Laramide Orogeny, these complexes are not associated with the Nevada hinterland of the Sevier Orogeny to the north (Figure 1.2; e.g., Coney, 1980). The development of metamorphic core complexes in southeastern California and Arizona can be studied as a distinct event unrelated to the Laramide Orogeny because these complexes either show no evidence of Laramide-style deformation or geologic mapping indicates Laramide-style deformation is older than metamorphic core complex

development. The ability to differentiate between Laramide-style deformation and the development of metamorphic core complexes in the southeastern California and Arizona core complexes is significant to studies of the formation, deformation, and metamorphism of all core complexes throughout the Cordillera.

The South Mountains are the only metamorphic core complex in Arizona that does not also exhibit evidence of Mesozoic plutonism or metamorphism. This is important because one issue central to a study of core complexes is determining that the footwall mylonitic zone is related to development of the metamorphic core complex (Price and Mountjoy, 1970; Davis et al., 1980; Davis et al., 1986; Reynolds et al., 1986; Davis and Lister, 1988; Lister and Davis, 1989; Reynolds and Lister, 1990). This relationship is difficult to conclude in the northern and central parts of the North American Cordillera, and can be complicated to determine in the southern part of the North American Cordillera as well.

The Catalina-Rincon Mountains in southeastern Arizona expose a metamorphic core complex along the northeast-southwest extending Catalina fault (e.g., Banks, 1980; Bykerk-Kauffman and Janecke, 1987; Bykerk-Kauffman, 1990; Bykerk-Kauffman, 2008). Although the complex is younger than Laramide-style deformation and is not associated with the Nevada hinterland, many questions remain unanswered. Radiometric studies return inconclusive results, meaning that the number and ages of deformations are unclear (e.g., Banks, 1977; Banks, 1980; Bykerk-Kauffman and Janecke, 1987; Gehrels and Smith, 1991). The plutons of the Catalina-Rincon Mountains may be Mesozoic in age (e.g., Banks, 1977; Banks, 1980; Bykerk-Kauffman and Janecke, 1987; Gehrels and Smith, 1991).

In the middle Tertiary, the Harcuvar metamorphic core complex developed in west-central Arizona (e.g., Rehrig and Reynolds, 1980). The Harcuvar complex is composed of the Harquahala, Harcuvar, Buckskin, and Rawhide Mountains (e.g., Rehrig and Reynolds, 1980). The complex is characterized by northeast-southwest-trending extension, a low-angle detachment fault surface, and mylonitic foliation with northeast-trending lineation in the footwall (e.g., Rehrig and Reynolds, 1980; Reynolds and Rehrig, 1980; Reynolds and Lister, 1990). While it is possible to correlate the mylonitization with the dated South Mountains metamorphic core complex and determine a tentative date of deformation at 25.3 Ma (Reynolds and Rehrig, 1980), the Harcuvar complex is not an ideal study area because of the complicating presence of additional Mesozoic intrusions and associated deformation (Davis et al., 1980).

A metamorphic core complex developed in the Whipple-Buckskin-Rawhide Mountains, located in southeastern California, in the middle Tertiary ~14-19 Ma (e.g., Davis et al., 1980; Davis et al., 1982; Davis et al., 1986; Lister and Davis, 1989). Although it is clear the deformation is younger than Laramide-style deformation (~ 80-30 Ma), (e.g., Coney, 1980; Reynolds and Rehrig, 1980; Reynolds et al., 1986), the Whipple-Buckskin-Rawhide Mountains show evidence of multiple episodes of mid-Tertiary deformation from ~19-14 Ma (e.g., Lister and Davis, 1989). There is evidence of at least two episodes of detachment faulting, rotation of the hanging-wall blocks, and lateral warping along northeast-southwest axes (e.g., Davis et al., 1986). The core complex is characterized by a low-angle detachment fault, associated brecciation, and a subhorizontal zone of mylonitization in the footwall (e.g., Davis et al., 1980; Davis et al., 1982; Davis et al., 1986). The Whipple-Buckskin-Rawhide metamorphic core complex

has a sufficient degree of complexity that it is worthwhile to find a more simple option for a rheological study of metamorphic core complexes.

The South Mountains metamorphic core complex, south of Phoenix, Arizona (Figure 1.8), exposes Tertiary extensional mylonites that formed coincident with intrusion of the footwall rocks (e.g., Reynolds and Rehrig, 1980; Reynolds, 1985; Reynolds et al., 1986). A study of cross-cutting relationships and geochronology allows the link between the footwall mylonites and the development of the metamorphic core complex to be determined (Reynolds and Rehrig, 1980; Reynolds, 1985; Reynolds et al., 1986). In addition, the lack of over-printing deformational episodes and the evidence of contemporaneous brittle and ductile deformation along the South Mountains detachment fault enables one to evaluate strain localization in continental crust in core complexes, which gives insight into the strength of continental crust.

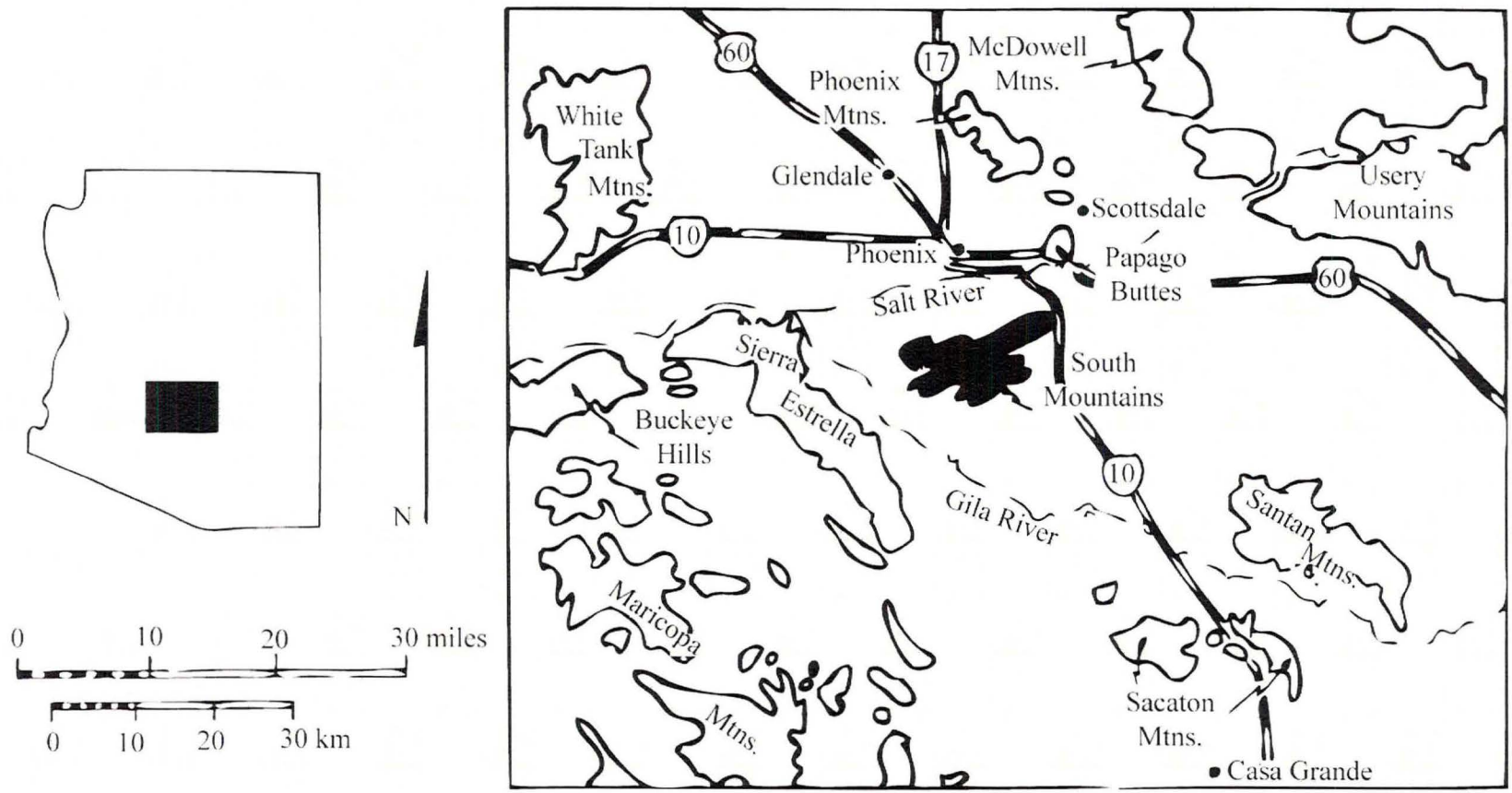

Figure 1.8 Map showing the location of the South Mountains and other local ranges. Modified from Reynolds (1985).

MOTIVATION OF PROJECT

The South Mountains, located south of Phoenix, Arizona (Figure 1.8), are host to a Miocene metamorphic core complex dominated by Tertiary intrusive rocks and associated Tertiary extensional mylonites (e.g., Reynolds, 1985; Reynolds et al., 1986). Geologic mapping indicates that since the Precambrian only one major episode of deformation has occurred in the South Mountains: the development of the Miocene metamorphic core complex (e.g., Reynolds, 1985). The lack of multiple deformational episodes in the South Mountains makes it an ideal location for a study of continental crust rheology during metamorphic core complex extension.

The Basin and Range Province is one of the best-known examples of continental extension in the world. It is also notable for the speed at which the metamorphic core complexes developed; for example, the South Mountains metamorphic core complex formed in ~1.5 million years (Reynolds et al., 1986). In addition, the footwall rocks of the South Mountains detachment fault contain evidence of both brittle and ductile deformation.

Prior studies of the South Mountains metamorphic core complex (e.g., Davis et al., 1986; Reynolds, 1985; Reynolds et al., 1986) were instrumental in defining the Tertiary origin of mylonites and the timing of formation of metamorphic core complexes. Strain localization of extensional provinces has yet to be comprehensively studied in the South Mountains metamorphic core complex. The rate of extension and speed at which these core complexes formed makes a rheological study essential to understanding how continental crust behaves during extension.

Studies of experimentally deformed quartz-rich rocks from the Ruby Gap duplex, Central Australia, the western Adirondacks, and other locations suggest that crystal plastic deformation of the crust is controlled by quartz (e.g., Hirth et al., 2001; Tullis, 2002; Gleason and DeSisto, 2008), but the flow laws utilized are constrained by a limited amount of field data. A field study of strain localization in the Tertiary South Mountains granodiorite mylonites can help lead to greater insight into the deformation mechanisms and conditions that promote strain localization in continental detachment fault systems. The results of this study will contribute to rheology studies of naturally deformed shear zone rocks (e.g., Hirth et al., 2001; Tullis, 2002; Gleason and DeSisto, 2008), that can be used to evaluate continental core complex development and continental crust rheology during extension.

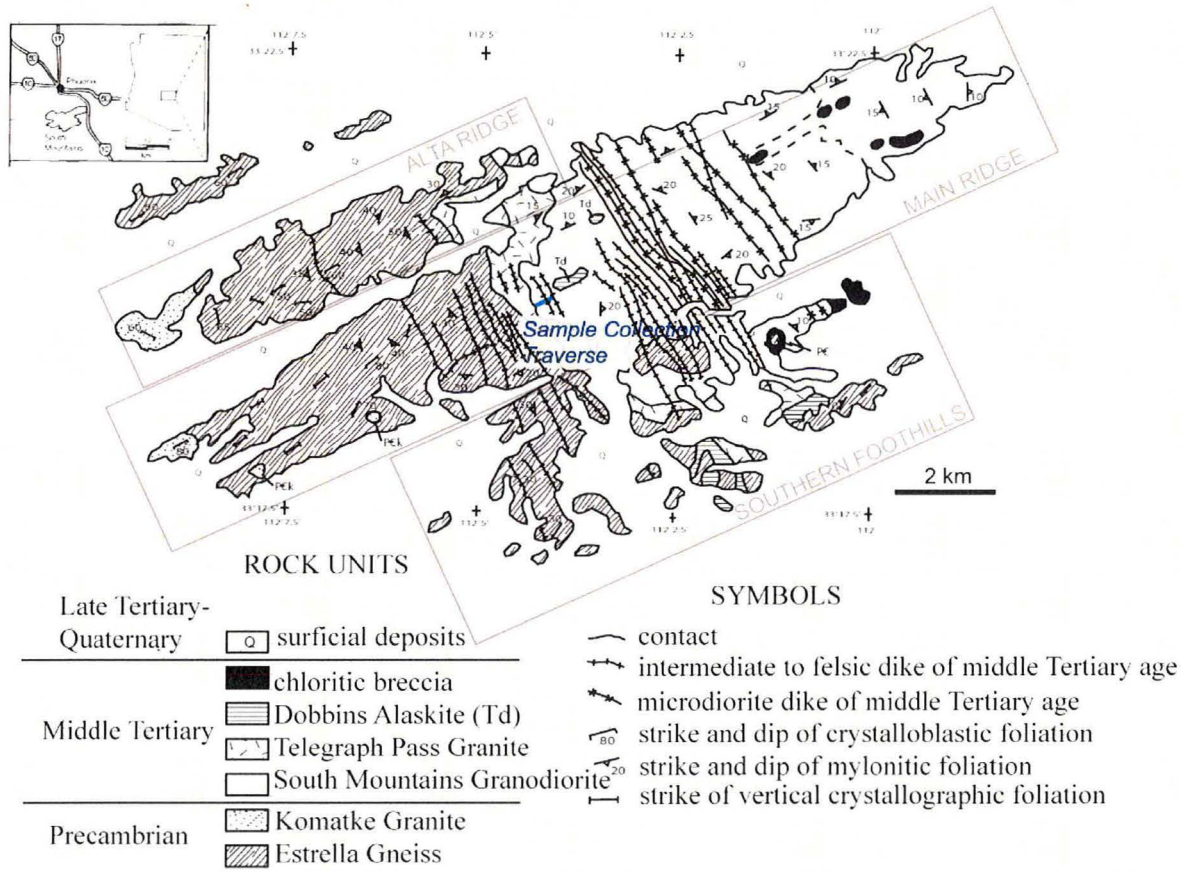

Figure 1.9 Geologic map of South Mountains. Modified from Reynolds (1985).

SOUTH MOUNTAINS GEOLOGY

Geographic Location

The South Mountains are located south of Phoenix, Arizona, in the City of Phoenix South Mountain Park (Figure 1.8; e.g., Avedisian, 1966; Reynolds, 1985). The South Mountains are an 18 km, northeast-trending metamorphic core complex (Figure 1.9), that is part of a series of metamorphic core complexes in southwestern Arizona (Figure 1.8; e.g., Rehrig and Reynolds, 1980; Reynolds and Rehrig, 1980; Reynolds, 1985). The South Mountains are located in the southern portion of the North American

Cordillera, and more specifically in the southwestern part of the Basin and Range Province (e.g., Wilson and Moore, 1959; Hayes, 1969; Rehrig and Reynolds, 1980).

Lithologic Units

Precambrian

Estrella Gneiss and Komatke Granite

The Proterozoic Estrella Gneiss is widely distributed and is visible on the North, Alta, and western half of Main ridges (Figure 1.9). It is dominantly quartzofeldspathic in composition with abundant amounts of amphibolite also present (Reynolds, 1985). Hornblende, plagioclase feldspar, biotite, and quartz are present, as is a crystalloblastic foliation (Reynolds, 1985). This is indicative of upper amphibolite-facies metamorphism (Reynolds, 1985). The Estrella Gneiss' protolith is most likely an intermediate to mafic plutonic rock or a metasedimentary rock (Reynolds, 1985). The Estrella Gneiss is Rb-Sr dated as 1.8-1.6 Ga (Reynolds, 1985), and was probably formed during a prior Precambrian period of intrusion and deformation (Reynolds, 1985).

The younger and more sparsely distributed Komatke Granite is found on the southwest sides of Alta Ridge and Main Ridge (Figure 1.9; Reynolds, 1985). The 1.6-1.7 Ga Komatke Granite is composed primarily of quartz, potassium feldspar, plagioclase feldspar, and variable amounts of biotite and hornblende (Reynolds, 1985). A crystalloblastic foliation is also present (Reynolds, 1985). This basement rock most likely formed during a later Precambrian intrusion, as evidence by its intrusive contact with the Estrella Gneiss (Reynolds, 1985).

Tertiary Intrusives

The eastern half of the South Mountains shows evidence of three major intrusive episodes that comprise a single composite pluton: the South Mountains Granodiorite, Telegraph Pass Granite, and Dobbins Alaskite (Figure 1.9; Reynolds, 1985; Reynolds et al., 1986). Additionally, two separate sets of extension-related, north-northwest trending dikes can be identified (Figure 1.9; Reynolds, 1985; Reynolds et al., 1986).

South Mountains Granodiorite

The ~24 Ma South Mountains Granodiorite is presumed to be the oldest of the three intrusive units, and it is also the most widely distributed (Reynolds, 1985; Reynolds et al., 1986). The South Mountains Granodiorite laterally extends to cover most of the eastern half of the range (Figure 1.9; Reynolds and Rehrig, 1980; Reynolds et al., 1986), and the best exposed outcrops are in the eastern part of Main Ridge and in the Southern Foothills (Figure 1.9; Reynolds, 1985). The South Mountains Granodiorite is comprised of quartz, potassium feldspar, and plagioclase feldspar, with variable amounts of biotite (Avedisian, 1966; Reynolds and Rehrig, 1980; Reynolds, 1985).

Telegraph Pass Granite

The ~22 Ma Telegraph Pass Granite is the middle-aged of the Tertiary intrusive units (Reynolds et al., 1986), and is best exposed in Telegraph Pass and in the central Southern Foothills (Figure 1.9; Reynolds, 1985). In Telegraph Pass it shares an intrusive contact with the Estrella Gneiss and a gradational intrusive contact with the South Mountains Granodiorite (Figure 1.9; Reynolds, 1985; Reynolds et al., 1986). In the Southern Foothills the Telegraph Pass Granite overlies the South Mountains Granodiorite

and underlies the Estrella Gneiss (Reynolds, 1985; Reynolds et al., 1986). Telegraph Pass Granite is compositionally similar to the South Mountains Granodiorite (Reynolds, 1985).

Dobbins Alaskite

Dobbins Alaskite is the youngest (~21 Ma) and least laterally extensive of the three Tertiary intrusive units (Reynolds et al., 1986). It is best exposed on Dobbins Lookout, Mount Suppoa, and in the Southern Foothills (Figure 1.9; Reynolds, 1985). Dobbins Alaskite is a white, fine-grained, quartz-rich rock (Reynolds and Rehrig, 1980; Reynolds, 1985).

Dikes

In the center of the South Mountains are two sets of middle Tertiary north-northwest – trending dike swarms (Figure 1.9; Reynolds and Rehrig, 1980; Reynolds, 1985). The older set of dikes is coarser-grained, dominantly granitic in composition (Reynolds et al., 1986), and has a mylonitic fabric (Reynolds, 1985). This older mid-Tertiary dike swarm is primarily found in the central to east portion of the range, with exposures east of Telegraph Pass and in the central Southern Foothills (Figure 1.9; Reynolds, 1985; Reynolds et al., 1986). The younger set is finer-grained, dioritic in composition (Reynolds et al., 1986), and does not show evidence of a mylonitic fabric (Reynolds, 1985). The younger dike swarm is exposed in the western Southern Foothills and west of Telegraph Pass on Main Ridge (Figure 1.9; Reynolds, 1985; Reynolds et al., 1986).

Tertiary Fault Rocks

Mylonites

Structurally below the Tertiary fault rocks associated with the South Mountains detachment fault is a less than 200-meter thick mylonitic shear zone (Reynolds and Rehrig, 1980; Davis et al., 1986). Some of the South Mountains Granodiorite has a mylonitic fabric, with the degree of mylonitization increasing up-structure towards the South Mountains detachment fault (Reynolds and Rehrig, 1980), toward its contact with the Precambrian Estrella Gneiss and Komatke Granite (Reynolds, 1985). The mylonitic South Mountains Granodiorite is characterized by smaller overall grain size and foliation shown by "smearing" of the biotite crystals (Reynolds, 1985). The Telegraph Pass Granite may also exhibit a mylonitic fabric (Reynolds, 1985). In contrast to the above units in which there is local evidence of a mylonitic fabric, the mylonitic gneiss and schist have an extremely pervasive mylonitic fabric in addition to also having undergone mineral replacement (Reynolds, 1985).

The mylonitic gneiss and schist are best exposed at Mount Suppoa and Dobbins Lookout (Figure 1.9; Reynolds, 1985). The mylonitic gneiss and schist overlie South Mountains Granodiorite (Figure 1.9; Reynolds and Rehrig, 1980) and underlie Estrella Gneiss (Reynolds, 1985). The mylonitic gneiss and schist have various protoliths including Estrella Gneiss, South Mountains Granodiorite, Telegraph Pass Granite, and Dobbins Alaskite (Reynolds and Rehrig, 1980; Reynolds, 1985).

Chloritic Breccia

The chloritic breccia is located in the footwall of the low-angle South Mountains detachment fault (Figure 1.9; Reynolds and Rehrig, 1980; Reynolds, 1985; Reynolds et al., 1986). It formed from brittle deformation of the South Mountains Granodiorite (Reynolds and Rehrig, 1980) in relation to movement along the South Mountains detachment fault (Reynolds and Rehrig, 1980; Reynolds, 1985). The South Mountains Granodiorite was fractured, faulted, and hydrothermally altered to become chloritic breccia (Reynolds, 1985). It is best exposed on the eastern ends of Main and Ahwatukee Ridges (Figure 1.9; Reynolds, 1985; Reynolds et al., 1986).

Microbreccia

The microbreccia is also located in the footwall of the low-angle South Mountains detachment fault (Figure 1.9; Reynolds and Rehrig, 1980; Reynolds, 1985; Reynolds et al., 1986). Formed from brittle deformation of the South Mountains Granodiorite (Reynolds and Rehrig, 1980), the microbreccia is structurally beneath the chloritic breccia (Reynolds and Rehrig, 1980). Microbreccia is distinguished from the chloritic breccia due to the much smaller size of the angular fragments and the presence of up to 90% matrix (Reynolds, 1985). Additionally, microbreccia contains less chlorite than the chloritic breccia (Reynolds, 1985).

Tertiary Structural Geology

The three episodes of middle Tertiary intrusion were accompanied by east-northeast directed extension of continental crust along the low-angle South Mountains detachment fault (Reynolds, 1985). The South Mountains detachment fault is only exposed in a small klippe on Ahwatukee Ridge in the Southern Foothills (Figure 1.9).

Due to the east-northeast directed extension along the South Mountains detachment fault, the geometry of the South Mountains is best described as an asymmetric antiformal dome (Reynolds and Rehrig, 1980; Reynolds, 1985; Reynolds et al., 1986). Evidence supportive of the dome structure includes the observation that the mylonitic foliation dips away from the crest of the antiform (Figure 1.9).

Cross-Cutting Relationships

A study of cross-cutting relationships and Rb-Sr, U-Th-Pb, and K-Ar geochronologic dating methods allowed the timing of deformation of the South Mountains metamorphic core complex to be determined (Reynolds et al., 1986). The mylonitization associated with the South Mountains detachment fault can be conclusively linked to the middle Tertiary plutonism through an analysis of cross-cutting relationships (Reynolds, 1985; Reynolds et al., 1986). The three intrusive phases of the composite pluton and two sets of dikes are positively identified as co-magmatic through a study of their gradational contacts and similar compositions (Reynolds, 1985).

There is evidence of the mylonitic fabric cutting the South Mountains granodiorite (Reynolds, 1985; Reynolds et al., 1986); the mylonitization is younger than the geochronologic date determined for the granodiorite (Reynolds, 1985; Reynolds et al., 1986). However, the mylonitic fabric is cut by both the Telegraph Pass Granite and Dobbins Alaskite (Reynolds, 1985; Reynolds et al., 1986); mylonitization is older than these two units (Reynolds, 1985; Reynolds et al., 1986). Mylonitization is also younger than the older, more granitic set of dikes, and older than the second, more dioritic set of dikes (Reynolds, 1985; Reynolds et al., 1986). Based on these relationships, it is plausible to assume that activation of the South Mountains detachment fault and the

associated development of mylonitic fabrics was contemporaneous with intrusion of the mid-Tertiary composite pluton (Reynolds, 1985; Reynolds et al., 1986).

Geochronology

Rb-Sr dating of the South Mountains Granodiorite yields a maximum age of 24.9 +/- 3.0 Ma (Reynolds et al., 1986). Telegraph Pass Granite has an Rb-Sr age of 27.6 +/- 11.9 Ma (Reynolds et al., 1986). Based on their comparable ages and nearly identical $^{87}Sr/^{86}Sr$ ratios of 0.7056 and 0.7062 respectively, the South Mountains Granodiorite and Telegraph Pass Granite are interpreted to be comagmatic at 25.0 Ma (Figure 1.10; Reynolds et al., 1986). U-Th-Pb analyses of zircon crystals from the South Mountains granodiorite yields an age of 22.0 +/- 4.1 Ma, further confirming a Miocene age of emplacement (Reynolds et al., 1986). K-Ar biotite dates from the South Mountains Granodiorite and Telegraph Pass Granite are 20-19 Ma (Reynolds et al., 1986). The K-Ar dates are interpreted as showing the composite pluton cooled below 250 °C within 3-6 million years of intrusion (Reynolds et al., 1986). Based on cross-cutting relationships, the dikes are also interpreted to be Miocene in age (Reynolds et al., 1986). Mylonitization of the rocks occurred ~22-25 Ma (Figure 1.10), based on cross-cutting relationships and isotopic dating methods (Reynolds et al., 1986). Mylonitization definitely ended by the K-Ar biotite date of 20-19 Ma (Reynolds et al., 1986). The South Mountains detachment fault was definitely not active until after intrusion ended 22-25 Ma (Figure 1.10; Reynolds et al., 1986). Because the fault has evidence of both ductile mylonitic fabrics and younger brittle deformation fabrics, it was active 19-20 Ma, and probably up until 17 Ma (Figure 1.10; Reynolds et al., 1986). Development of the South

Mountains metamorphic core complex is thus dated as early Miocene (~20-17 Ma) in age (Reynolds et al., 1986).

Structural Evolution of the South Mountains Metamorphic Core Complex

In the early Miocene, 22-25 Ma, the composite pluton that primarily makes up the South Mountains metamorphic core complex was emplaced, disrupting the Precambrian crystalline basement (Reynolds et al., 1986). After intrusion was completed, the South Mountains detachment fault was active from ~20 Ma until ~17 Ma (Reynolds et al., 1986). Associated mylonitic fabrics formed ~19-20 Ma (Reynolds et al., 1986). It has been hypothesized that the South Mountains metamorphic core complex formed in an evolving crustal shear zone that accommodated middle Tertiary extension (Figure 1.11; e.g., Davis, 1983; Reynolds, 1985; Davis et al., 1986; Reynolds et al., 1986; Lister and Davis, 1989; Reynolds and Lister, 1990).

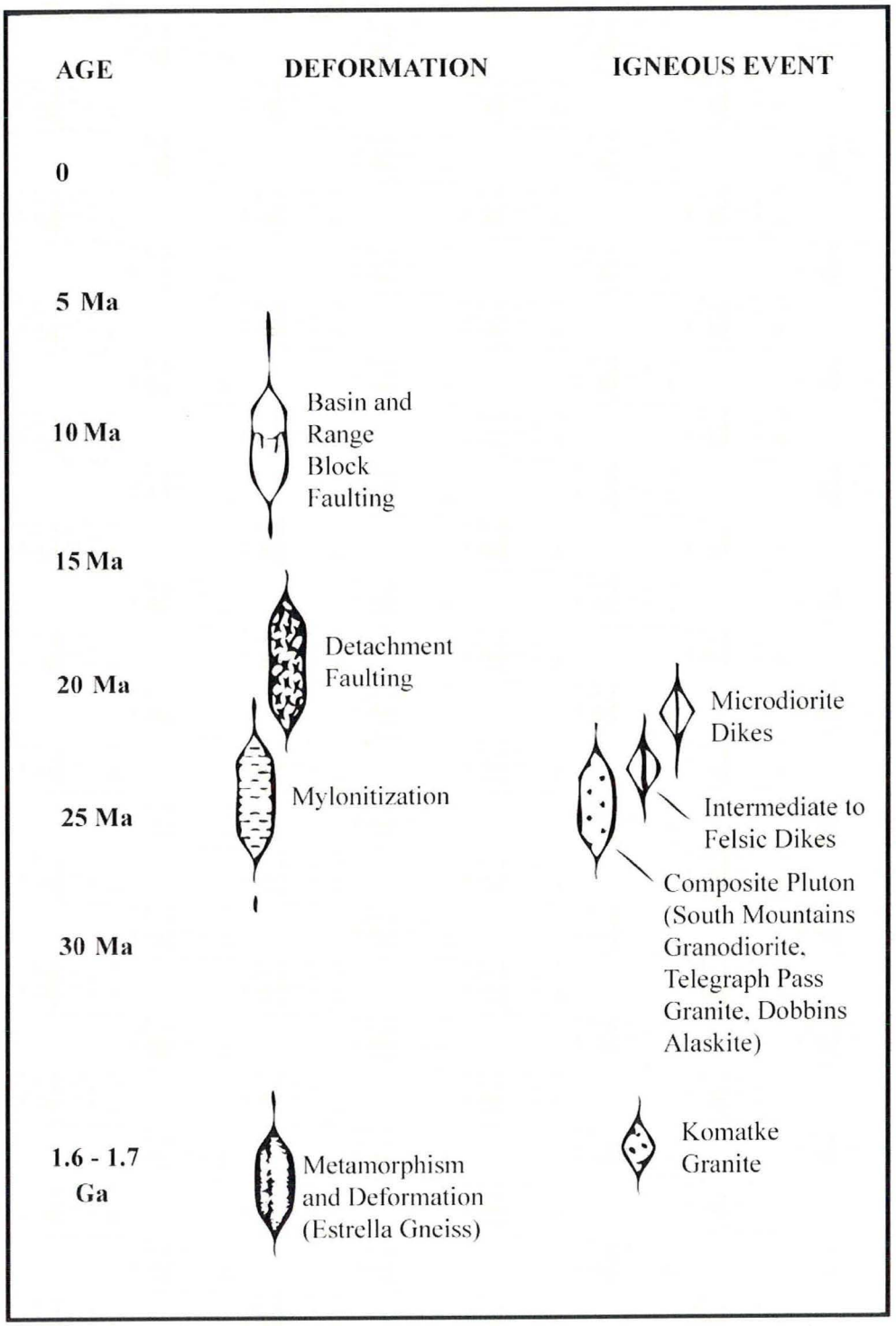

Figure 1.10 Chronology of geologic events in the South Mountains. Modified from Reynolds (1985).

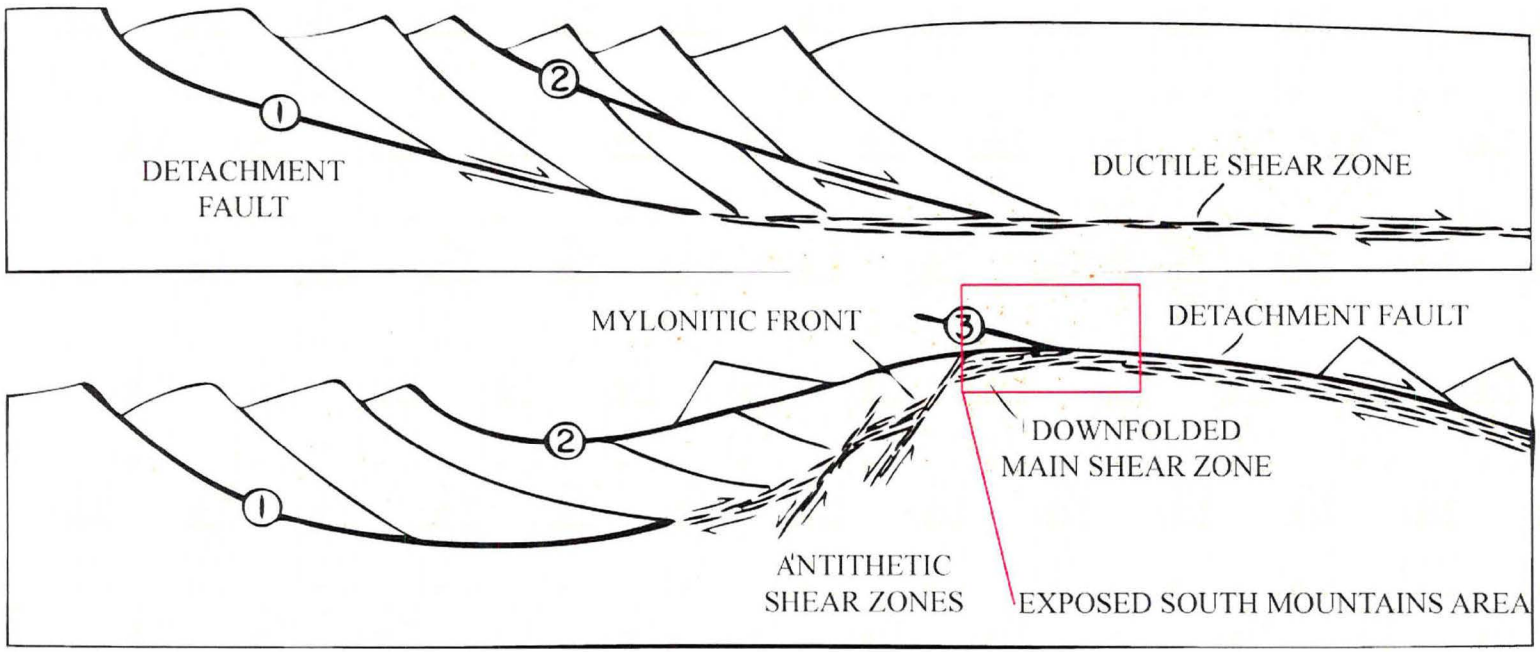

Figure 1.11 Interpreted evolution of low-angle normal shear zones, showing progressive arching of basement culmination leading to formation of back-dipping zone and antithetic shear zones within back-dipping zone. Successive splays of detachment fault, numbered 1 to 3 in order of their formation, form in response to arching, youngest fault (3) being most planar. Modified from Reynolds and Lister (1990).

THESIS WORK

In Chapter 2, I present a microstructural and electron backscatter diffraction (EBSD) study of naturally deformed shear zone rocks from the footwall of the South Mountains, Arizona, core complex to interpret the deformation mechanisms associated with strain localization along the South Mountains detachment fault. Chapter 2 is written as a manuscript draft intended for submission to the Journal of Structural Geology. My thesis work is focused on the evaluation of strain localization processes that promote detachment faulting in the Miocene South Mountains Granodiorite and Telegraph Pass Granite intrusive units. Previous fieldwork indicates the footwall of the South Mountains core complex is dominated by the Miocene composite pluton that exhibits Miocene extensional mylonitic fabrics associated with the structural development of the core complex (e.g., Reynolds, 1985; Reynolds et al., 1986).

I conducted a microstructural and EBSD study of the Tertiary South Mountains Granodiorite and Telegraph Pass Granite mylonites to determine the deformation mechanisms that promote strain localization. The seven oriented samples were collected on an up-structure traverse through the ~60 m thick mylonitic shear zone towards the interpreted detachment fault surface. Deformational microstructures were identified through microstructural analysis of quartz, plagioclase feldspar, and potassium feldspar grains. I used the identified microstructures to interpret dynamic recrystallization Regimes 2 and 3 for quartz grains, and dynamic recrystallization Regime 1 for the plagioclase feldspar and potassium feldspar grains.

I used EBSD data from granodiorite mylonites in the shear zone to interpret a lattice-preferred orientation in quartz grains. Pole figures of quartz data exhibit c-axis

maxima that we interpret as evidence of lattice-preferred orientation. The locations of the maxima are indicative of rhomb <a> slip and prism <a> slip. Based on the interpreted slip systems, we infer that deformation of quartz occurred at moderate temperatures of 500-650°C.

Based on the microstructural evidence for crystal plasticity and the interpreted lattice preferred orientation, I suggest that quartz deforms by dislocation creep. In contrast, microstructural observations of the feldspar grains indicate limited crystal plasticity, suggesting that feldspar was more rheologically competent during this period of fabric development, and deformed dominantly by microfracturing. The microstructural and EBSD study results for these naturally deformed shear zone rocks can be used to help evaluate strain localization and the strength of continental crust during the development of metamorphic core complexes along low-angle detachment faults.

CHAPTER 2: STRAIN LOCALIZATION IN QUARTZOFELDSPATHIC MYLONITES: A MICROSTRUCTURAL AND ELECTRON BACKSCATTER DIFFRACTION (EBSD) STUDY OF THE SOUTH MOUNTAINS CORE COMPLEX, ARIZONA

INTRODUCTION

The evaluation of strain localization in detachment fault shear zones is essential to the study of continental core complex development and permits insight into continental crust rheology during extension. I present a microstructural and electron backscatter diffraction (EBSD) study of naturally deformed shear zone rocks from the footwall of the South Mountains, Arizona, metamorphic core complex to interpret the deformation mechanisms that lead to strain localization along the detachment fault. I hypothesize that the strength of quartz strongly influences strain localization in the naturally deformed granodiorite mylonites and granite mylonites.

A key issue to consider when undertaking a study of metamorphic core complexes is how and why these structures develop at such a rapid speed. The formation of metamorphic core complexes is not well understood. For example, the South Mountains metamorphic core complex developed in ~1.5 million years (e.g., Reynolds et al., 1986), but no sufficient explanation for the speed at which the brittle detachment fault slips has been hypothesized.

Strength envelopes of experimentally deformed quartzofeldspathic rocks suggest quartz accommodates dislocation or diffusion creep of the lower crust (e.g., Gleason and Tullis, 1995; Stockhert et al., 1999; Hirth et al., 2001; Rutter and Brodie, 2004). There is also a possible transition in deformation mechanisms from dislocation creep to diffusion creep. This transition can promote dynamic recrystallization or strain localization of the quartz grains.

A metamorphic core complex often exposes lower crustal rocks in the footwalls, and this is where shearing associated with brittle detachment faulting begins. A study of the shear zone rocks associated with the South Mountains metamorphic core complex can lead to a greater understanding of how and why strain localization occurs so quickly. Additionally, this study can give us insight into the temperature conditions, deformation mechanisms, and dynamic recrystallization regimes present during strain localization of naturally deformed shear zone rocks.

GEOLOGIC SETTING

The Basin and Range Province

The Basin and Range Province is one of the best-known continental extensional tectonic provinces in the world (e.g., Coney, 1980). The present-day Basin and Range Province may be the site of continental breakup over a diffuse boundary. Evidence supportive of this hypothesis is that the Basin and Range Province developed during several episodes of Tertiary crustal extension (e.g., Coney, 1987), one of which resulted in the development of metamorphic core complexes.

Metamorphic Core Complexes in the North American Cordillera

In the northern part of the North American Cordillera, metamorphic core complex development is superimposed on structures associated with Mesozoic compression (Figure 2.1; e.g., Coney, 1980). In contrast, the metamorphic core complexes in the southern part of the North American Cordillera, specifically the southeastern California and Arizona metamorphic core complexes, generally do not have multiply deformed, older Mesozoic rocks in the footwall (e.g., Coney, 1980). Of the southeastern California and Arizona core complexes, there is one that does not also exhibit evidence of Mesozoic

or early Tertiary plutonism or metamorphism: the South Mountains metamorphic core complex, south of Phoenix, Arizona (Figure 2.2; e.g., Reynolds et al., 1986). The South Mountains expose intrusive rocks that are Tertiary in age, so a study to understand extension and the strain localization processes that lead to metamorphic core complex development is best located in the South Mountains.

The South Mountains Metamorphic Core Complex

The South Mountains are located just south of Phoenix, Arizona, in the City of Phoenix South Mountain Park (Figure 2.2; e.g., Avedisian, 1966; Reynolds, 1985). The South Mountains are an 18 km-long, northeast-trending metamorphic core complex that is part of a series of metamorphic core complexes in southwestern Arizona (e.g., Rehrig and Reynolds, 1980; Reynolds and Rehrig, 1980; Reynolds, 1985). The South Mountains are located in the southern portion of the North American Cordillera, and more specifically in the southwestern part of the Basin and Range Province (Figure 2.1; e.g., Wilson and Moore, 1959; Hayes, 1969; Rehrig and Reynolds, 1980).

The footwall of the South Mountains metamorphic core complex is dominated by a Miocene composite pluton that exhibits extensional mylonitic fabrics associated with the structural development of the core complex (e.g., Reynolds and Rehrig, 1980; Reynolds, 1985; Reynolds et al., 1986). The composite pluton is composed of South Mountains Granodiorite, Telegraph Pass Granite, and Dobbins Alaskite, but the South Mountains Granodiorite is the most voluminous of the intrusive units (Figure 2.2; e.g., Reynolds and Rehrig, 1980; Reynolds, 1985; Reynolds et al., 1986). The composite pluton intruded the Precambrian Estrella Gneiss and Komatke Granite basement rocks

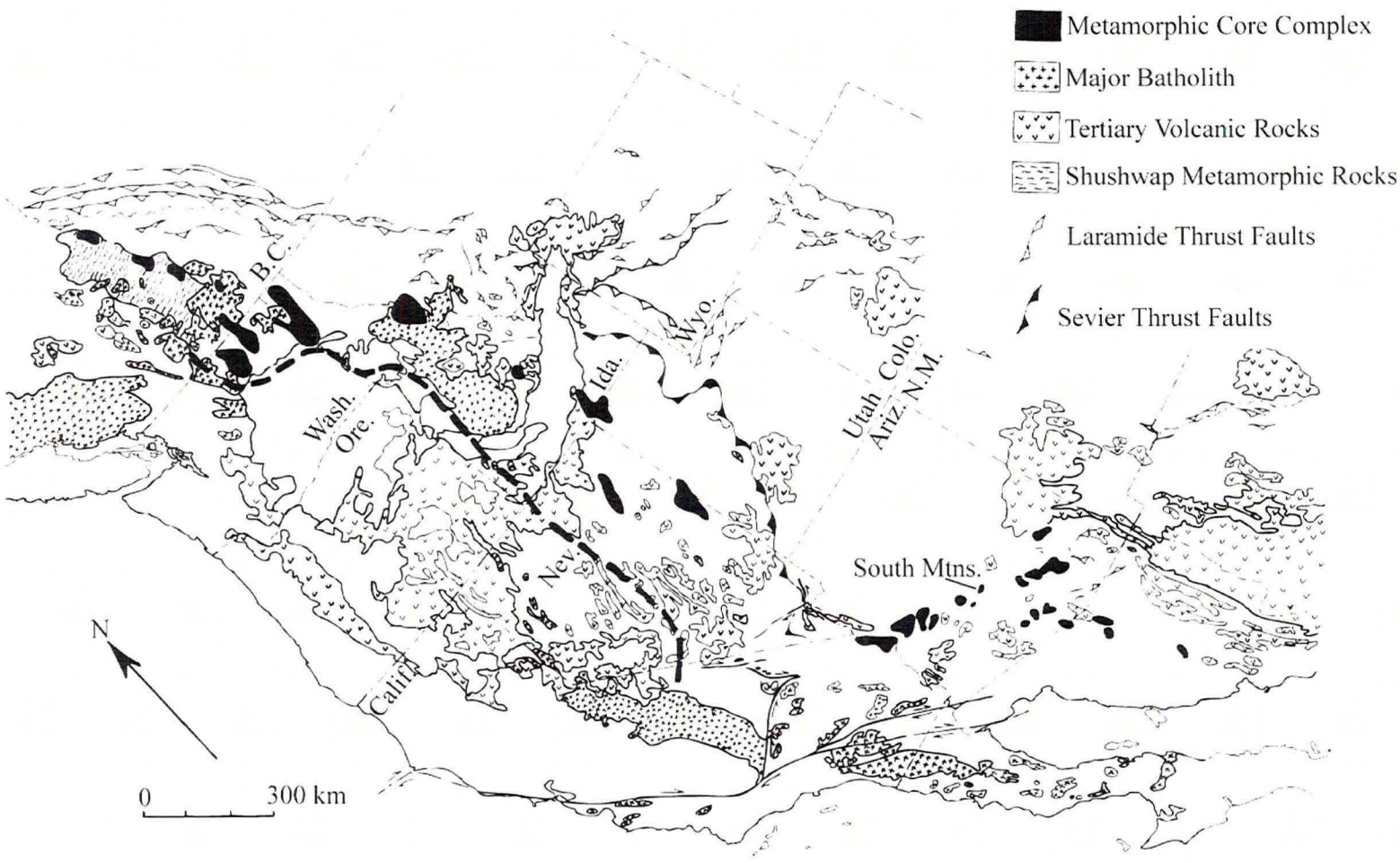

Figure 2.1 Map showing the geographic extent of the North American Cordillera, as well as the areas affected by the Laramide and Sevier Orogenies. Modified from Coney (1980).

(Figure 2.2; Reynolds, 1985; Reynolds et al., 1986). The three episodes of middle Tertiary intrusion that comprise the composite pluton were accompanied by east-northeast directed extension of continental crust along the low-angle South Mountains detachment fault (Figure 2.2; e.g., Reynolds, 1985).

The South Mountains detachment fault shear zone is developed within the South Mountains Granodiorite and Telegraph Pass Granite intrusive units (e.g., Reynolds, 1985; Reynolds et al., 1986). Structurally below the South Mountains detachment fault are a mylonitic shear zone and associated chloritic breccia and microbreccia fault rocks (Figure 2.2; Reynolds, 1985; Reynolds et al., 1986). Additionally, two separate sets of extension-related, middle Tertiary north-northwest trending dike swarms can be identified (Figure 2.2; Reynolds, 1985; Reynolds et al., 1986).

Previous studies of cross-cutting relationships and Rb-Sr, U-Th-Pb, and K-Ar geochronologic dating methods show that the composite pluton intrusion is Tertiary in age (e.g., Davis et al., 1986; Reynolds et al., 1986). Mapped cross-cutting relationships show that intrusion of the composite pluton and the formation of Miocene ductile mylonitic fabrics during detachment faulting occurred at the same time (e.g., Reynolds, 1985). Therefore, the mylonites and fault breccias can be dated as Tertiary because geochronologic dating methods determined the composite pluton is Tertiary in age (Reynolds et al., 1986).

Additionally, the detachment fault linked to formation of the metamorphic core complex and the development of mylonitic fabrics in the footwall were further related through the use of microstructures (i.e. S-C fabrics) to document a top-to-the-northeast

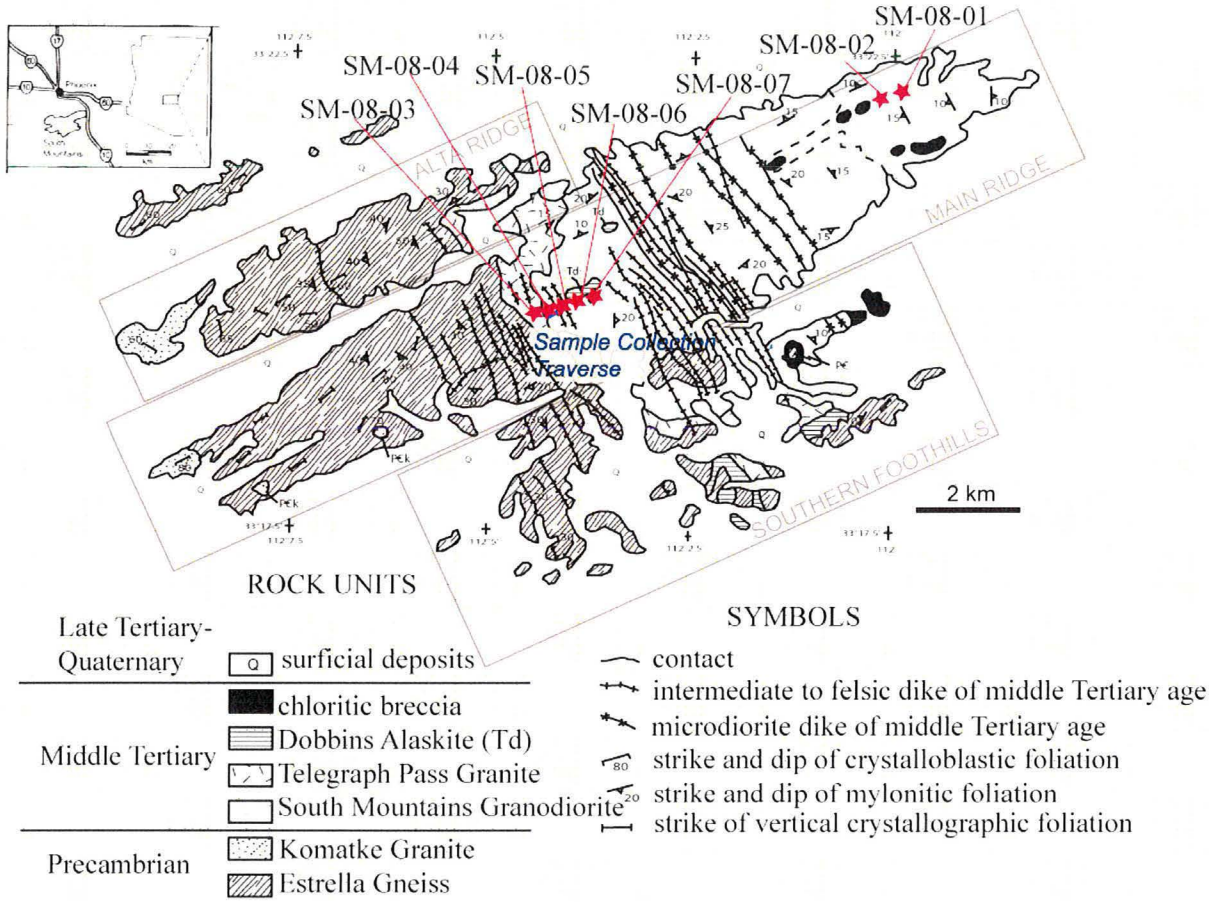

Figure 2.2 Geologic map of South Mountains. Stars indicate sample locations. Modified from Reynolds (1985).

sense of shear consistent with kinematic indicators observed in the field (Davis et al., 1986). Mylonitic fabrics in the footwall and fault breccias in the structurally shallowest portions of the footwall were also linked to formation of the core complex through microstructural studies (Davis et al., 1986).

From prior studies of geochronologic dating and mapped cross-cutting relationships, the following Tertiary chronologic history of the South Mountains was determined (Figure 2.3). In the early Miocene, 22-25 Ma, the composite pluton that primarily makes up the South Mountains metamorphic core complex was emplaced,

disrupting the Precambrian crystalline basement (Reynolds et al., 1986). Geochronologic dating and mapped cross-cutting relationships indicates that after intrusion was completed ~20 Ma, the South Mountains detachment fault was active from ~20 Ma until ~17 Ma (Reynolds et al., 1986). Associated mylonitic fabrics formed ~19-20 Ma (Reynolds et al., 1986).

MATERIALS AND METHODS

Sample Collection

We collected seven samples from the exposed footwall rocks for microstructural and electron backscatter diffraction evaluation of strain localization processes. Samples SM-08-03 through SM-08-07 are South Mountains Granodiorite and Telegraph Pass Granite footwall rocks that were collected on an up-structure traverse through the ~60 meter thick mylonitic shear zone towards the interpreted detachment fault surface (Figure 2.2). Samples SM-08-01 and SM-08-02 are also South Mountains Granodiorite footwall rocks, but were collected in the northeastern part of the South Mountains (Figure 2.2; Reynolds, 1985). Of the seven samples, SM-08-01 and SM-08-02 were structurally closest to the interpreted detachment fault surface (Figure 2.4). All samples were removed with respect to the in situ orientation of the rocks.

Thin Section Preparation

The oriented samples SM-08-01 through SM-08-07 were cut parallel to lineation and perpendicular to foliation with a water-cooled rock saw into ~1 in thick slices. Study areas on each hand sample were selected and the 1 in thick slices were further cut into areas close to the size of a standard thin section. Following this, standard thin sections (30 μm thick) of each of the seven samples were prepared.

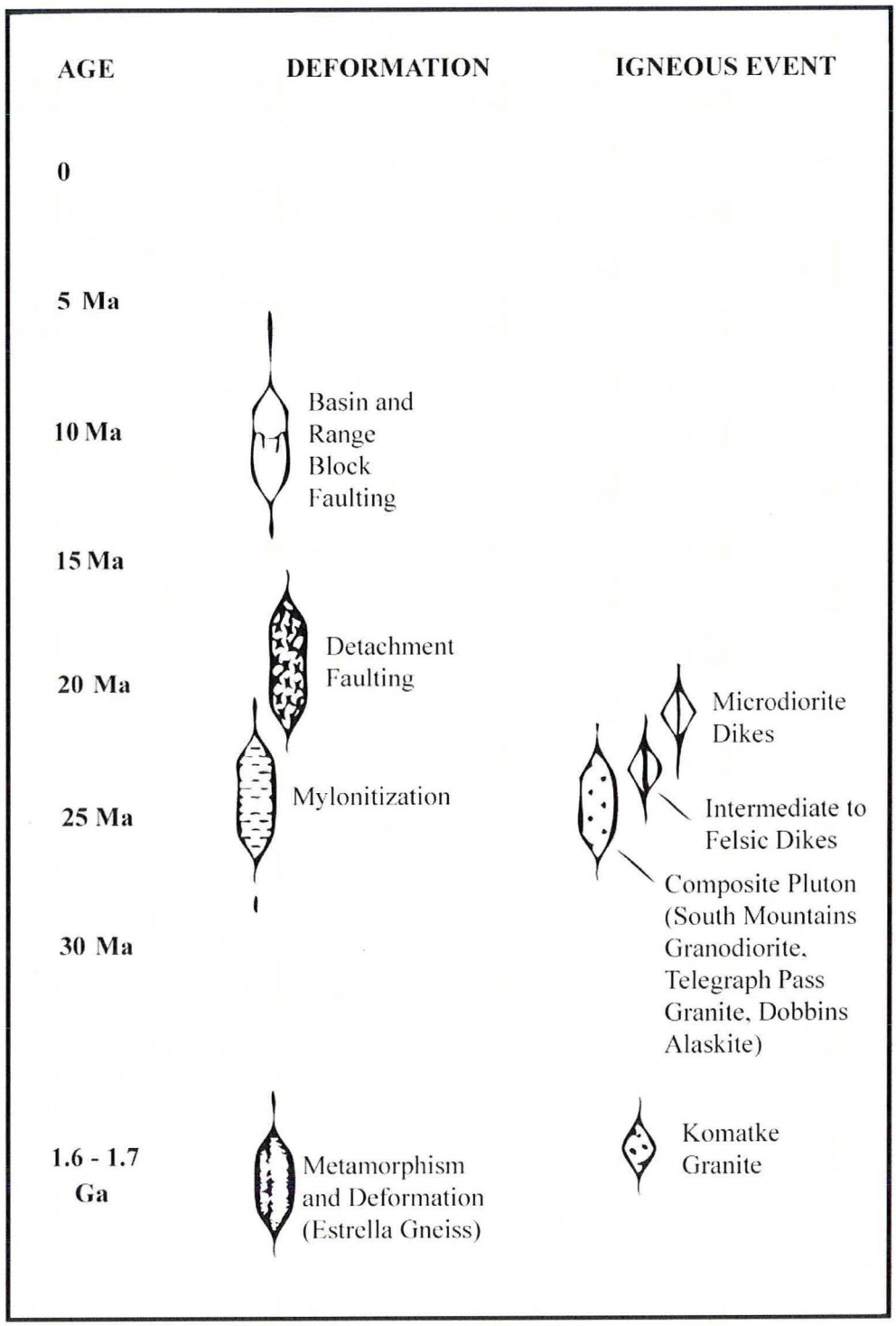

Figure 2.3 Chronology of geologic events in the South Mountains. Modified from Reynolds (1985).

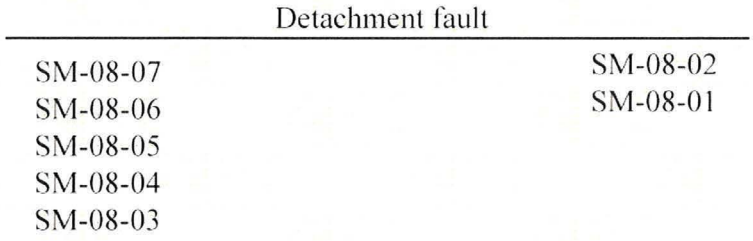

Figure 2.4 Relative structural depth of samples SM-08-01 through SM-08-07 with respect to the interpreted detachment fault surface.

Microstructural Analysis

I conducted a microstructural analysis of all samples prior to the electron backscatter diffraction study. This preliminary analysis was undertaken to identify the primary mineralogy, microstructures of the primary mineralogy, and any secondary alteration and associated alteration microstructures (Appendix C). There are three main purposes of the microstructural analysis. The first goal is to identify the microstructures present, determine the proportion of brittle to ductile deformation, and to make a preliminary interpretation as to under what conditions the samples deformed.

The second purpose of the microstructural analysis is to identify samples and potential study sites to look at in the electron backscatter diffraction study. The four samples chosen for EBSD analysis are located at different structural depths within the mylonitic shear zone. The third purpose of the microstructural analysis is to interpret the deformation mechanisms operative during crystal plastic deformation in the shear zone.

EBSD Preparation

Probe-polished thin sections require a secondary polishing procedure before EBSD analysis to remove any remaining surface damage or imperfections on the slides (Appendix A). The secondary polishing procedure consists of three separate rounds of

polishing with progressively finer-grained polishing solutions. In the first round, the slide was polished for 60 minutes with a 6-micron diamond suspension fluid. In the second round, the slide was polished for 60 minutes with a 1-micron diamond suspension fluid, and then in the third round the slide was polished for 60 minutes with a colloidal silica solution fluid. Several measures were undertaken to prevent contamination between rounds of polishing. Each of the three rounds was completed with different polishing trays, and between each round the slides were rinsed and then washed in an ultrasonic bath for 2-3 minutes to remove any remaining polishing solution.

EBSD Analysis

Electron backscatter diffraction is used to measure lattice preferred orientation in minerals. A lattice preferred orientation is indicated where individual grains align their crystallographic axes. With an oriented thin section, EBSD enables us to detect grain boundaries and determine the crystallographic orientations of different phases on the nanometer scale. This is all displayed on a beam map. The grain orientation and possible lattice preferred orientations are determined from a pole figure of the c-axis. In addition, EBSD allows the interpretation of deformation mechanisms active during crystal plastic deformation in the shear zone.

EBSD data were collected at both the University of California Santa Barbara and California State University Northridge. Therefore, two separate EBSD preparation procedures were followed. At UCSB, the thin sections were carbon-coated to prevent any charging from occurring while the slide was under the scanning electron microscope (SEM). At CSUN, the thin sections were palladium-gold (Pd-Au) coated. After being

coated, the thin sections were attached to the SEM mount with copper tape to further prevent charging.

Once the slide was in the SEM, the desired EBSD analysis site was located. To begin EBSD data collection, as a general rule the mounted slide is tilted 70°. At UCSB this rotation was done before the site for analysis was found. At CSUN the slide was tilted after the site was located. EBSD data collection and subsequent analyses were completed with the CHANNEL5 program at both UCSB and CSUN (Appendices B, D).

RESULTS

Microstructural Observations

Quartz Microstructures

The South Mountains Granodiorite and Telegraph Pass Granite samples (Appendix C; Table 1) show several different quartz microstructures (Table 2). Predominantly arranged as parallel, elongate ribbons (Figure 2.11c), the quartz grains show evidence of subgrain development and bulging of grain boundaries (Figures 2.5b, 2.8b). Quartz grains within the elongate ribbons decrease in grain size when pinched between larger feldspar porphyroclasts (Figures 2.5c, 2.8c). With increasing structural proximity to the interpreted detachment fault surface, quartz grains exhibit sinuous grain boundaries (Figure 2.10d). Quartz grain boundary migration is indicated where the sinuous grain boundaries close off to form new grain boundaries (Figure 2.9c).

Feldspar Microstructures

The plagioclase and potassium feldspar grains are generally larger in size than the quartz grains (Table 3; Figure 2.7c). With increasing structural proximity to the interpreted detachment fault surface, feldspar grains decrease in size and are present as

rounded neoblasts (Figure 2.11c). Feldspar grains exhibit microfracturing (Figure 2.9d), slight zoning, and some bulging of grain boundaries (Figures 2.9c, 2.10e).

Sample	Rock Name	Modal % Quartz	Modal % Feldspar	Modal % Biotite	Modal % Oxides
SM-08-01	South Mountains Granodiorite	40%	45%	10%	5%
SM-08-02	South Mountains Granodiorite	40%	50%	7%	3%
SM-08-03	South Mountains Granodiorite	50%	45%	5%	Trace
SM-08-04	South Mountains Granodiorite	50%	42%	8%	Trace
SM-08-05	South Mountains Granodiorite	45%	50%	5%	Trace
SM-08-06	Telegraph Pass Granite	50%	40%	5%	5%
SM-08-07	South Mountains Granodiorite	50%	35%	7%	8%

Table 1 Modal proportions of samples SM-08-01 through SM-08-07.

Sample	Quartz Microstructures	Matrix %
SM-08-01	Elongate ribbons, subgrain development, bulging of grain boundaries	30%
SM-08-02	Elongate ribbons, subgrain development, sinuous grain boundaries	25%
SM-08-03	Subgrain development, bulging of grain boundaries	<5%
SM-08-04	Elongate ribbons, subgrain development, sinuous grain boundaries	60%
SM-08-05	Elongate ribbons, subgrain development, sinuous grain boundaries, grain boundary recrystallization	40%
SM-08-06	Elongate ribbons, subgrain development, sinuous grain boundaries, grain boundary recrystallization with overprinted bulging of grain boundaries	70%
SM-08-07	Elongate ribbons, subgrain development, sinuous grain boundaries	70%

Table 2 Quartz microstructures displayed in samples SM-08-01 through SM-08-07.

Sample	Feldspar Microstructures	Porphyroclast %	P-clast Size
SM-08-01	Microfracturing, zoning, bulging of grain boundaries	70%	2-20 μm
SM-08-02	Microfracturing, zoning, bulging of grain boundaries	75%	2-30 μm
SM-08-03	Microfracturing, zoning	>95%	2-50 μm
SM-08-04	Microfracturing, zoning, bulging of grain boundaries	40%	1-20 μm
SM-08-05	Microfracturing	60%	5-50 μm
SM-08-06	Bulging of grain boundaries, grain boundary migration	30%	<1-5 μm
SM-08-07	Bulging of grain boundaries	30%	<1-5 μm

Table 3 Feldspar microstructures displayed in samples SM-08-01 through SM-08-07.

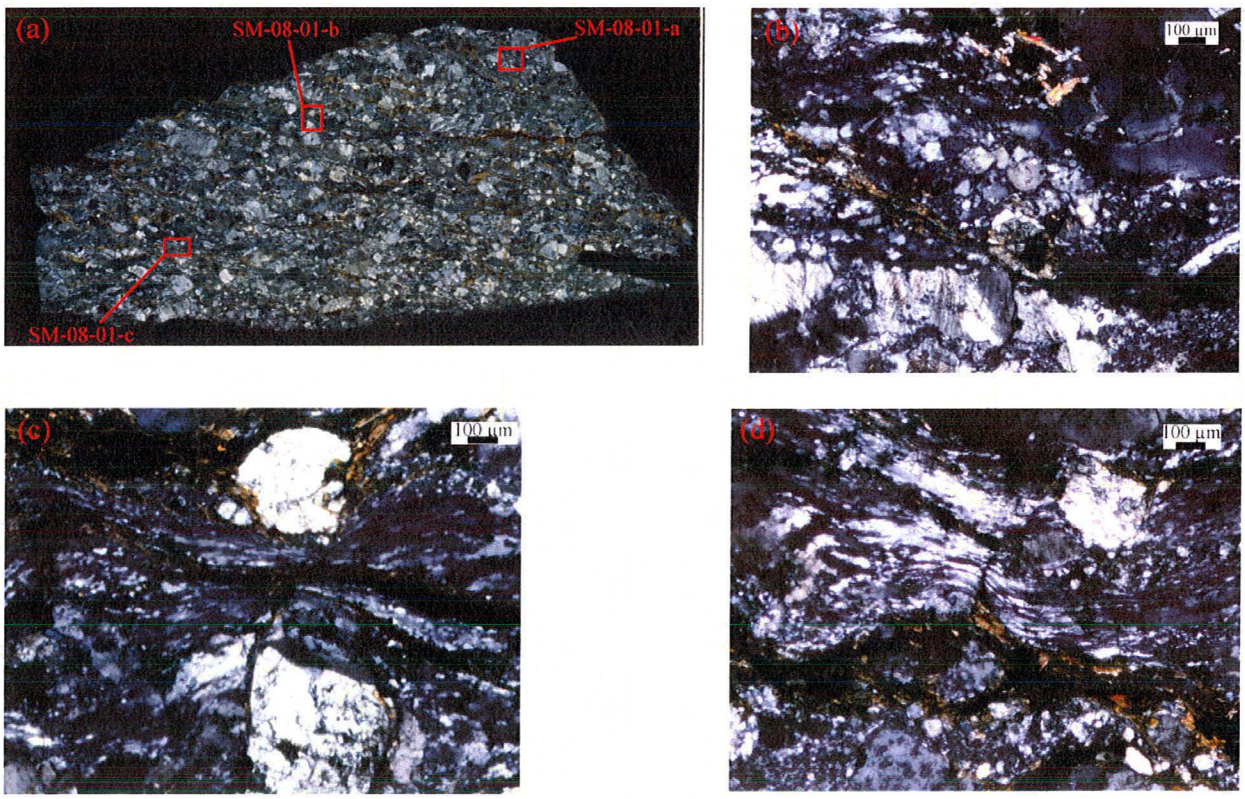

Figure 2.5 (a) Whole thin section scan of SM-08-01 in cross-polar light. Squares denote locations of photomicrographs. (b) Photomicrograph of SM-08-01-a. Quartz subgrain development along the edges of elongate quartz ribbons. (c) Photomicrograph of SM-08-01-b. Sinuous, elongate quartz ribbons pinch out between fractured feldspar porphyroclasts. (d) Photomicrograph of SM-08-01-c. Recrystallization of quartz grain boundaries on the edges of quartz subgrains.

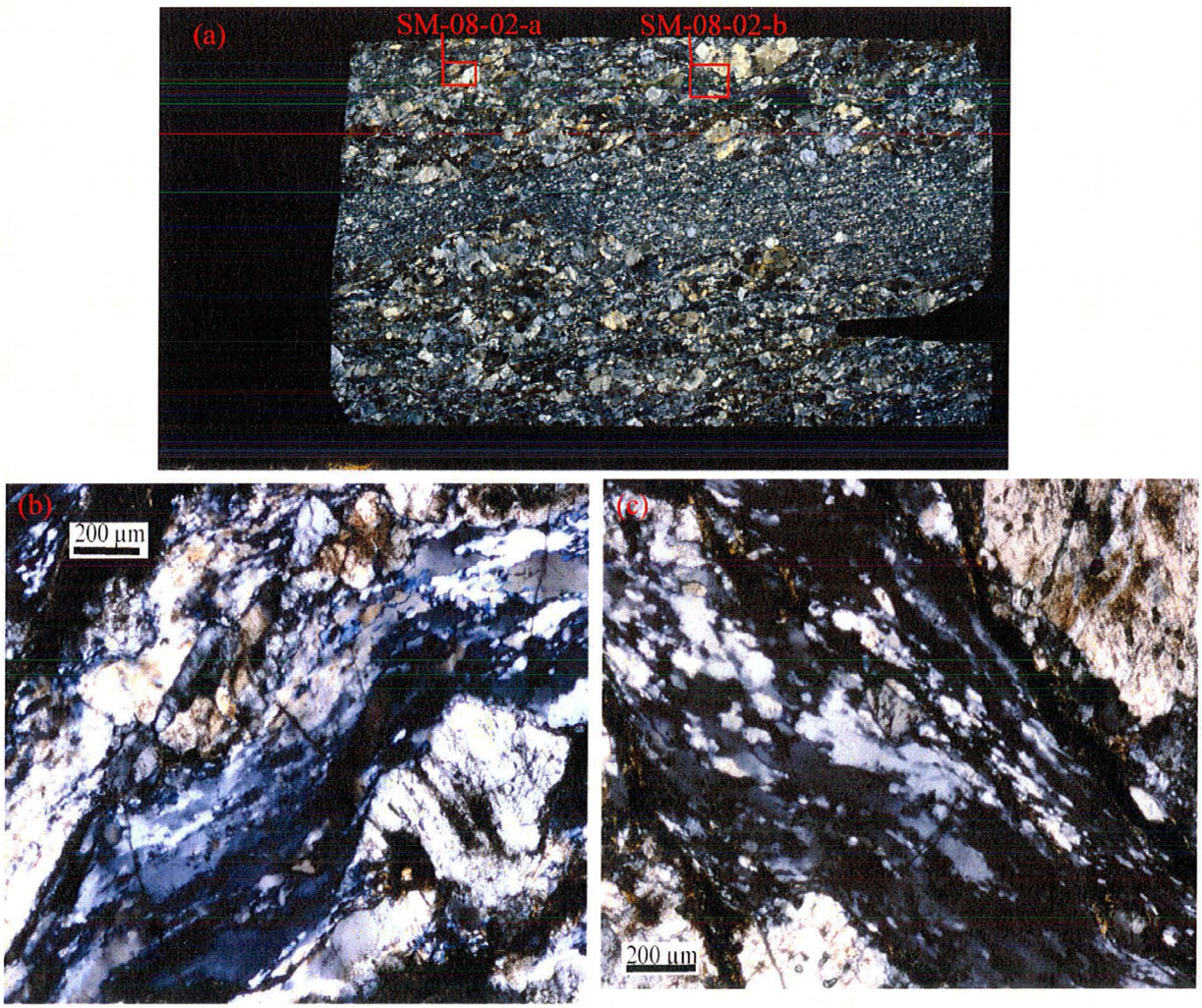

Figure 2.6 (a) Whole thin section scan of SM-08-02 in cross-polar light. Squares denote locations of photomicrographs. (b) Photomicrograph of SM-08-02-a. Quartz subgrain development along sinuous grain boundaries. (c) Photomicrograph of SM-08-02-b. Elongate quartz ribbons between microfractured and zoned feldspar grains.

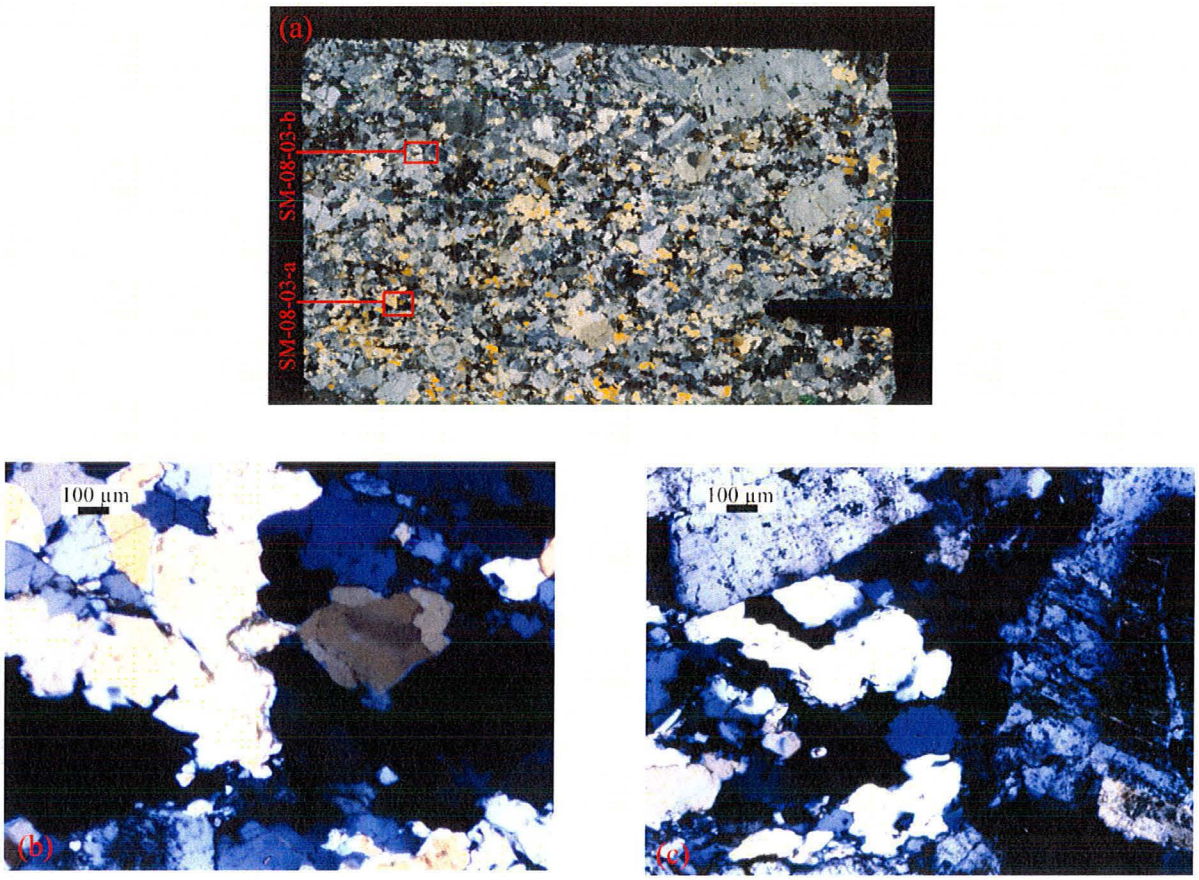

Figure 2.7 (a) Whole thin section scan of SM-08-03 in cross-polar light. Boxes denote photomicrograph locations. (b) Photomicrograph of SM-08-03-a. Bulging and recrystallization of quartz grain boundaries, as well as quartz subgrain development within the grains. (c) Photomicrograph of SM-08-03-b. Fractured and zoned feldspars are larger than the quartz grains.

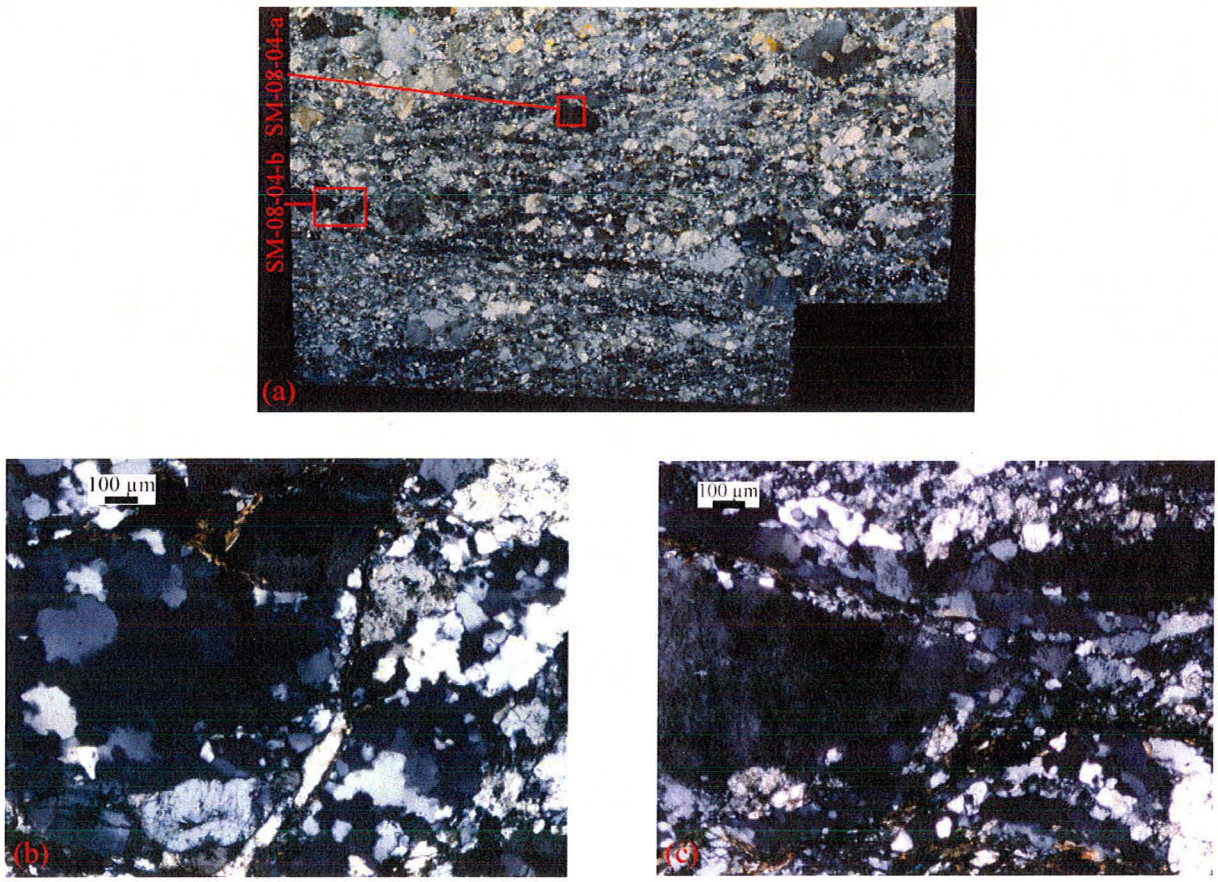

Figure 2.8 (a) Whole thin section scan of SM-08-04 in cross-polar light. Boxes denote photomicrograph locations. (b) Photomicrograph of SM-08-04-a. Elongate quartz ribbons have sinuous grain boundaries and subgrain development. (c) Photomicrograph of SM-08-04-b. Quartz ribbons pinch out between fractured feldspar porphyroclasts.

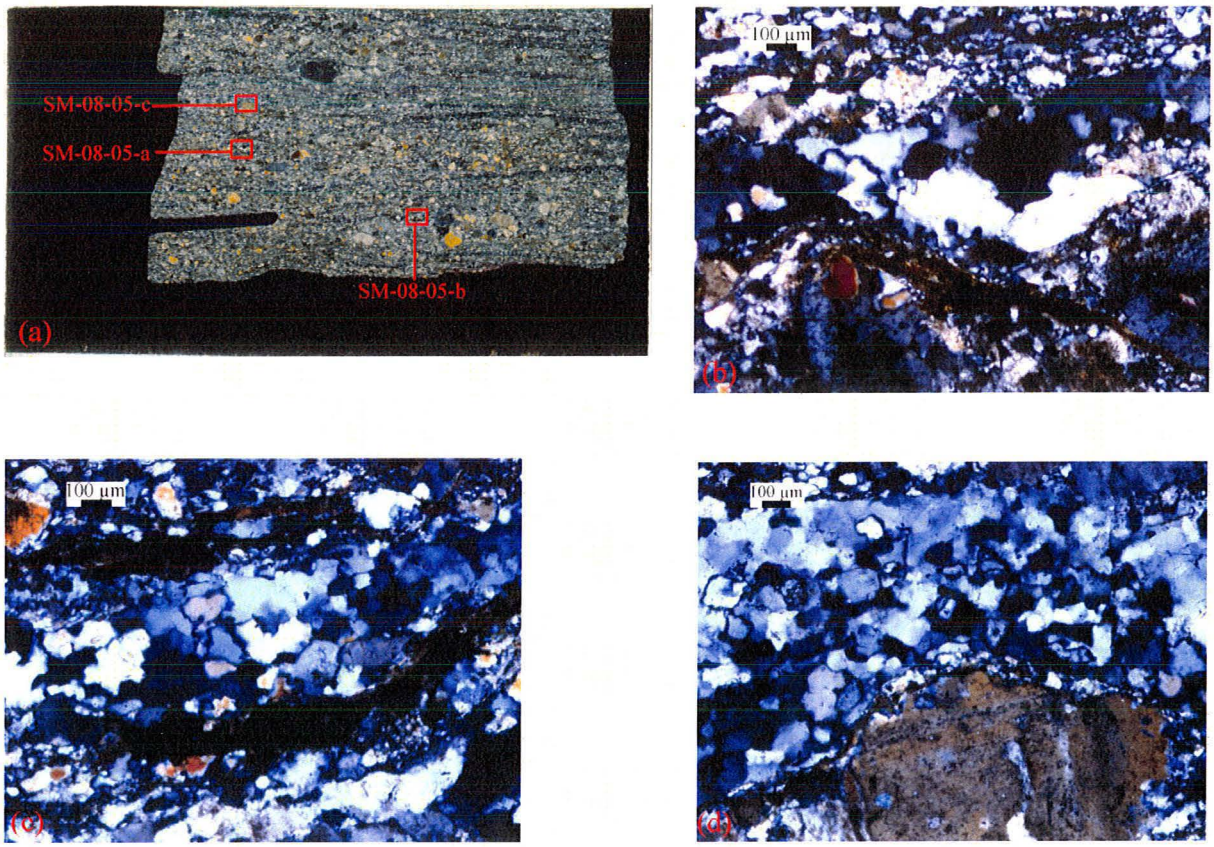

Figure 2.9 (a) Whole thin section scan of SM-08-05 in cross-polar light. Boxes indicate photomicrograph locations. (b) Photomicrograph of SM-08-05-a. Quartz subgrain development along sinuous quartz grain boundaries. (c) Photomicrograph of SM-08-05-b. Elongate quartz ribbons with recrystallization along sinuous grain boundaries. (d) Photomicrograph of SM-08-05-c. Quartz subgrain development within elongate ribbons alongside larger, fractured feldspar porphyroclasts.

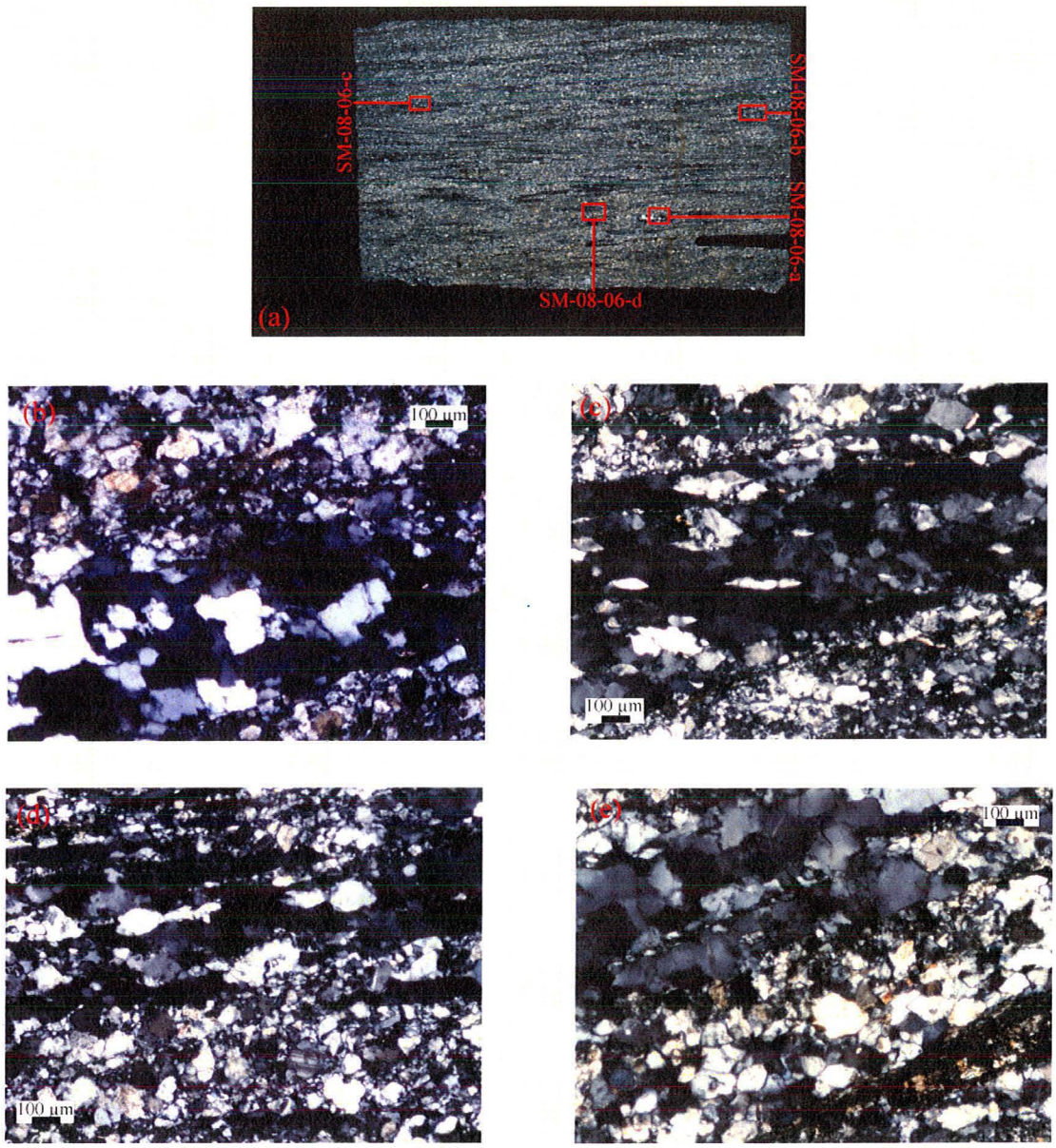

Figure 2.10 (a) Whole thin section scan of SM-08-06 in cross-polar light. Boxes indicate photomicrograph locations. (b) Photomicrograph of SM-08-06-a. Evidence of recrystallization of quartz grain boundaries and quartz subgrain development. (c) Photomicrograph of SM-08-06-b. Elongate quartz ribbon with bulging of grain boundaries. (d) Photomicrograph of SM-08-06-c. Sinuous quartz grain boundaries along elongate quartz ribbon. (e) Photomicrograph of SM-08-06-d. Sinuous quartz grain boundaries and bulging of feldspar grain boundaries.

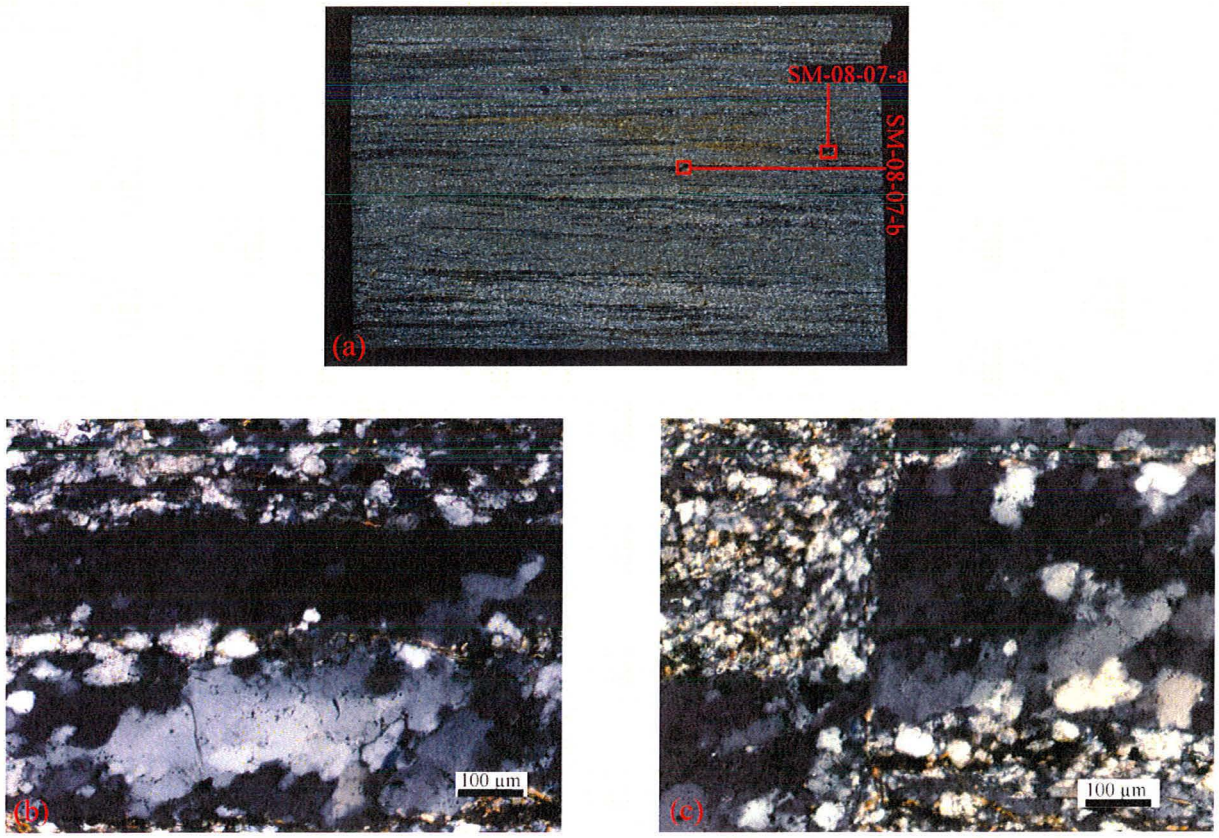

Figure 2.11 (a) Whole thin section scan of SM-08-07 in cross-polar light. Boxes indicate photomicrograph locations. (b) Photomicrograph of SM-08-07-a. Elongate quartz ribbon with sinuous quartz grain boundaries and subgrain development. Feldspar grain boundaries show evidence of bulging. (c) Photomicrograph of SM-08-07-b. Offset elongate quartz ribbons. Small feldspar grains with bulging of grain boundaries.

EBSD Data

On the EBSD band contrast and Euler angle beam maps produced for the samples, a change in color on the beam map indicates a different Euler angle orientation. Gradual color changes indicate subgrains. Black lines denote grain boundaries, and thinner gray lines mark subgrains. The corresponding scatter plot and contour pole figures have one point per quartz grain represented in order to prevent over-sampling.

SM-08-01-b

The EBSD beam map for SM-08-01-b (Appendix D; Figure 2.12b) displays the smaller quartz grains arranged in elongate ribbons that pinch out between larger plagioclase and potassium feldspar porphyroclasts. The quartz grains exhibit bulging of grain boundaries. Additionally, while the quartz grains are smaller in size than the feldspar grains as a whole, the quartz grains decrease in size and increase in the degree of grain boundary migration when closer to a pinch-out between two feldspar porphyroclasts. The scatter plot pole figure indicates the quartz c-axis orientations are clustered to the upper right and lower left of the crosshairs (Figure 2.12c). The contour pole figure (Figure 2.12d) shows the c-axis maxima are centralized in the lower left quadrant next to the crosshairs. These maxima are consistent with a lattice preferred orientation along the rhomb <a> and prism <a> slip systems.

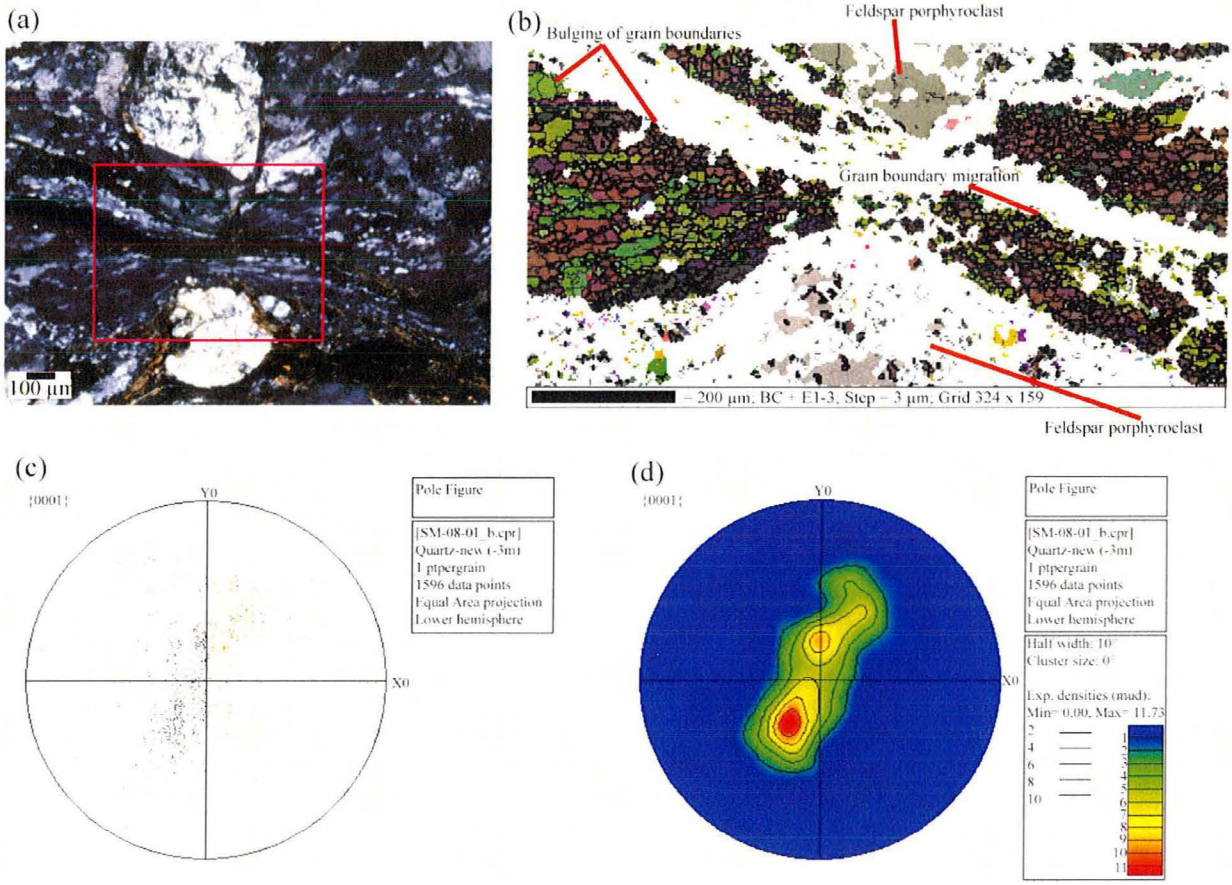

Figure 2.12 EBSD data for SM-08-01-b. (a) Photomicrograph of SM-08-01-b. Red box denotes where the EBSD beam map is located. (b) EBSD beam map of SM-08-01-b. Band contrast and Euler angle beam map of quartz, orthoclase, and bytownite. White space is non-indexed minerals. Black lines are grain boundaries. Gray lines are subgrains (> 5°). (c) Equal area projection scatter plot pole figure of quartz grain c-axes, with 1 point per grain. (d) Equal area projection contour pole figure of quartz grain c-axes, with 1 point per grain.

SM-08-03-a

SM-08-03-a (Appendix D; Figure 2.13b) shows evidence of bulging of quartz grain boundaries and quartz subgrain development. Minor amounts of grain boundary migration along the quartz grain boundaries are present. The plagioclase and orthoclase feldspar grains are brittlely deformed with no evidence of bulging of grain boundaries or subgrain rotation. There is no indication of a strong mylonitic fabric within the large, block-like quartz and feldspar grains. The two pole figures (Figures 2.13c, 2.13d) show

the quartz grains do not have a strong lattice preferred orientation. Quartz c-axis orientations are scattered randomly around the crosshairs (Figure 2.13c). In the contour pole figure the c-axis maxima are located in the northern hemisphere (Figure 2.13d). These maxima are consistent with rhomb <a> and prism <a> slip.

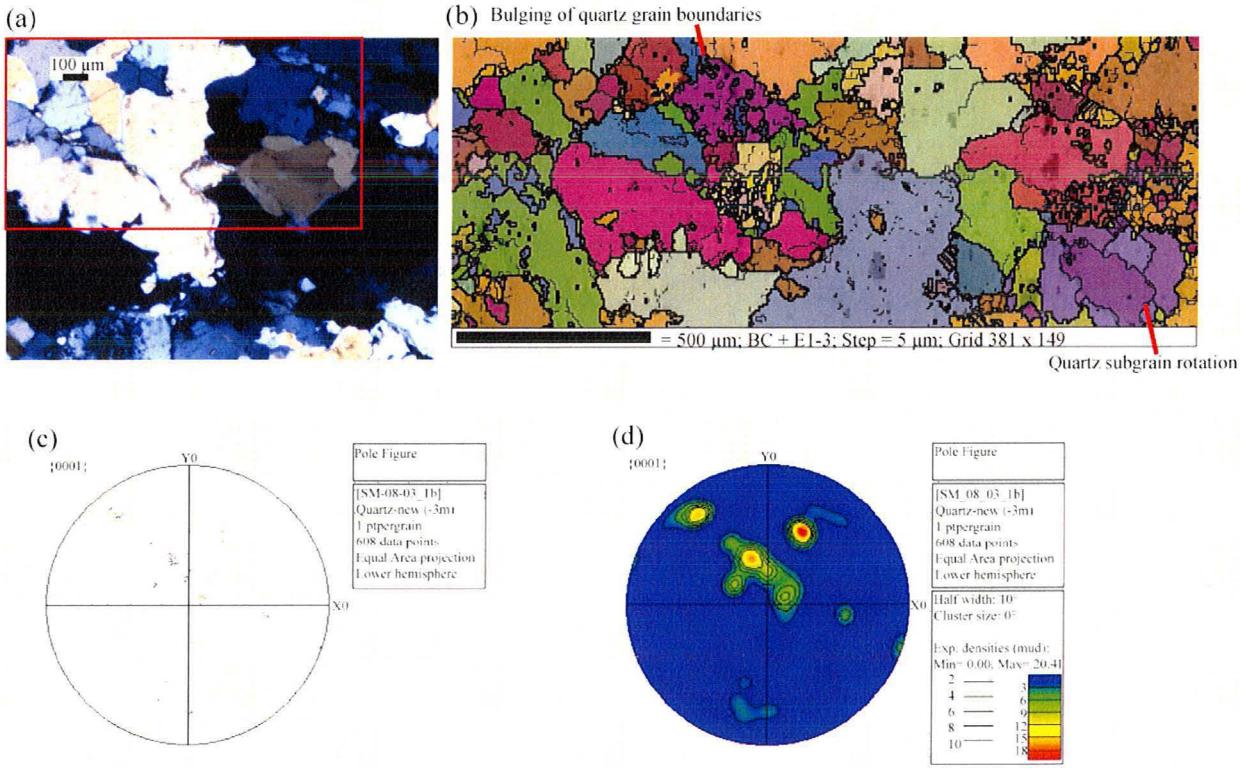

Figure 2.13 EBSD data for SM-08-03-a. (a) Photomicrograph of SM-08-03-a. Red box denotes where the EBSD beam map is located. (b) EBSD beam map of SM-08-03-a. Band contrast and Euler angle beam map of quartz, orthoclase, and bytownite. White space is non-indexed minerals. Black lines are grain boundaries. Gray lines are subgrains (> 2°). (c) Equal area projection scatter plot pole figure of quartz grain c-axes, with 1 point per grain. (d) Equal area projection contour pole figure of quartz grain c-axes, with 1 point per grain.

SM-08-05-a

SM-08-05-a (Appendix D; Figure 2.14b) shows evidence of bulging of quartz grain boundaries and quartz grain boundary migration. The elongate quartz ribbons are composed of smaller quartz grains with sinuous grain boundaries. A decrease in grain size and increase in grain boundary migration is observed when the elongate quartz

ribbons are between two feldspar porphyroclasts. The larger, more block-like plagioclase and potassium feldspar grains show some bulging of grain boundaries and subgrain rotation. The quartz c-axis orientations are scattered randomly around the crosshairs on the scatter plot pole figure (Figure 2.14c). However, the equal area projection contour pole figure shows the c-axis maxima are centralized just above the crosshairs (Figure 2.14d). These c-axis maxima are indicative of a lattice preferred orientation along the rhomb <a> and prism <a> slip systems.

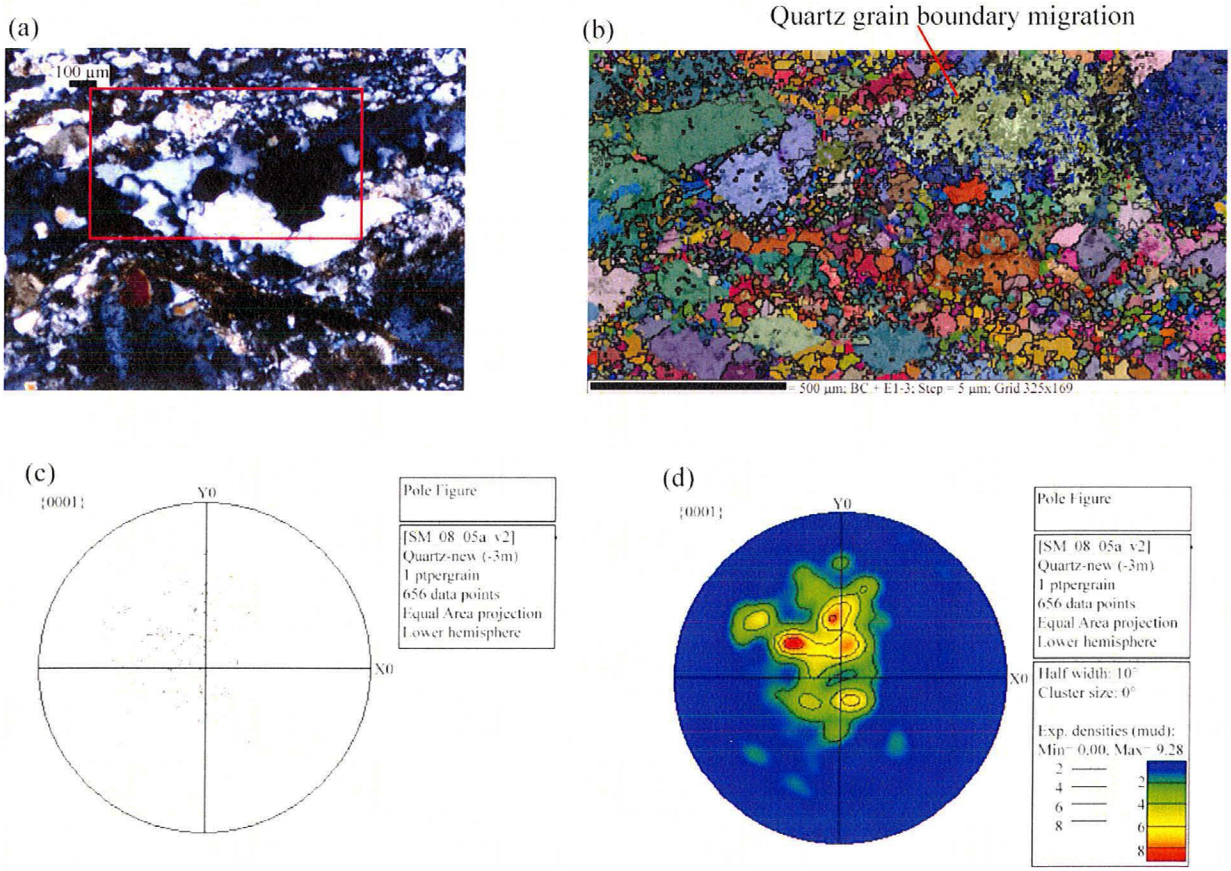

Figure 2.14 EBSD data for SM-08-05-a. (a) Photomicrograph of SM-08-05-a. Red box denotes where EBSD beam map is located. (b) EBSD beam map of SM-08-05-a. Band contrast and Euler angle beam map of quartz, orthoclase, and bytownite. White space is non-indexed minerals. Black lines are grain boundaries. Gray lines are subgrains (> 1°). (c) Equal area projection scatter plot pole figure of quartz grain c-axes, with 1 pointper grain. (d) Equal area projection contour pole figure of quartz grain c-axes, with 1 point per grain.

SM-08-06-a

SM-08-06-a (Appendix D; Figure 2.15b) displays evidence of bulging of quartz grain boundaries, quartz subgrain development, and quartz grain boundary migration. Parallel elongate quartz ribbons are observed between plagioclase and potassium feldspar porphyroclasts. The feldspar grains exhibit bulging of grain boundaries and some grain boundary migration. With all quartz grains represented on the scatter plot pole figure, the quartz c-axis orientations are clustered above the crosshairs toward the center (Figure 2.15c). These c-axis maxima are consistent with a lattice preferred orientation with rhomb <a> and prism <a> slip.

DISCUSSION

Microstructural Analysis

In the first phase of analysis I identified the microstructures associated with quartz and feldspar grains. The identified microstructures allow interpretation of the mechanisms of dynamic recrystallization, all of which are indicative of dislocation creep. A correct interpretation of the dynamic recrystallization regimes is important to understanding the processes and conditions under which deformation occurred.

Three dynamic recrystallization regimes associated with the dislocation creep deformation mechanism have been identified in experimentally deformed quartz aggregates (e.g., Hirth and Tullis, 1992). Regime 1 is termed 'bulging grain boundary migration' recrystallization (e.g., Hirth and Tullis, 1992). Regime 1 is grain-size insensitive and occurs under high stress conditions (e.g., Hirth and Tullis, 1992; Passchier and Trouw, 1998). It is identified microstructurally in the South Mountains samples as bulging of quartz grain boundaries (Figure 2.10c).

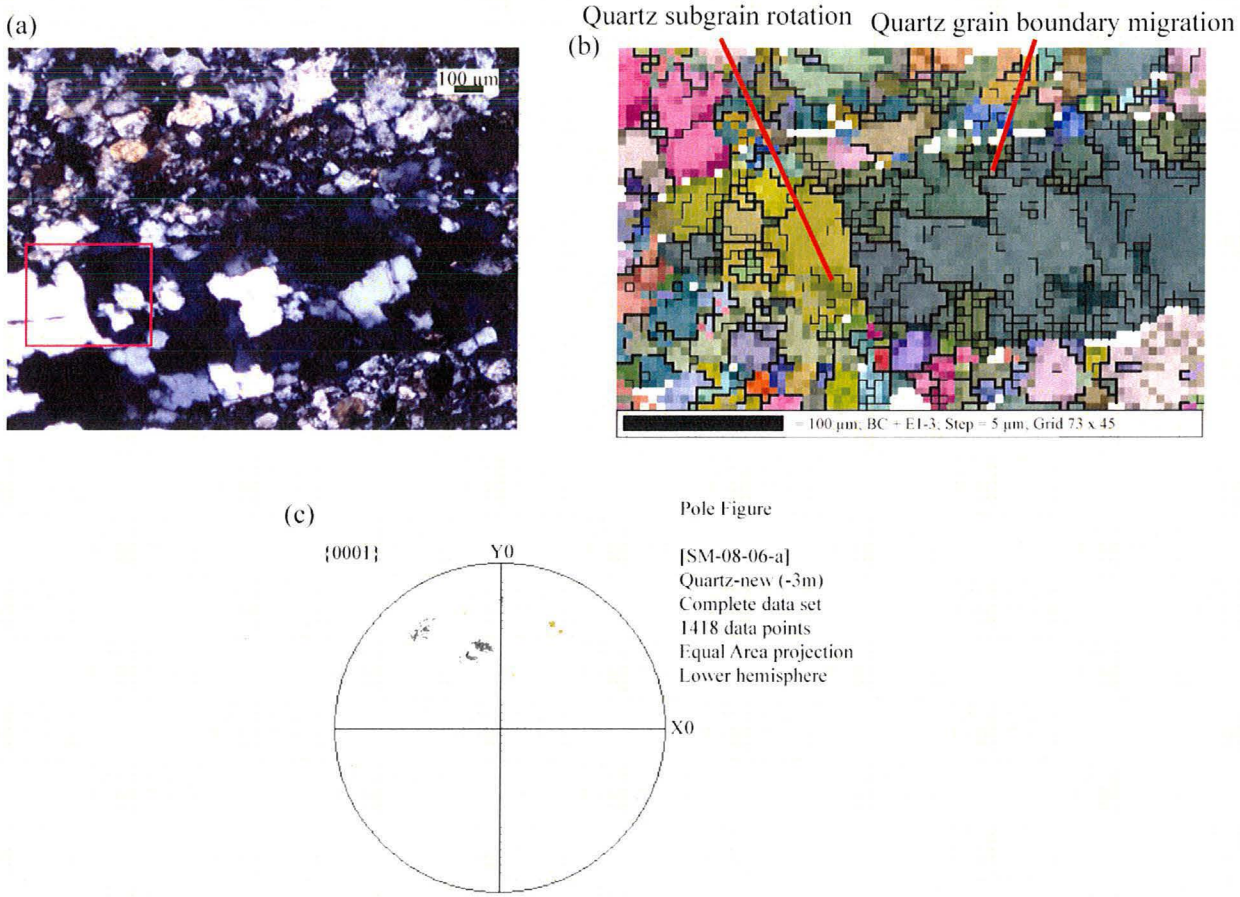

Figure 2.15 EBSD data for SM-08-06-a. (a) Photomicrograph of SM-08-06-a. Red box denotes where EBSD beam map is located. (b) EBSD beam map of SM-08-06-a. Band contrast and Euler angle beam map of quartz, orthoclase, and bytownite. White space is non-indexed minerals. Black lines are grain boundaries. Gray lines are subgrains (> 5°). (c) Equal area projection scatter plot pole figure of all quartz c-axes.

Regime 2 is described as 'subgrain rotation' recrystallization (e.g., Hirth and Tullis, 1992; Passchier and Trouw, 1998). Regime 2 is grain-size insensitive and occurs under moderate stress conditions (e.g., Hirth and Tullis, 1992; Passchier and Trouw, 1998). It is identified microstructurally in the South Mountains samples as undulose extinction in the quartz grains and as elongate quartz ribbons (e.g., Figures 2.6b, 2.8b).

Regime 3 is described as 'grain boundary migration' recrystallization (e.g., Hirth and Tullis, 1992; Passchier and Trouw, 1998). Regime 3 is grain-size insensitive and

occurs under low stress conditions (e.g., Hirth and Tullis, 1992; Passchier and Trouw, 1998). It is identified microstructurally in the South Mountains samples as sinuous quartz grain boundaries (e.g., Figures 2.9c, 2.10d).

Microstructural observation of quartz grains in the South Mountains Granodiorite and Telegraph Pass Granite protomylonites and mylonites reveals the presence of elongate ribbon grains with subgrain development (grain boundary migration) along the rims of these grains, and irregular and sinuous sutured grain boundaries (e.g., Figures 2.10d, 2.11b). These microstructures are interpreted as evidence of dynamic recrystallization Regimes 2 and 3 (e.g., Hirth and Tullis, 1992; Passchier and Trouw, 1998). As one progress structurally further up the sample collection traverse toward the interpreted detachment fault surface (Figures 2.2, 2.4; Reynolds, 1985; Reynolds et al., 1986), dynamic recrystallization Regime 3 appears to become dominant over dynamic recrystallization Regime 2. This is based on the presence of increasingly lobate structures and larger grain sizes.

Three regimes of recrystallization have been identified in feldspar grains (e.g., Fitz Gerald and Stunitz, 1993; Lafrance et al., 1996). The first regime occurs at lower temperatures and is apparent by grain boundary bulging (e.g., Lafrance et al., 1996). The moderate and high temperature regimes of subgrain rotation recrystallization and "fast" grain boundary migration (e.g., Lafrance et al., 1996) are not observed in the South Mountains samples. In contrast to the quartz grains in the South Mountains Granodiorite and Telegraph Pass Granite samples, the plagioclase feldspar and potassium feldspar crystals are not deformed under the higher temperature regimes. The feldspar grains are predominantly microfractured with limited development of bulging grain boundaries on

the rims of the feldspar grains (e.g., Figures 2.8c, 2.11c). The occurrence of bulging of feldspar grain boundaries increases with structural proximity to the interpreted detachment fault surface. These microstructures are interpreted as evidence of grain boundary bulging recrystallization (e.g., Lafrance et al., 1996).

EBSD Analysis

Confirmation of Microstructures

EBSD beam maps are used to confirm the microstructures observed under the petrographic microscope. My focus was on the determination of grain boundaries and on the shape of grain boundaries. Subgrain rotation of quartz grains is indicative of Regime 2 dynamic recrystallization. On the EBSD beam maps subgrain boundaries are apparent as thin gray lines (e.g., Figure 2.15b). Similar color on either side of a subgrain boundary indicates subgrain recrystallization. Subgrains are defined as low-angle boundaries. The criteria for determining a subgrain varied with each EBSD sample (Appendix B), but were always less than 5°. Subgrains are primarily located in the center of large quartz grains (e.g., Figure 2.15b), or along the edges of extremely sinuous quartz grain boundaries (e.g., Figure 2.14b).

An analysis of grain boundaries on the EBSD beam maps is used to differentiate between Regime 1 (grain boundary bulging) and Regime 3 (grain boundary migration) dynamic recrystallization. Although possible to differentiate between the two regimes in the microscope, neoblasts from Regime 1 are extremely small (<1 μm) and typically not observed. Grain boundaries are high-angle boundaries indicated on the EBSD beam maps as thick black lines. The criteria for determining a subgrain varied with each EBSD sample (Appendix B), but were always greater than 1°. Dynamic recrystallization

Regimes 1 and 3 are similar in that both are grain-size insensitive. The difference is that the bulges associated with Regime 1 dynamic recrystallization are low-angle and less distinct (e.g., Figure 2.12b). Plagioclase and potassium feldspar grains show evidence of Regime 1 dynamic recrystallization. Regime 3 dynamic recrystallization is characterized by curvaceous, sinuous, lobate structures with larger grains than associated with Regime 1. When these sinuous grain boundaries pinch off, new grains form on the rims of larger grains. This is apparent on the quartz grains in the EBSD samples. Grain boundary migration is indicated by small squares (e.g., Figures 2.14b, 2.15b).

Deformation Mechanisms

The combination of the microstructural evidence for crystal plasticity and the interpreted lattice preferred orientation indicates that the quartz grains deformed by dislocation creep (e.g., Hirth and Tullis, 1992; Passchier and Trouw, 1998). Based on the prevalence of dynamic recrystallization Regimes 2 and 3 in the quartz grains, the South Mountains Granodiorite and Telegraph Pass Granite samples did not undergo either brittle or semi-brittle deformation. There are three primary reasons the results are more compatible with dislocation creep than diffusion creep.

First, diffusion creep does not produce a lattice preferred orientation. The samples show evidence of a well-developed lattice preferred orientation (Figures 2.12, 2.14), and a moderately developed lattice preferred orientation (Figures 2.13, 2.15). Second, diffusion creep is grain-size sensitive (e.g., Hirth and Tullis, 1992; Gleason and Tullis, 1995; Rutter and Brodie, 2004). The neoblasts within the samples should all be of a small (< 5 μm), homogeneous grain-size (e.g., Hirth and Tullis, 1992), in contrast to

what is observed in the South Mountains. The wide variation in grain size within the samples (Appendix C) makes the results more compatible with dislocation creep.

Third, although the quartz grains show microstructural evidence for crystal plasticity, microstructural observations of the feldspar grains indicate limited crystal plasticity, suggesting that feldspar was more rheologically competent, and deformed dominantly by microfracturing. This indicates the temperature of deformation was still relatively low. Based on this and the interpreted rhomb <a> and prism <a> slip systems, it is inferred that deformation occurred at moderate temperatures of 500-650°C (Passchier and Trouw, 1998). Diffusion creep requires a higher temperature of deformation than dislocation creep (e.g., Passchier and Trouw, 1998).

Identification of Lattice Preferred Orientation

EBSD data from granodiorite and granite mylonites in the shear zone are used to interpret a lattice-preferred orientation in quartz grains (e.g., Figures 2.12d, 2.14d). Contoured pole figures of quartz data exhibit c-axis maxima that are interpreted as evidence of lattice preferred orientation (e.g., Figures 2.12d, 2.14d). The locations of the maxima are indicative of rhomb <a> slip and prism <a> slip (Passchier and Trouw, 1998).

EBSD data from South Mountains Granodiorite mylonites at both the bottom and the top of the mylonitic shear zone (Figures 2.12, 2.14) show evidence of a lattice preferred orientation in quartz grains (Figures 2.12d, 2.14d). Both the scatter plot and contoured pole figures of quartz data indicate the c-axis maxima are located just adjacent to the crosshairs (Figures 2.12c-d, 2.14c-d). The concentration of c-axis maxima is

interpreted as evidence of lattice preferred orientation with slip along the rhomb <a> and prism <a> slip systems (Passchier and Trouw, 1998).

The equal area projection scatter plot pole figure compiled from EBSD data from Telegraph Pass Granite mylonite sample SM-08-06 displays an interpreted breakdown of a lattice preferred orientation in the quartz grains (Figure 2.15c). The plotted c-axis maxima are scattered across the upper hemisphere of the pole figure (Figure 2.15c). Although the locations of these plotted points are still indicative of rhomb <a> slip and prism <a> slip (Passchier and Trouw, 1998), the c-axis maxima are less centralized than in the other samples.

Implications for Strain Localization

The microstructural and EBSD results indicate the shear zone rocks deformed primarily by dislocation creep. However, it is important to revisit the apparent breakdown of lattice preferred orientation in Telegraph Pass Granite sample SM-08-06 (Figure 2.15). Evidence shows the randomization of lattice preferred orientation with structural proximity to the interpreted detachment fault surface. Dislocation creep may have begun to incorporate grain-boundary sliding diffusion creep, thus weakening the lattice preferred orientation. This implies that during detachment fault shearing, strain is not necessarily localized with just one deformation mechanism.

Strain was localized dominantly by crystal-plastic deformation of quartz grains. Feldspar grains did incorporate some of that crystal-plastic strain with increasing proximity to the interpreted detachment fault surface. This is indicated by the progressive decrease in feldspar grain size and increase in the degree of Regime 1

dynamic recrystallization seen in the feldspar grains. Future studies should investigate this apparent transition from dislocation creep to grain-size sensitive creep.

CONCLUSION

The microstructural and electron backscatter diffraction study of the granodiorite and granite mylonites within the South Mountains mylonitic shear zone yielded several valuable conclusions. The plagioclase and potassium feldspar grains are more rheologically competent than the quartz grains, which indicate quartz controls strain localization in these shear zone rocks. The crystal plasticity and interpreted lattice preferred orientation in the quartz grains indicates the quartz grains deformed by dislocation creep at moderate temperatures of 500-650°C. In future studies, the feldspar grains of the South Mountains mylonitic shear zone should be more closely studied to document the apparent transition from dislocation creep to diffusion creep. In addition, the results of this microstructural and EBSD study on naturally deformed shear zone rocks can be used to help evaluate experimental flow laws for both mono-and polymineralic aggregates.

REFERENCES

Armstrong, R.L., 1968. Sevier orogenic belt in Nevada and Utah. Geological Society of America Bulletin 79, 429-458.

Armstrong, R.L., 1982. Cordilleran metamorphic core complexes – from Arizona to southern Canada. Annual Review of Earth and Planetary Sciences 83, 1729-1754.

Atwater, T., 1970. Implications of plate tectonics for the Cenozoic tectonic evolution of western North America. Geological Society of America Bulletin 81, 3513-3536.

Atwater, T., 1998. Plate Tectonic History of Southern California with emphasis on the Western Transverse Ranges and Santa Rosa Island. In: Weigand, P.W. (Ed.), Contributions to the geology of the Northern Channel Islands, Southern California. American Association of Petroleum Geologists, Pacific Section, MP 45, 1-8.

Avedisian, G.E., 1966. Geology of the western half of Phoenix South Mountains Park, Arizona [M.S. thesis]. Tempe, Arizona State University, 52 p.

Banks, N.G., 1977. Geologic setting and interpretation of a zone of middle Tertiary igneous-metamorphic complexes in south-central Arizona. U.S. Geological Survey Open-file Report 77-376, 29 p.

Banks, N.G., 1980. Geology of a zone of metamorphic core complexes in southeastern Arizona. In: Crittenden, M.D., Coney, P.J., Davis, G.H. (Eds.), Cordilleran Metamorphic Core Complexes. Geological Society of America Memoir 153, 177-215.

Bird, Peter, 1984. Laramide crustal thickening event in the Rocky Mountain foreland and Great Plains. Tectonics 3, 741-758.

Bykerk-Kauffman, A., 1990. Structural evolution of the northeastern Santa Catalina Mountains, Arizona: a glimpse of the pre-extension history of the Catalina complex [Ph.D. thesis]. Tucson, Arizona, University of Arizona.

Bykerk-Kauffman, A., 2008. Geologic Map of the Southeastern Santa Catalina Mountains, Pima County, Arizona. Arizona Geological Survey CM-08-A.

Bykerk-Kauffman, A., Janecke, S.U., 1987. Late Cretaceous to early Tertiary ductile deformation: Catalina-Rincon metamorphic core complex, southeastern Arizona. Geology 15, 462-465.

Coney, P.J., 1979. Tertiary evolution of Cordilleran metamorphic core complexes. In: Armentrout, J.W., Cole, M.R., Terbest, H. (Eds.), Cenozoic Paleogeography of Western United States. Society of Economic Paleontologists and Mineralogists,

Pacific Section, Pacific Coast Paleogeography Symposium 3, 15-28.

Coney, P.J., 1980. Cordilleran metamorphic core complexes: An overview. In: Crittenden, M.D., Coney, P.J., Davis, G.H. (Eds.), Cordilleran Metamorphic Core Complexes. Geological Society of America Memoir 153, 7-31.

Coney, P.J., 1987. The regional tectonic setting and possible causes of Cenozoic extension in the North American Cordillera. In: Coward, M.P., Dewey, J.F., Hancock, P.L. (Eds.), Continental Extensional Tectonics. Geological Society Special Publication 28, 177-186.

Coney, P.J., Reynolds, S.J., 1977. Cordilleran Benioff zones. Nature 270, 403-406.

Cooper, F.J., Platt, J.P., 2008. Thermobarometric constraints on the tectonic evolution of the Northern Snake Range metamorphic core complex, Eastern Nevada. Geological Society of America Abstracts with Programs 40, 76.

Crouch, J.K., Suppe, J., 1993. Late Cenozoic tectonic evolution of the Los Angeles basin and inner California borderland: A model for core complex-like crustal extension. Geological Society of America Bulletin 105, 1415-1434.

Davis, G.A., Anderson, J.L., Frost, E.G., Shackelford, T.J., 1980. Mylonitization and detachment faulting in the Whipple-Buckskin-Rawhide Mountains terrane, southeastern California and western Arizona. In: Crittenden, M.D., Coney, P.J., Davis, G.H. (Eds.), Cordilleran Metamorphic Core Complexes. Geological Society of America Memoir 153, 79-129.

Davis, G.A., Anderson, J.L., Martin, D.L., Krummenacher, D., Frost, E.G., Armstrong, R.L., 1982. Geologic and geochronologic relations in the lower plate of the Whipple detachment fault. In: Frost, E.G., Martin, D.L. (Eds.), Mesozoic-Cenozoic tectonic evolution of the Colorado River Region. San Diego, California, Cordilleran Publishing, 408-432.

Davis, G.A., Lister, G.S., 1988. Detachment faulting in continental extension: perspectives from the southwestern U.S. Cordillera, John Rodgers symposium volume. Geological Society of America Special Paper 218, 133-159.

Davis, G.A., Lister, G.S., Reynolds, S.J., 1986. Structural evolution of the Whipple and South mountains shear zones, southwestern United States. Geology 14, 7-10.

Davis, G.H., 1980. Structural characteristics of metamorphic core complexes, southern Arizona. In: Crittenden, M.D., Coney, P.J., Davis, G.H. (Eds.), Cordilleran Metamorphic Core Complexes. Geological Society of America Memoir 153, 35-77.

Davis, G.H., 1983. Shear-zone model for the origin of metamorphic core complexes. Geology 11, 342-347.

DeCelles, P.G., 2004. Late Jurassic to Eocene evolution of the Cordilleran thrust belt and foreland basin system, western U.S.A. American Journal of Science 304, 105-168.

Dewey, J.F., 1980. Episodicity, sequence, and style of convergent plate boundaries. In: Strangway, D.W. (Ed.), The Continental Crust and its Mineral Deposits. Geological Association of Canada Special Paper 20, 553-573.

Dickinson, W.R., 1981. Plate tectonic evolution of the southern Cordillera. In: Dickinson, W.R., Payne, W.D. (Eds.), Relations of Tectonics to Ore Deposits in the Southern Cordillera. Arizona Geological Society Digest 14, 113-135.

Dickinson, W.R., Snyder, W.S., 1979. Geometry of subducted slabs related to San Andreas transform. Journal of Geology 87, 609-627.

Dumitru, T.A., 1990. Subnormal Cenozoic geothermal gradients in the extinct Sierra Nevada magmatic arc: consequences of Laramide and post-Laramide shallow-angle subduction. Journal of Geophysical Research 95, 4925-4941.

Fitz Gerald, J.D., Stunitz, H., 1993. Deformation of granitoids at low metamorphic grades: I. Reactions and grain size reduction. Tectonophysics 221, 269-297.

Gehrels, G.E., Smith, C.H., 1991. U-Pb geochronologic constraints on the age of thrusting, crustal extension, and peraluminous plutonism in the Little Rincon Mountains, southern Arizona. Geology 19, 238-241.

Gleason, G.C., Tullis, J., 1995. A flow law for dislocation creep of quartz aggregates determined with the molten salt cell. Tectonophysics 247, 1-23.

Hayes, P.T., 1969. Geology and topography. In: Mineral and water resources of Arizona. Arizona Bureau of Mines Bulletin 180, 35-57.

Hirth, G., Tullis, J., 1992. Dislocation creep regimes in quartz aggregates. Journal of Structural Geology 14, 145-159.

Hirth, G., Teyssier, C., Dunlap, W.J., 2001. An evaluation of quartzite flow laws based on comparisons between experimentally and naturally deformed rocks. International Journal of Earth Sciences 90, 77-87.

Lafrance, B., John, B.E., Scoates, J.S., 1996. Syn-emplacement recrystallization and deformation microstructures in the Poe Mountain anothosite, Wyoming. Contrib Mineral Petrol 122, 431-440.

Lister, G.S., Davis, G.A., 1989. The origin of metamorphic core complexes and detachment faults formed during Tertiary continental extension in the northern Colorado River region, U.S.A. Journal of Structural Geology 11, 65-94.

Luyendyk, B.P., 1991. A model for Neogene crustal rotations, transtension, and transpression in southern California. Geological Society of America Bulletin 103, 1528-1536.

Misch, P., 1960. Regional structural reconnaissance in central-northeast Nevada and some adjacent areas: Observations and interpretations. Intermountain Association of Petroleum Geologists Guidebook for 11th Annual Field Conference, 17-42.

Niemi, N.A., Wernicke, B.P., Brady, R.J., Saleeby, J.B., Dunne, G.C., 2001. Distribution and provenance of the middle Miocene Eagle Mountain Formation, and implications for regional kinematic analysis of the Basin and Range province. Geological Society of America Bulletin 113, 419-442.

Parsons, T., 1995. The Basin and Range Province. In: Olsen, K. (Ed.), Continental Rifts: evolution, structure, and tectonics, 277-324.

Passchier, C.W., Trouw, R.A.J., 1998. Microtectonics. Springer, Berlin.

Price, R.A., Mountjoy, E.W., 1970. Geologic structure of the Canadian Rocky Mountains between Bow and Athabasca Rivers – a progress report. Geological Association of Canada Special Paper 6, 7-25.

Rehrig, W.A., Reynolds, S.J., 1980. Geologic and geochronologic reconnaissance of a northwest-trending zone of metamorphic core complexes in southern and western Arizona. In: Crittenden, M.D., Coney, P.J., Davis, G.H. (Eds.), Cordilleran Metamorphic Core Complexes. Geological Society of America Memoir 153, 131-157.

Reynolds, S.J., 1985. Geology of the South Mountains, central Arizona. Arizona Bureau of Geology and Mineral Technology Bulletin 195, 61 p., scale 1:24,000.

Reynolds, S.J., Lister, G.S., 1987. Structural aspects of fluid-rock interactions in detachment zones. Geology 15, 362-366.

Reynolds, S.J., Lister, G.S., 1990. Folding of mylonitic zones in Cordilleran metamorphic core complexes: Evidence from near the mylonitic front. Geology 18, 216-219.

Reynolds, S.J., Rehrig, W.A., 1980. Mid-Tertiary plutonism and mylonitization, South Mountains, central Arizona. In: Crittenden, M.D., Coney, P.J., Davis, G.H. (Eds.), Cordilleran Metamorphic Core Complexes. Geological Society of America Memoir 153, 159-174.

Reynolds, S.J., Shafiqullah, M., Damon, P.E., DeWitt, E., 1986. Early Miocene mylonitization and detachment faulting, South Mountains, central Arizona. Geology 14, 283-286.

Rutter, E.H., Brodie, K.H., 2004. Experimental grain size-sensitive flow of hot-pressed Brazilian quartz aggregates. Journal of Structural Geology 26, 2011-2023.

Severinghaus, J., Atwater, T., 1990. Cenozoic geometry and thermal state of the subducting slabs beneath western North America. In: Wernicke, B.P. (Ed.), Basin and Range extensional tectonics near the latitude of Las Vegas, Nevada. Geological Society of America Memoir 176, 1-22.

Stockhert, B., Brix, M.R., Kleinschrodt, R., Hurford, A.J., Wirth, R., 1999. Thermochronometry and microstructures of quartz – a comparison with experimental flow laws and predictions on the temperature of the brittle-plastic transition. Journal of Structural Geology 21, 351-369.

Tullis, J., 2002. Deformation of granitic rocks; experimental studies and natural examples. In: Plastic deformation of minerals and rocks. Reviews in Mineralogy and Geochemistry 51, 51-95.

Wells, R.E., Hillhouse, J.W., 1989. Paleomagnetism and tectonic rotation of the lower Miocene Peach Springs Tuff: Colorado Plateau, Arizona, to Barstow, California. Geological Society of America Bulletin 101, 846-863.

Wernicke, B., 1981. Low-angle normal faults in the Basin and Range Province: nappe tectonics in an extending orogen. Nature 291, 645-648.

Wernicke, B., Axen, G.J., Snow, J.K., 1988. Basin and Range extensional tectonics at the latitude of Las Vegas, Nevada. Geological Society of America Bulletin 100, 1738-1757.

Wilson, E.D., Moore, R.T., 1959. Structure of Basin and Range Province in Arizona. Arizona Geological Society, Southern Arizona Guidebook II, 89-105.

APPENDIX A: PROBE POLISHING PROCEDURE

Date	Sample Number	Time: 6 μm	Time: 1 μm	Time: Silica	Pressure	RPM
8/13/09	SM-08-06-b	60 min.	60 min.	60 min.	4 lb	25
8/13/09	SM-08-06-a	90 min.	60 min.	60 min.	4 lb	25
8/14/09	SM-08-01-a	60 min.	60 min.	60 min.	4 lb	25
10/12/09	SM-08-03	60 min.	60 min.	60 min.	4 lb	25
12/2/09	SM-08-05	60 min.	60 min.	60 min.	4 lb	25
12/4/09	SM-08-04	60 min.	60 min.	60 min.	4 lb	25

The probe polishing procedure consists of three separate rounds of polishing with the Buehler MiniMet 1000 Grinder-Polisher. Preparation involves applying a Buehler adhesive-backed polishing microcloth to a glass plate, which fits into a polishing bowl. A different glass plate and polishing bowl are used for each round of polishing. The polishing bowl is placed on the Grinder-Polisher under the load arm and aligned with the locating pins. Slides are mounted on the specimen holder with distilled water and set into the load pin of the load arm.

In the first round of polishing, the slide is polished for 60-90 minutes. Three pumps of Metadi II Paste 6-micron diamond suspension fluid and distilled water are applied to the polishing cloth. In the second round of polishing, the slide is polished for 60 minutes. Four to five pumps of Metadi II Paste 1-micron diamond suspension fluid and distilled water are applied to the polishing cloth. In the third round of polishing the slide is again polished for 60 minutes. MasterMet 2 non-crystallizing colloidal silica polishing suspension is poured into the polishing bowl until the slide and glass plate are covered. Between each round of polishing the slides are rinsed with distilled water and then washed with distilled water in a Fisher Scientific Tabletop Ultrasonic Cleaner for 3

minutes to remove any remaining polishing solution. Slides are wiped dry with Kimtech Science Kimwipes to prevent any abrasions to the newly polished surface.

APPENDIX B: ELECTRON BACK-SCATTER DIFFRACTION RE-INDEXING AND PROCESSING PROCEDURES

SM-08-01-b

EBSD data was collected at University of California Santa Barbara. No re-indexing was completed before the data were processed at California State University Northridge with the CHANNEL5 suite. Standard noise reduction was conducted in which wild spikes were extrapolated, and all zero solutions were extrapolated from 'high' to 'medium.' The Kuwahara filter was also applied. A minimum angle of 5° was set to define a grain boundary. In addition to grain boundaries, the beam map displays band contrast and all three indexed phases: quartz, orthoclase feldspar, and bytownite, which was substituted for plagioclase feldspar.

SM-08-03-b

EBSD data was collected at California State University Northridge with the CHANNEL5 suite. No reindexing was completed in Flamenco before the data were processed in Tango. Standard noise reduction was conducted in which wild spikes were extrapolated, and all zero solutions were extrapolated from 'high' to 'medium.' The Kuwahara filter was also applied. All pseudosymmetric indexings were removed. A minimum angle of 2° was set to define a grain boundary. This allowed a more accurate evaluation of subgrain rotation in quartz grains. In addition to grain boundaries, the beam map displays band contrast and all three indexed phases: quartz, orthoclase feldspar, and bytownite, which was substituted for plagioclase feldspar.

	Maximum Bands	Minimum Bands	MAD	Calibration File
Initial	6	4	< 1.0	WD 10.0 mm, 175.5 mm

SM-08-05-a

EBSD data were collected at California State University Northridge with the CHANNEL5 suite. The initial data were re-indexed three times in Flamenco before the data was processed in Tango. Standard noise reduction was conducted in which wild spikes were extrapolated, and all zero solutions were extrapolated from 'high' to 'medium.' All pseudosymmetric indexings were removed. A minimum angle of 1° was set to define a grain boundary. In addition to grain boundaries, the beam map displays band contrast and all three indexed phases: quartz, orthoclase feldspar, and bytownite, which was substituted for plagioclase feldspar.

	Maximum Bands	Minimum Bands	MAD	Calibration File	Other Changes
Initial	6	4	< 1.0	WD 10.0 mm, 175.5 mm	
Re-index #1	8	7	< 1.0	WD 10.0 mm, 175.5 mm	Hough resolution = 70
Re-index #2	7	6	< 1.0	WD 10.0 mm, 175.5 mm	Advanced fit 'on'
Re-index #3	6	5	< 1.5	WD 10.0 mm, 175.5 mm	

SM-08-06-a

EBSD data were collected with the CHANNEL5 suite at California State University Northridge. The initial data were re-indexed three times in Flamenco before the data were processed in Tango. Standard noise reduction was conducted in which wild spikes were extrapolated, and all zero solutions were extrapolated from 'high' to 'medium.' A minimum angle of 5° was set to define a grain boundary. In addition to grain boundaries, the beam map displays band contrast and all three indexed phases: quartz, orthoclase feldspar, and bytownite, which was substituted for plagioclase feldspar.

	Maximum Bands	Minimum Bands	MAD	Calibration File	Other Changes
Initial	6	4	< 1.0	WD 10.0 mm, 175.5 mm	
Re-index #1	8	7	< 1.0	WD 10.0 mm, 175.5 mm	Hough resolution = 70, advanced fit 'on'
Re-index #2	7	6	< 1.0	WD 10.0 mm, 175.5 mm	
Re-index #3	7	6	< 1.0	WD 10.0 mm, 175.5 mm	'Lock phase' box checked

APPENDIX C: MICROSTRUCTURAL ANALYSES, SCANS, AND PHOTOMICROGRAPHS

Sample No.	SM-08-01		
Field Area Location	Northeast area of South Mountains		
Latitude/Longitude	33°21'39.3" N, 112°00'54.1" W		
Protolith Rock Name	South Mountains Granodiorite		
Fault Rock Name	Granodiorite proto-mylonite		
Primary Mineralogy	**Minerals**	**Modal Abundance**	
	Quartz	40%	
	Feldspar	45%	
	Biotite	10%	
	Oxides	5%	
	Zircon	trace	
Microstructures of Primary Mineralogy	Quartz:	Bulging of grain boundaries, subgrain rotation, elongate ribbons, grain boundary migration	
	Feldspar:	Fractures, zoned plagioclase, slight bulging of some grain boundaries	
	Primary Mineral	**Replaced With**	**Modal %**
Secondary Alteration	Biotite	Chlorite	<1%
Microstructures of Alteration Minerals	None		
Estimated Porphyroclast %	70%		
Range in P-clast Size	2-20 microns		
Estimated Matrix %	30%		

Microstructural analysis template for SM-08-01.

Plane light scan of SM-08-01.

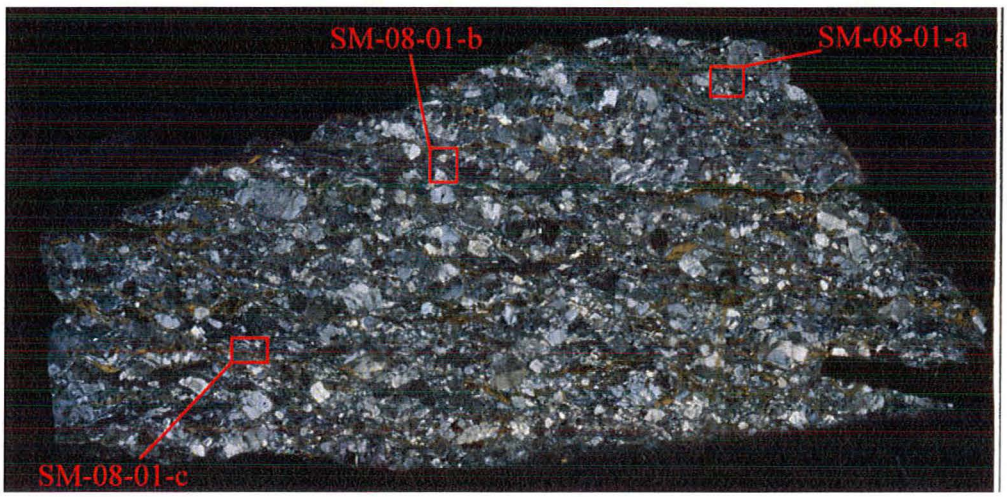

Polarized light scan of SM-08-01. Microstructural analysis locations are outlined in red.

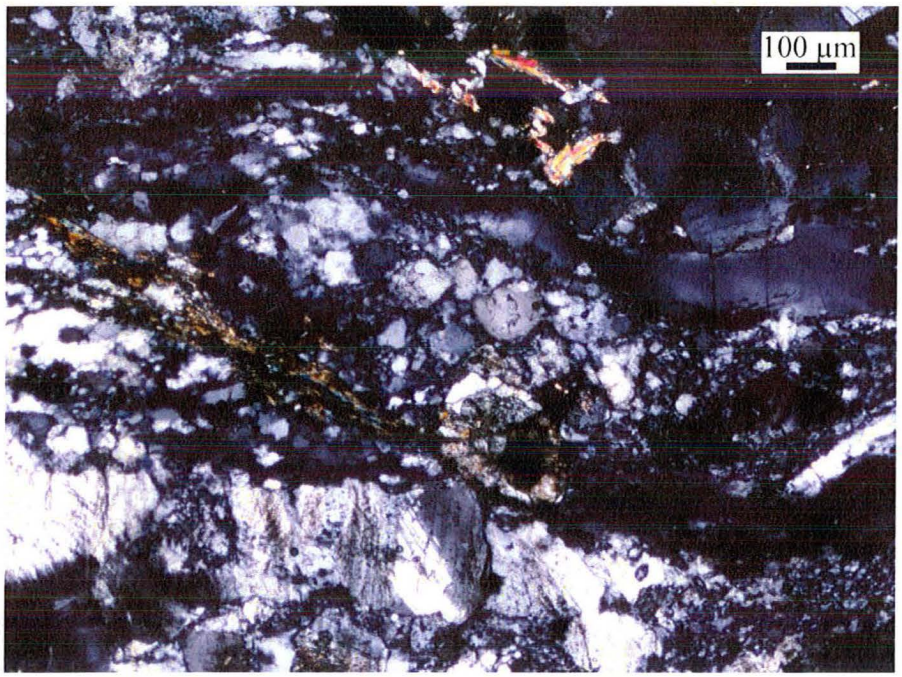

Photomicrograph of SM-08-01-a under cross-polars at 5x.

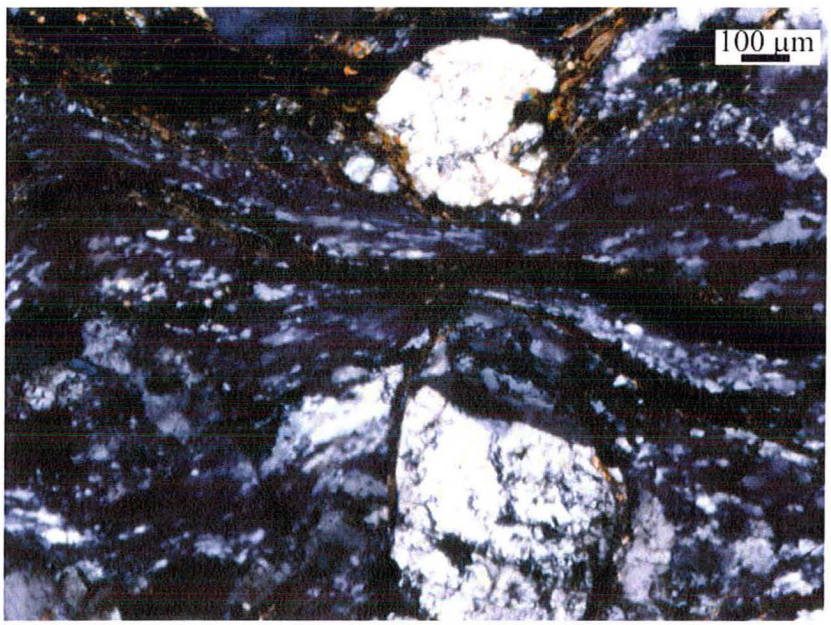

Photomicrograph of SM-08-01-b under cross-polars at 5x.

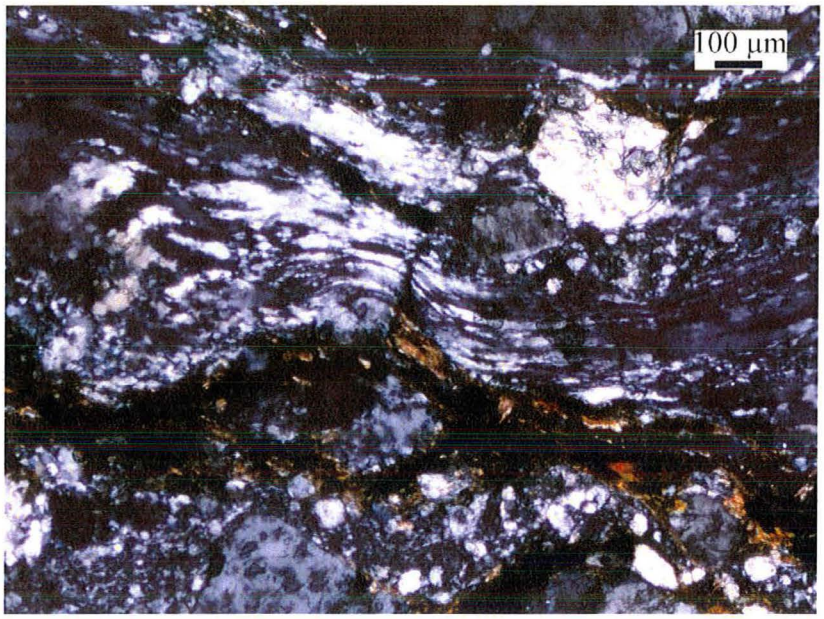

Photomicrograph of SM-08-01-c under cross-polars at 5x.

Sample No.	**SM-08-02**		
Field Area Location	Northeast area of South Mountains		
Latitude/Longitude	33°21'38.7" N, 112°00'57.1" W		
Protolith Rock Name	South Mountains Granodiorite		
Fault Rock Name	Granodiorite proto-mylonite		
Primary Mineralogy	**Minerals**	**Modal abundance**	
	Quartz	40%	
	Feldspar	50%	
	Biotite	7%	
	Oxides	3%	
Microstructures of Primary Mineralogy	Quartz:	Bulging of grain boundaries, subgrain rotation, elongate ribbons, grain boundary migration	
	Feldspar:	Fractures, zoned plagioclase, tartan twinning	
	Primary Mineral	**Replaced With**	**Modal %**
Secondary Alteration	Biotite	Chlorite	<1%
Microstructures of Alteration Minerals	None		
Estimated Porphyroclast %	75%		
Range in P-clast Size	2-30 microns		
Estimated Matrix %	25%		

Microstructural analysis template for SM-08-02.

Plane light scan of SM-08-02.

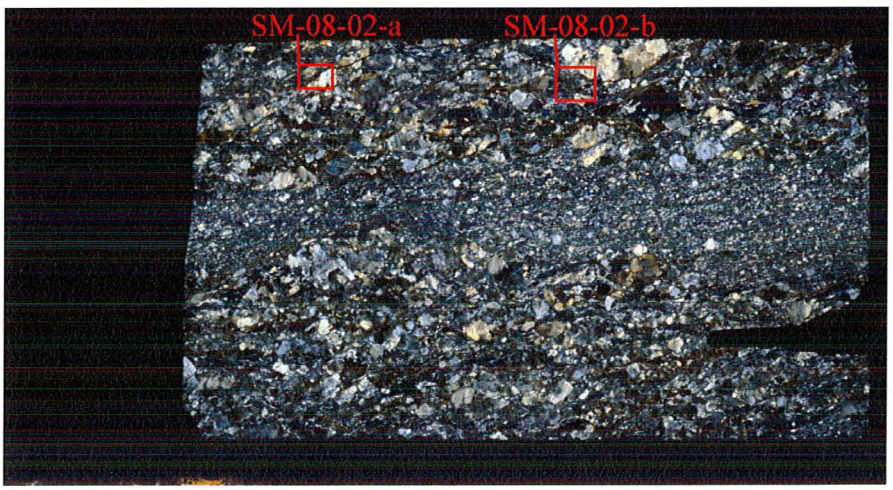

Polarized light scan of SM-08-02. Microstructural analysis locations are outlined in red.

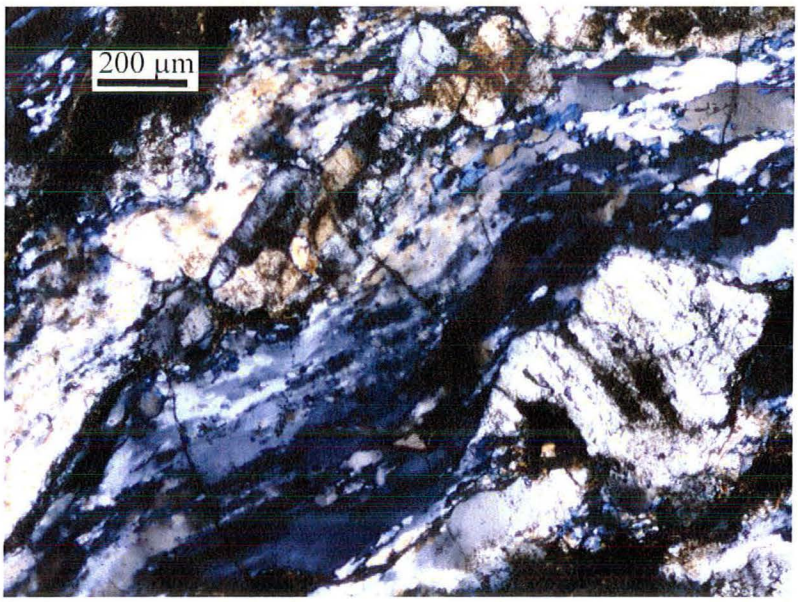

Photomicrograph of SM-08-02-a under cross-polars at 5x.

Photomicrograph of SM-08-02-b under cross-polars at 5x.

Sample No.	SM-08-03		
Field Area Location	Southwest area of South Mountains		
Latitude/Longitude	33°19'50.1" N, 112°04'08.8" W		
Protolith Rock Name	South Mountains Granodiorite		
Fault Rock Name	Granodiorite proto-mylonite		
Primary Mineralogy	**Minerals**	**Modal abundance**	
	Quartz	50%	
	Feldspar	45%	
	Biotite	5%	
	Oxides	trace	
Microstructures of Primary Mineralogy	Quartz:	Bulging of grain boundaries, subgrain rotation, grain boundary migration on rims	
	Feldspar:	Fractures, large, blocky	
	Primary Mineral	**Replaced With**	**Modal %**
Secondary Alteration	None		
Microstructures of Alteration Minerals	None		
Estimated Porphyroclast %	> 95%		
Range in P-clast Size	2-50 microns		
Estimated Matrix %	< 5%		

Microstructural analysis template for SM-08-03.

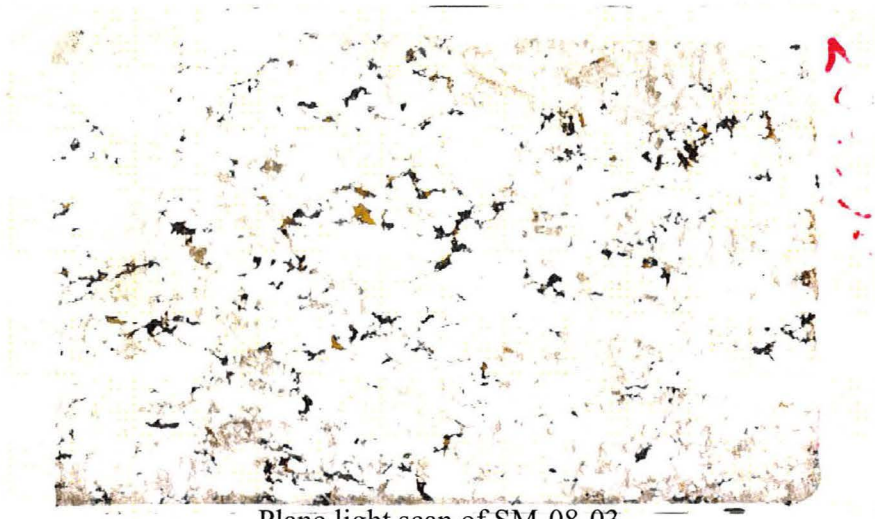

Plane light scan of SM-08-03.

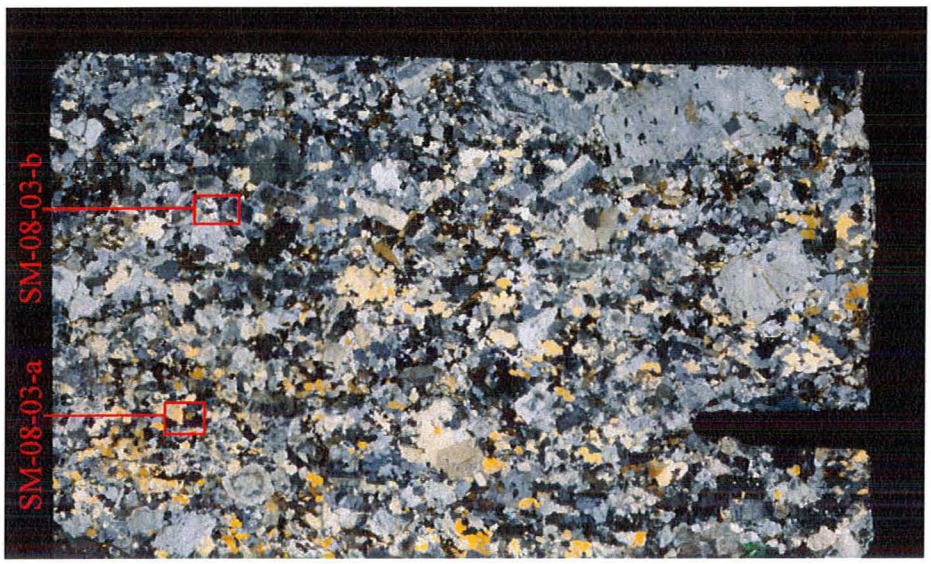

Polarized light scan of SM-08-03. Microstructural analysis locations are outlined in red.

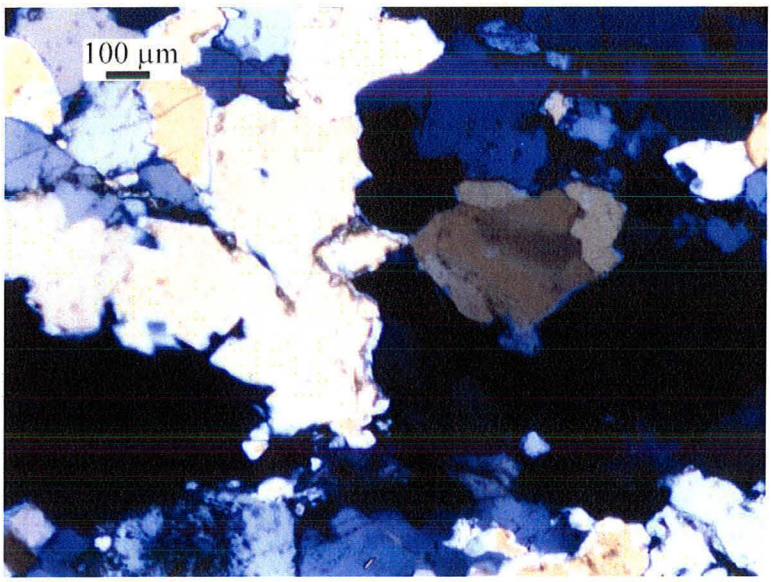

Photomicrograph of SM-08-03-a under cross-polars at 5x.

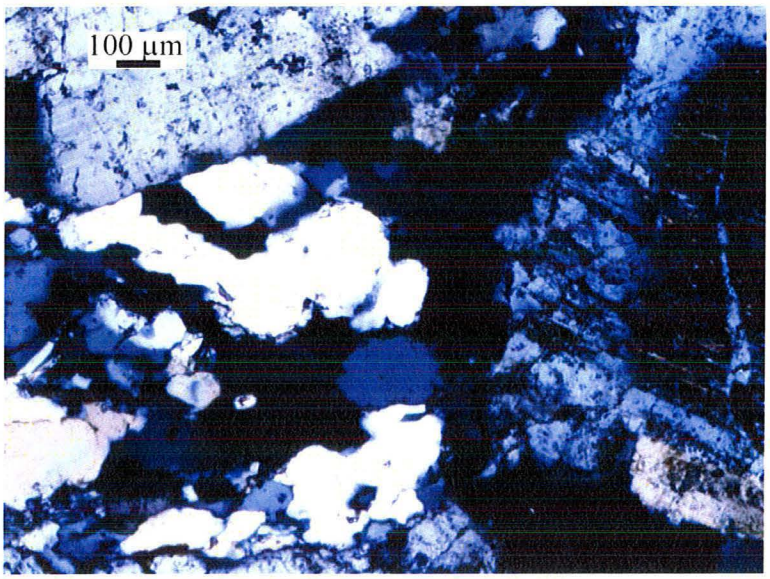

Photomicrograph of SM-08-03-b under cross-polars at 5x.

Sample No.	SM-08-04		
Field Area Location	Southwest area of South Mountains		
Latitude/Longitude	33°19'51.2" N, 112°04'06.0" W		
Protolith Rock Name	South Mountains Granodiorite		
Fault Rock Name	Granodiorite mylonite		
Primary Mineralogy	**Minerals**	**Modal abundance**	
	Quartz	50%	
	Feldspar	42%	
	Biotite	8%	
	Oxides	trace	
Microstructures of Primary Mineralogy	Quartz:	Bulging of grain boundaries, subgrain rotation, elongate ribbons, grain boundary migration	
	Feldspar:	Fractures, more rounded, incorporated into quartz ribbons	
Secondary Alteration	**Primary Mineral**	**Replaced With**	**Modal %**
	Biotite	Chlorite	< 1%
	Oxides	Rust	trace
Microstructures of Alteration Minerals	None		
Estimated Porphyroclast %	40%		
Range in P-clast Size	1-20 microns		
Estimated Matrix %	60%		

Microstructural analysis template for SM-08-04.

Plane light scan of SM-08-04.

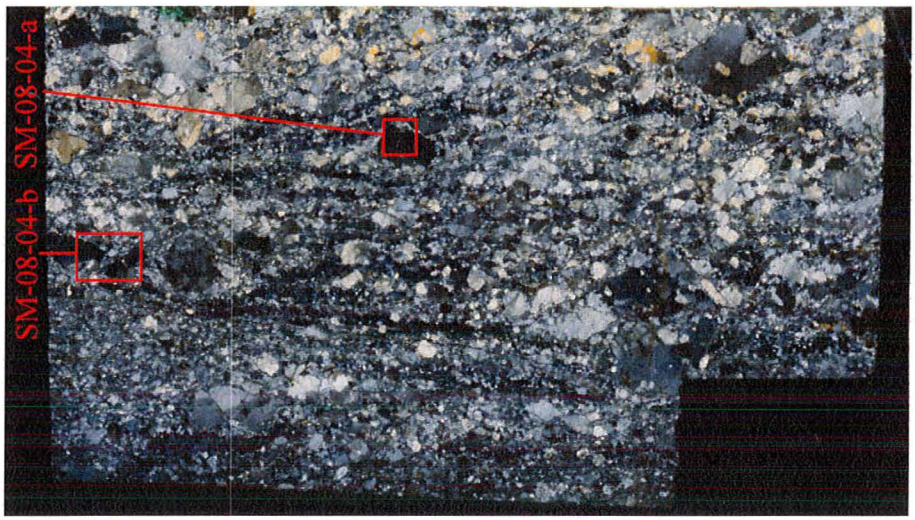

Polarized light scan of SM-08-04. Microstructural analysis locations are outlined in red.

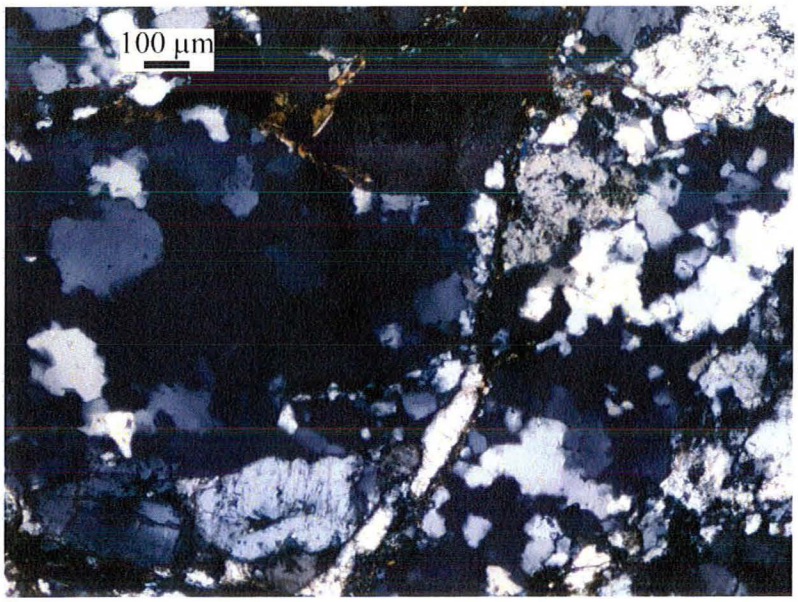

Photomicrograph of SM-08-04-a under cross-polars at 5x.

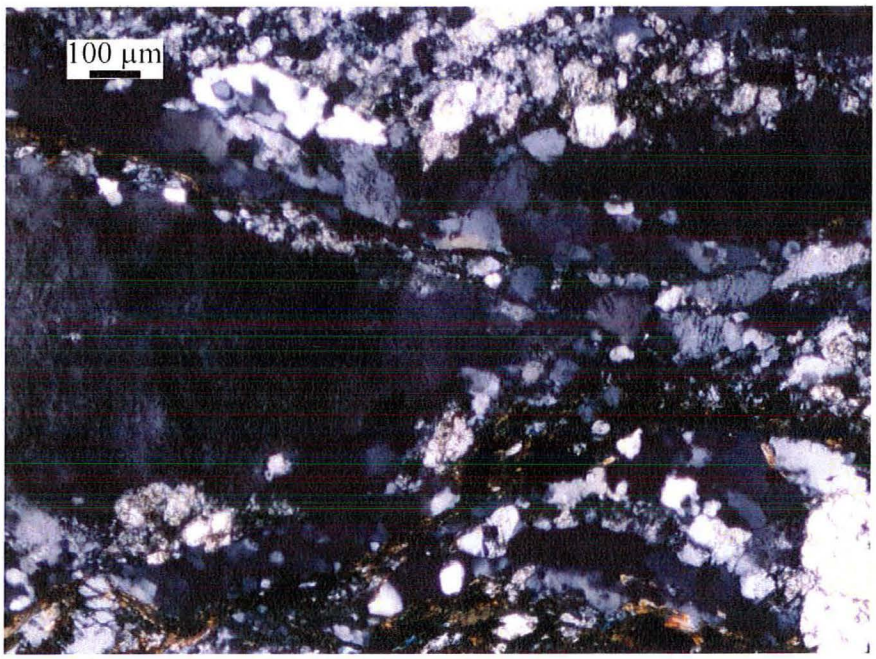

Photomicrograph of SM-08-04-b under cross-polars at 5x.

Sample No.	SM-08-05		
Field Area Location	Southwest area of South Mountains		
Latitude/Longitude	33°19'52.0" N, 112°04'05.2" W		
Protolith Rock Name	South Mountains Granodiorite		
Fault Rock Name	Granodiorite proto-mylonite		
Primary Mineralogy	**Minerals**	**Modal abundance**	
	Quartz	45%	
	Feldspar	50%	
	Biotite	5%	
	Oxides	trace	
Microstructures of Primary Mineralogy	Quartz:	Bulging of grain boundaries, subgrain rotation, elongate ribbons, grain boundary migration	
	Feldspar:	Fractures, some bulging of grain boundaries	
	Primary Mineral	**Replaced With**	**Modal %**
Secondary Alteration	None		
Microstructures of Alteration Minerals	None		
Estimated Porphyroclast %	60%		
Range in P-clast Size	5-50 microns		
Estimated Matrix %	40%		

Microstructural analysis template for SM-08-05.

Plane light scan of SM-08-05.

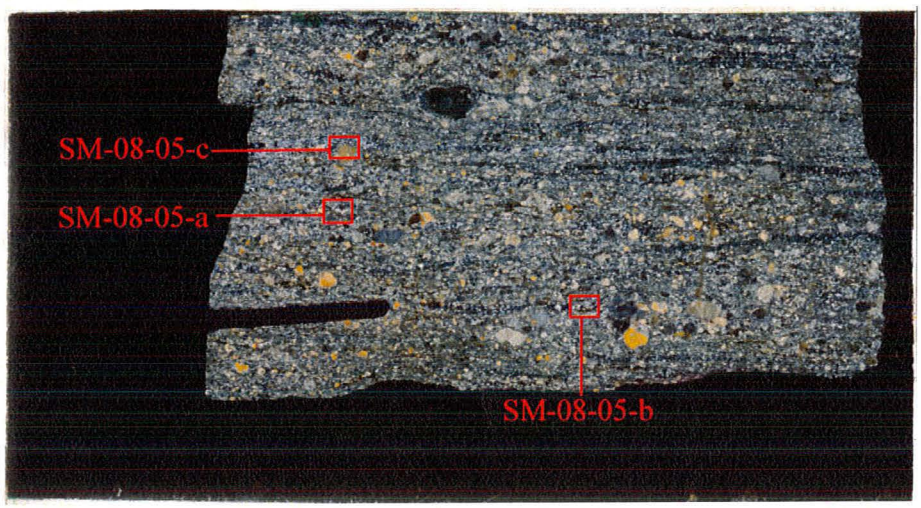

Polarized light scan of SM-08-05. Microstructural analysis locations are outlined in red.

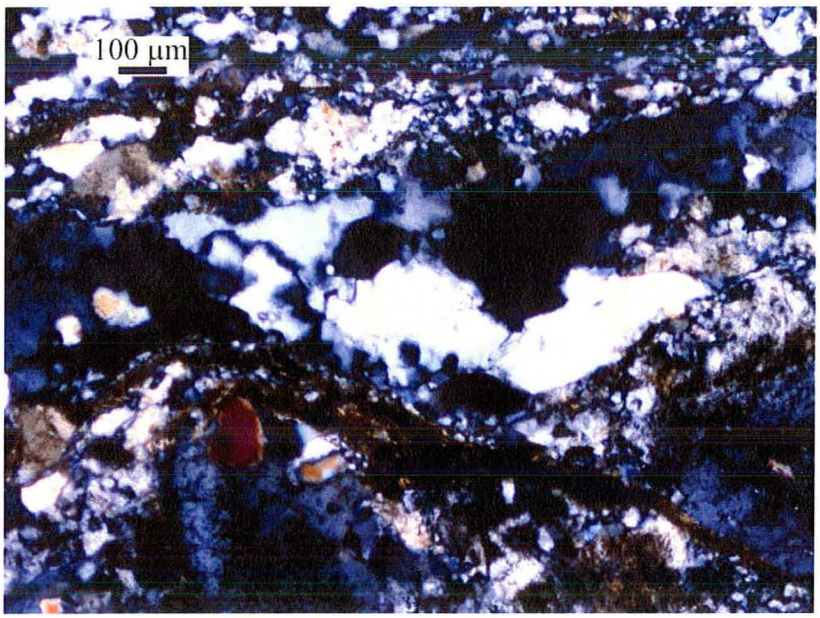

Photomicrograph of SM-08-05-a under cross-polars at 5x.

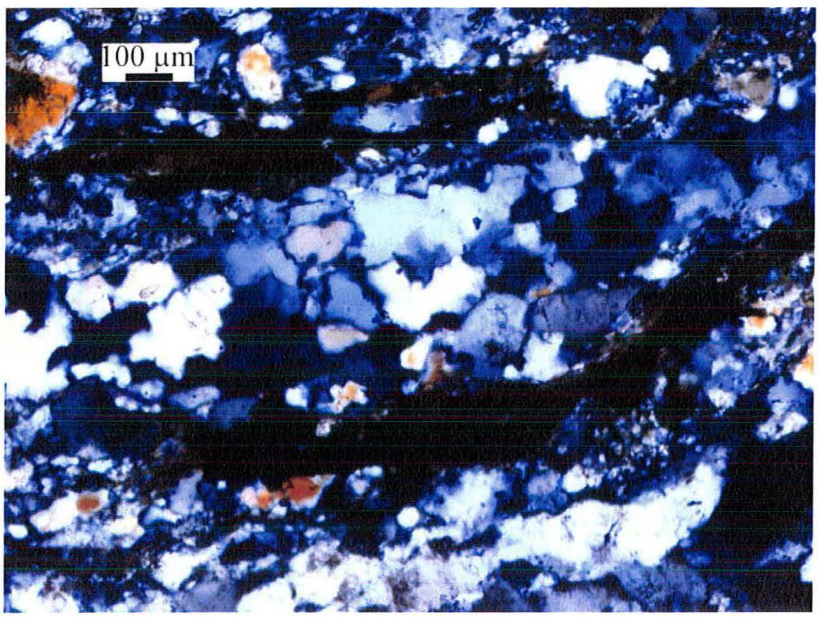

Photomicrograph of SM-08-05-b under cross-polars at 5x.

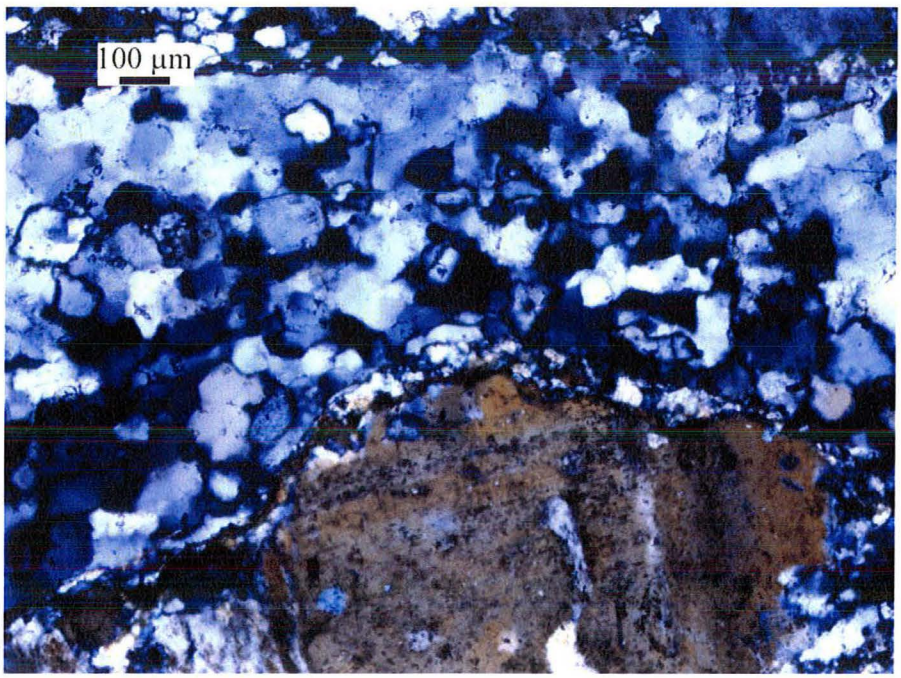

Photomicrograph of SM-08-05-c under cross-polars at 5x.

Sample No.	SM-08-06		
Field Area Location	Southwest area of South Mountains		
Latitude/Longitude	33°19'52.3" N, 112°04'05.0" W		
Protolith Rock Name	Telegraph Pass Granite		
Fault Rock Name	Granite mylonite		
Primary Mineralogy	**Minerals**	**Modal abundance**	
	Quartz	50%	
	Feldspar	40%	
	Biotite	5%	
	Oxides	5%	
Microstructures of Primary Mineralogy	Quartz:	Bulging of grain boundaries, elongat ribbons, grain boundary migration	
	Feldspar:	Bulging of grain boundaries, some grain boundary migration	
	Primary Mineral	**Replaced With**	**Modal %**
Secondary Alteration	None		
Microstructures of Alteration Minerals	None		
Estimated Porphyroclast %	30%		
Range in P-clast Size	<1-5 microns		
Estimated Matrix %	70%		

Microstructural analysis template for SM-08-06.

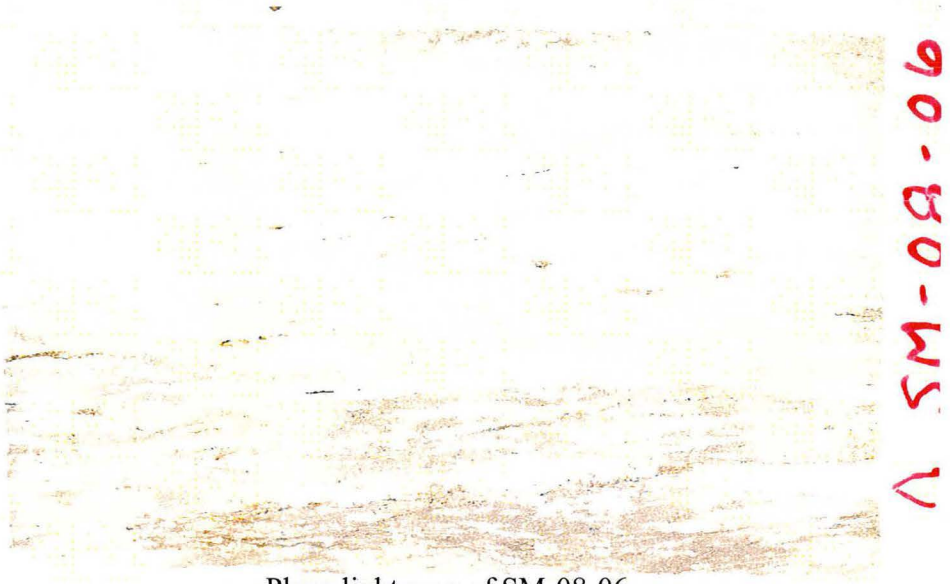

Plane light scan of SM-08-06.

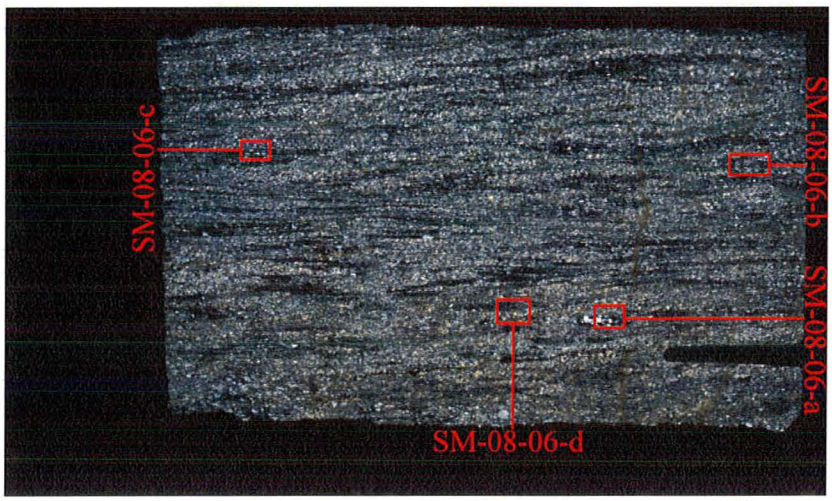

Polarized light scan of SM-08-06. Microstructural analysis locations are outlined in red.

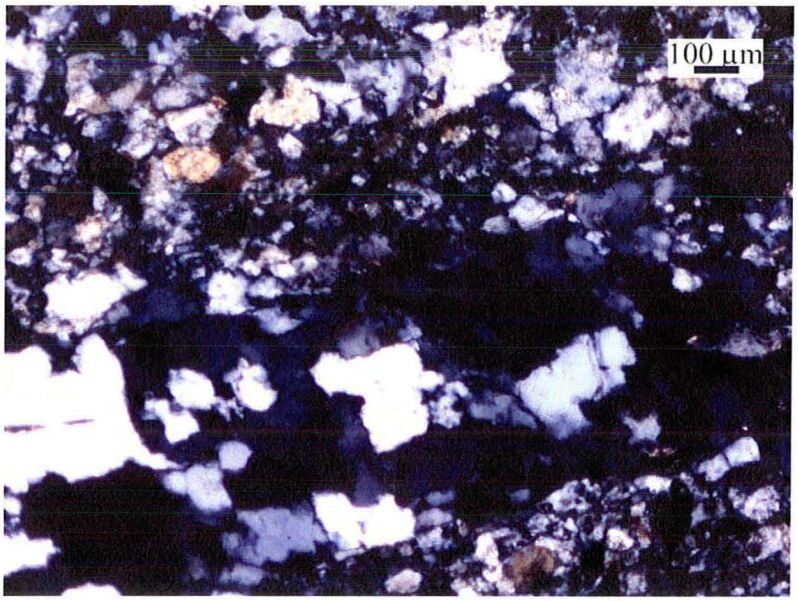

Photomicrograph of SM-08-06-a under cross-polars at 5x.

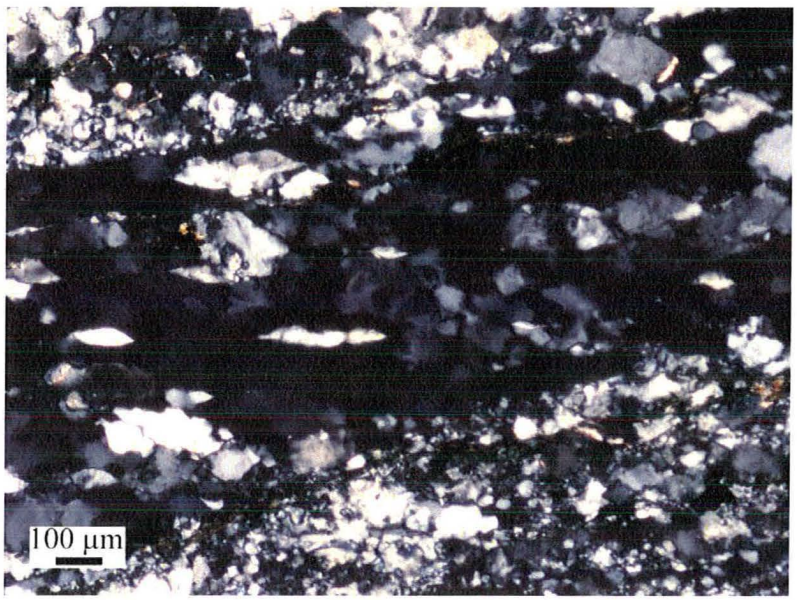

Photomicrograph of SM-08-06-b under cross-polars at 5x.

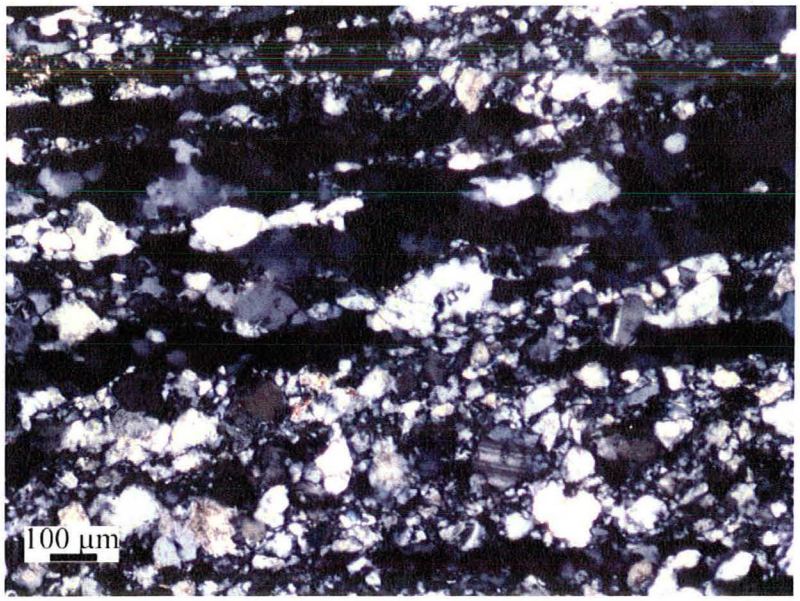

Photomicrograph of SM-08-06-c under cross-polars at 5x.

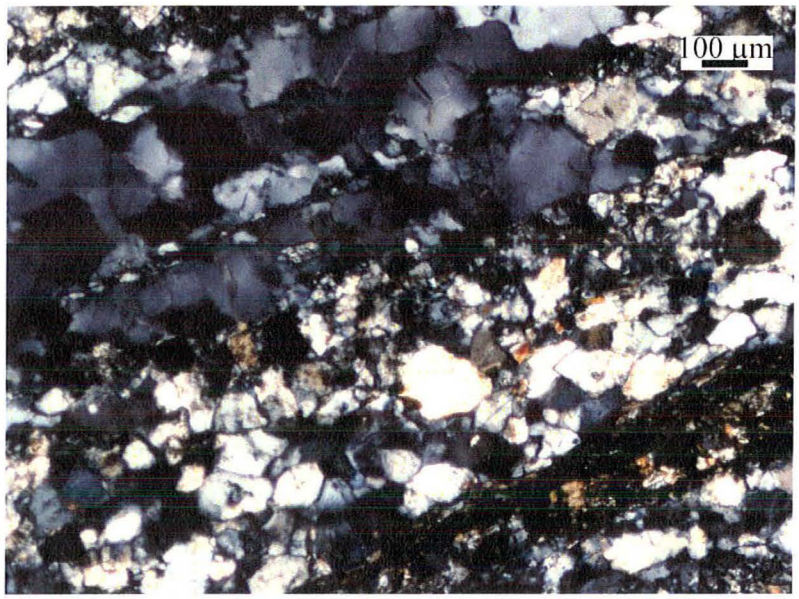

Photomicrograph of SM-08-06-d under cross-polars at 5x.

Sample No.	SM-08-07		
Field Area Location	Southwest area of South Mountains		
Latitude/Longitude	33°19'53.5" N, 112°04'04.8" W		
Protolith Rock Name	South Mountains Granodiorite		
Fault Rock Name	Granodiorite mylonite		
Primary Mineralogy	**Minerals**	**Modal abundance**	
	Quartz	50%	
	Feldspar	35%	
	Biotite	7%	
	Oxides	8%	
Microstructures of Primary Mineralogy	Quartz:	Bulging of grain boundaries, elongat ribbons, grain boundary migration	
	Feldspar:	Some grain boundary migration	
	Primary Mineral	**Replaced With**	**Modal %**
Secondary Alteration	None		
Microstructures of Alteration Minerals	None		
Estimated Porphyroclast %	30%		
Range in P-clast Size	<1-5 microns		
Estimated Matrix %	70%		

Microstructural analysis template for SM-08-07.

Plane light scan of SM-08-07.

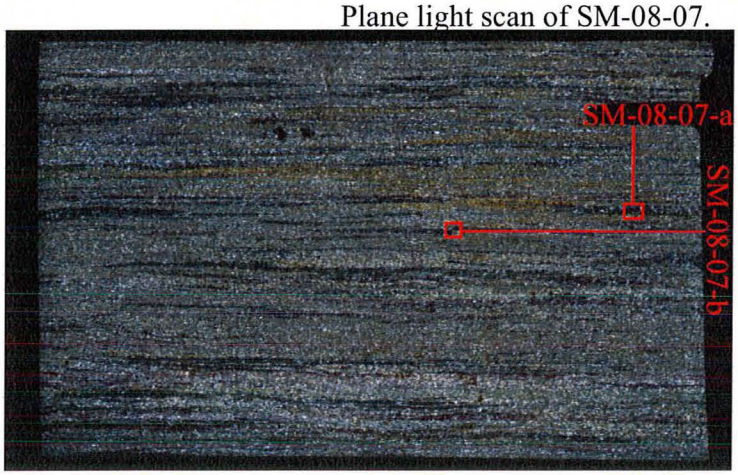

Polarized light scan of SM-08-07. Microstructural analysis locations are outlined in red.

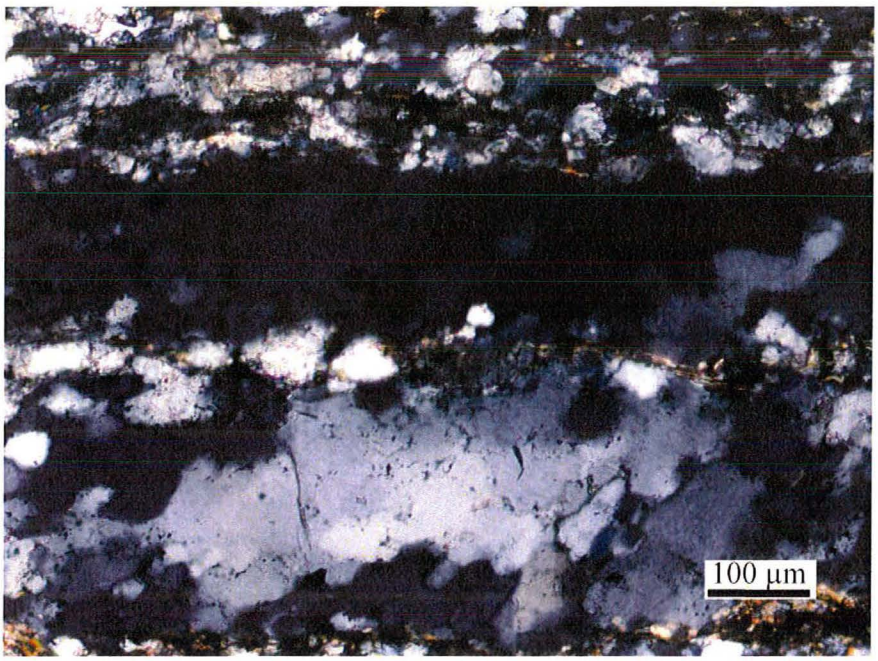

Photomicrograph of SM-08-07-a under cross-polars at 5x.

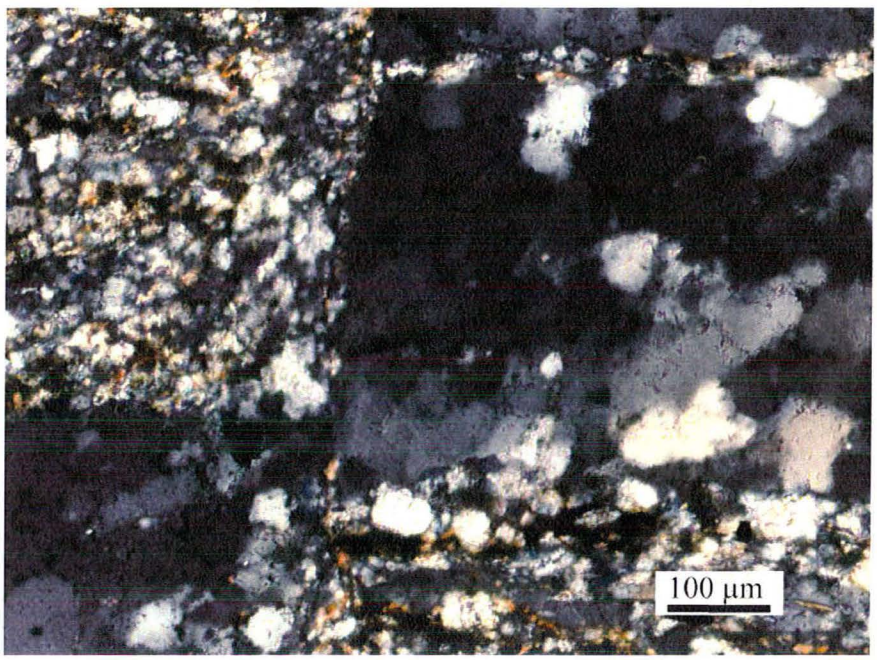

Photomicrograph of SM-08-07-b under cross-polars at 5x.

APPENDIX D: EBSD BEAM MAPS AND POLE FIGURES

SM-08-01:

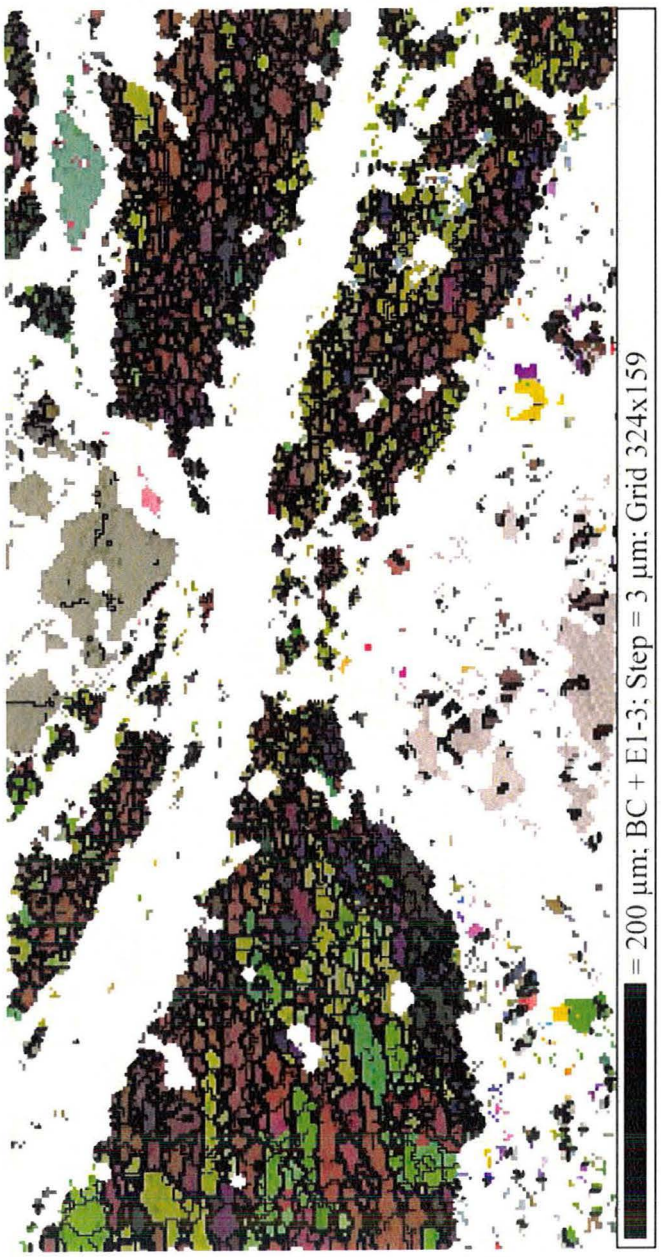

EBSD beam map of SM-08-01-b. Band contrast and Euler angle beam map of quartz, orthoclase, and bytownite. White space is non-indexed minerals. Black lines are grain boundaries. Gray lines are subgrains (> 5°).

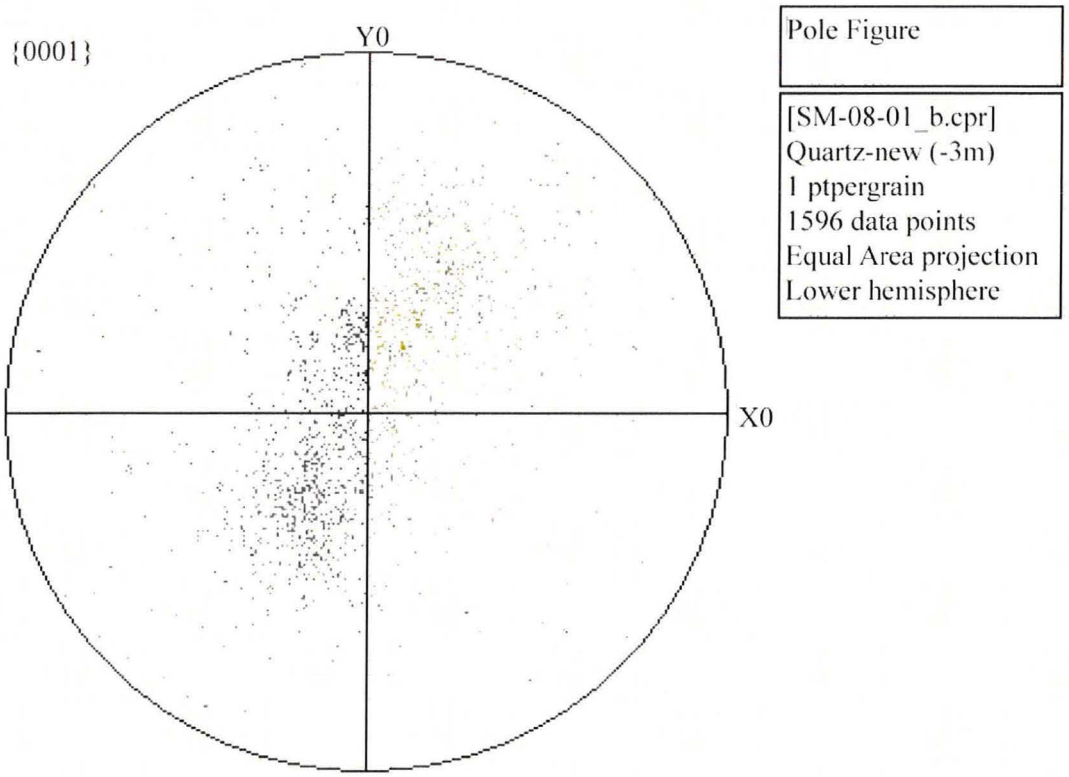

Equal area projection scatter plot pole figure of quartz grain c-axes, with 1 point per grain.

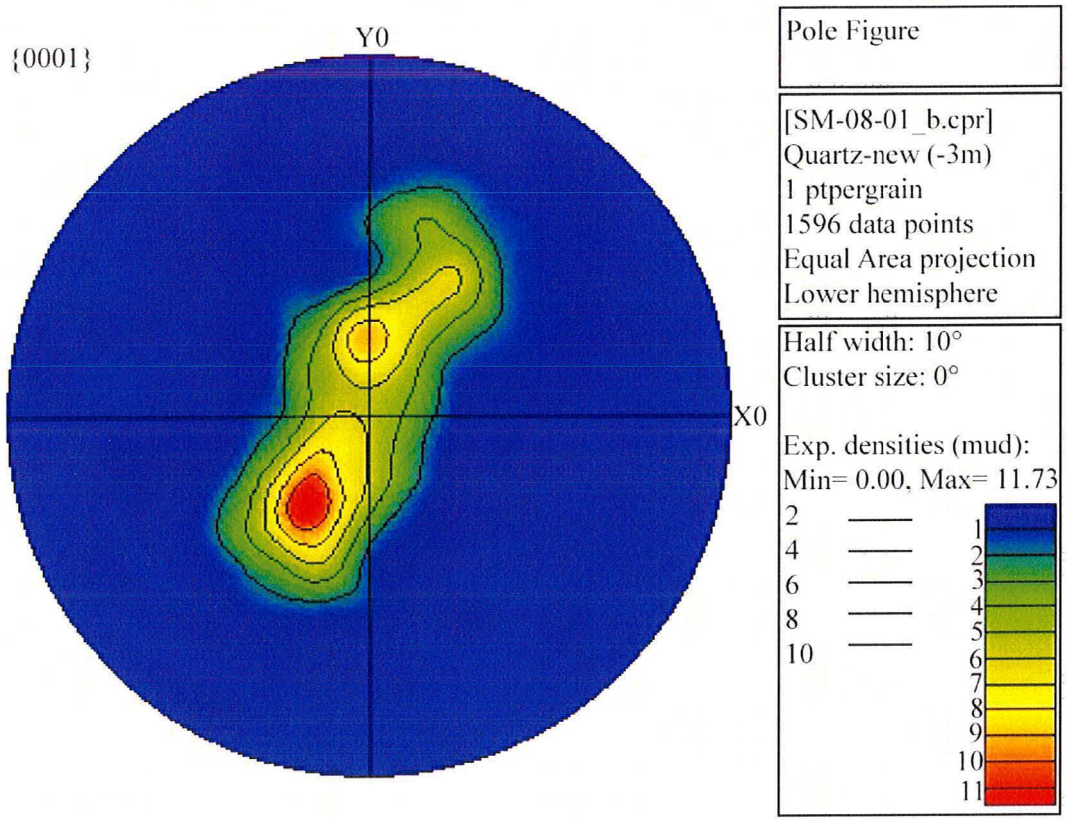

Equal area projection contour pole figure of quartz grain c-axes, with 1 point per grain.

SM-08-03:

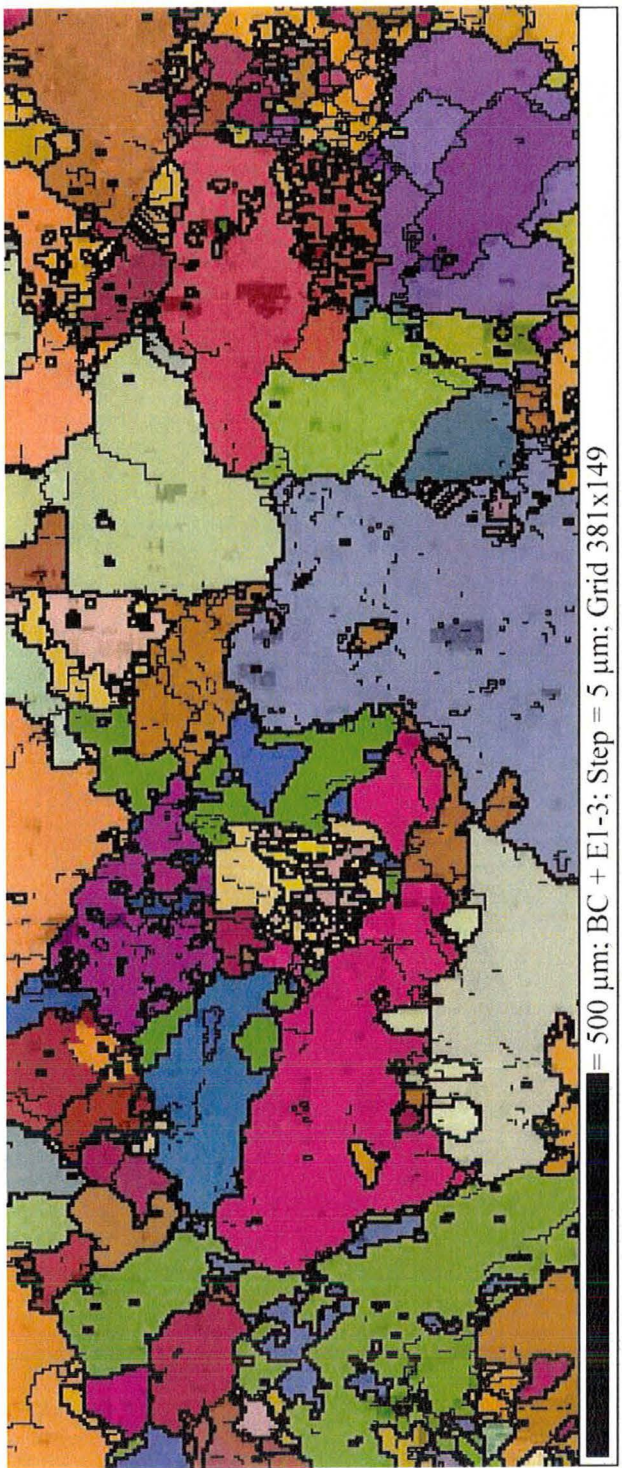

EBSD beam map of SM-08-03-a. Band contrast and Euler angle beam map of quartz, orthoclase, and bytownite. White space is non-indexed minerals. Black lines are grain boundaries. Gray lines are subgrains (> 2°).

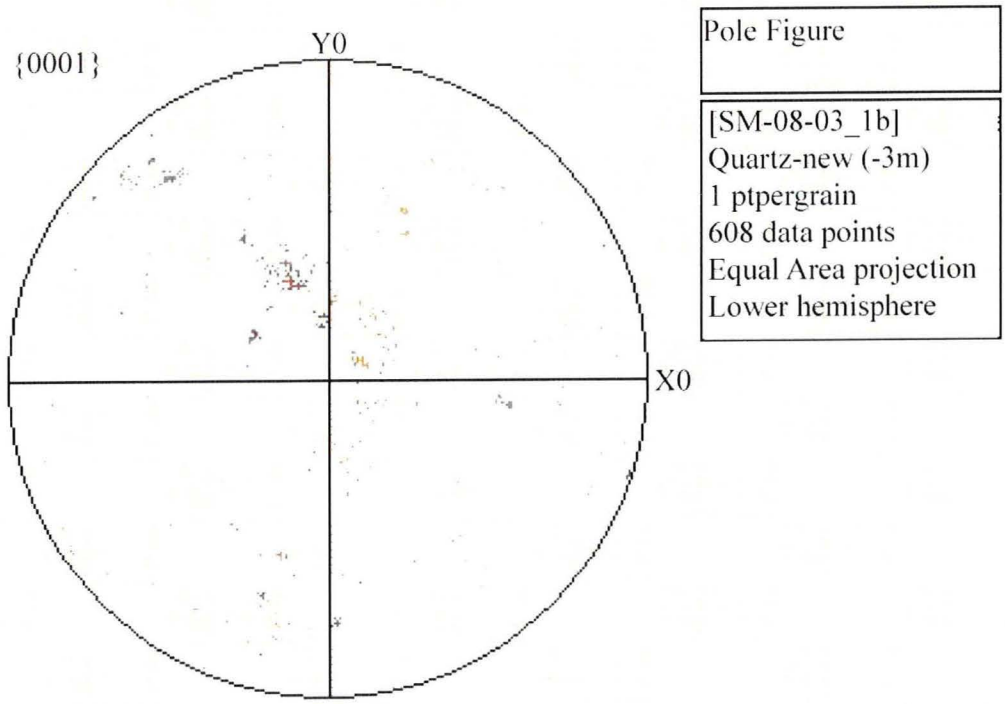

Equal area projection scatter plot pole figure of quartz grain c-axes, with 1 point per grain.

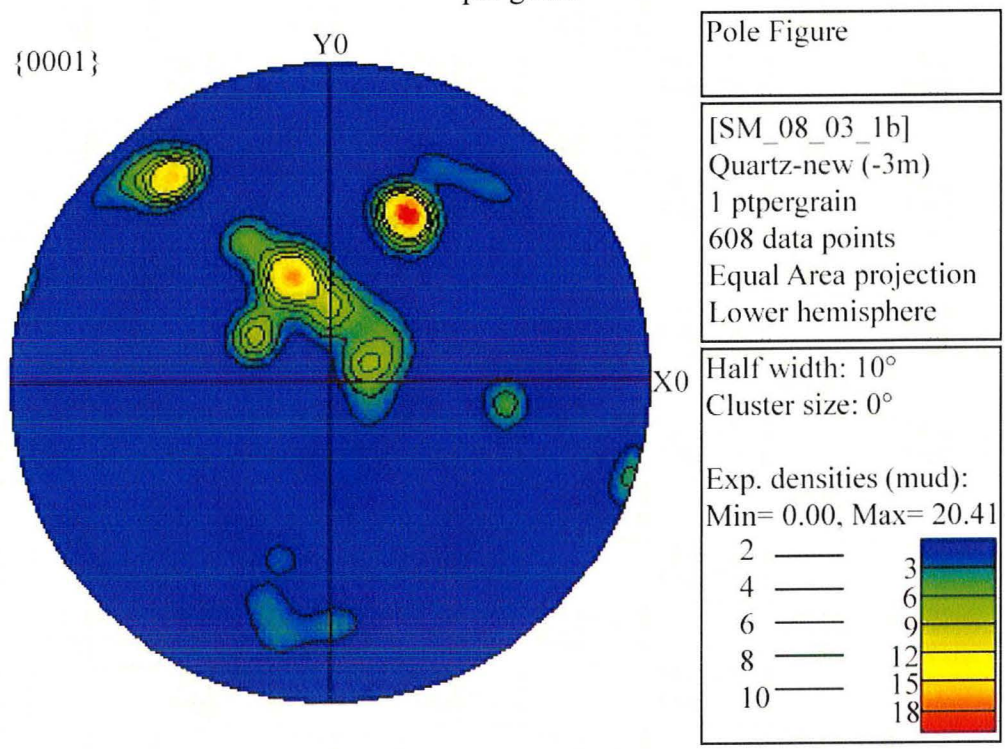

Equal area projection contour pole figure of quartz grain c-axes, with 1 point per grain.

SM-08-05:

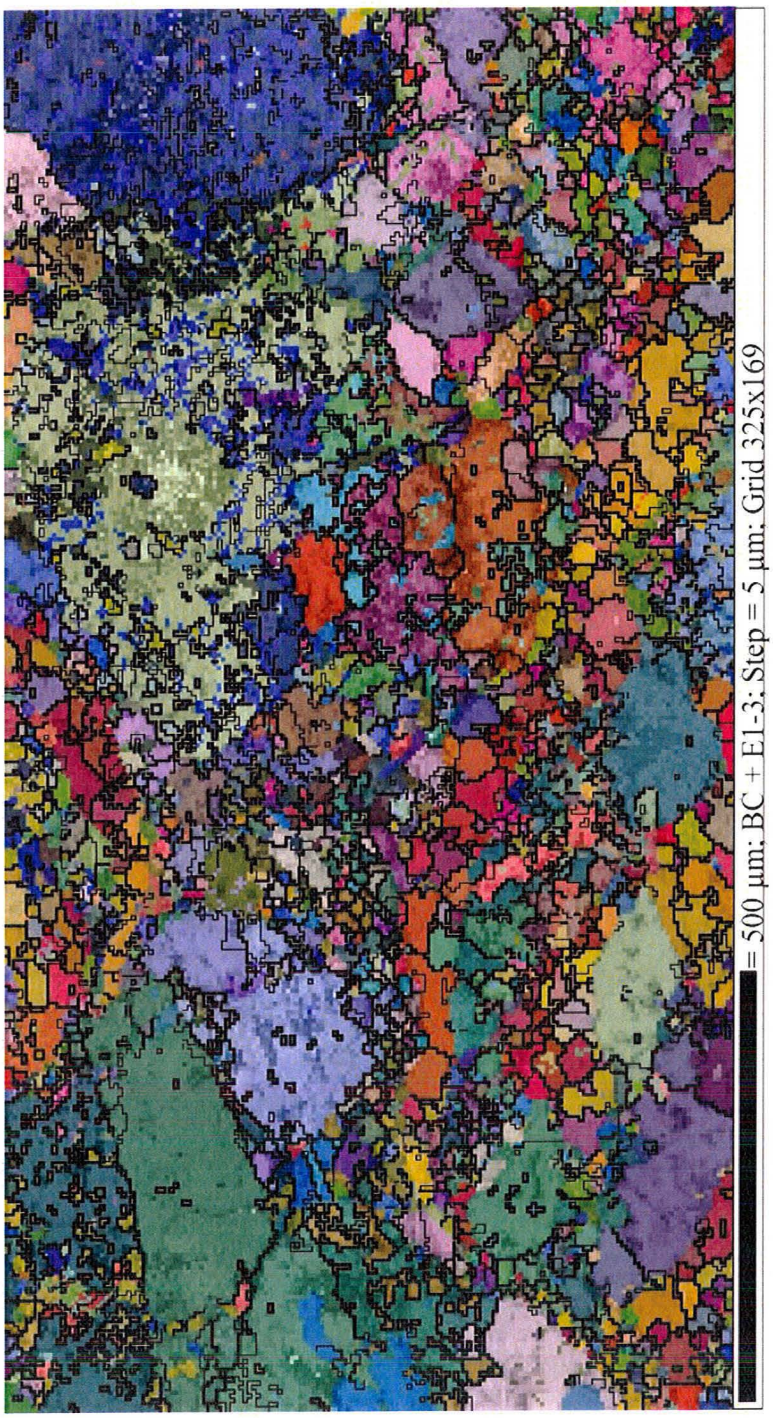

EBSD beam map of SM-08-05-a. Band contrast and Euler angle beam map of quartz, orthoclase, and bytownite. White space is non-indexed minerals. Black lines are grain boundaries. Gray lines are subgrains (> 1°).

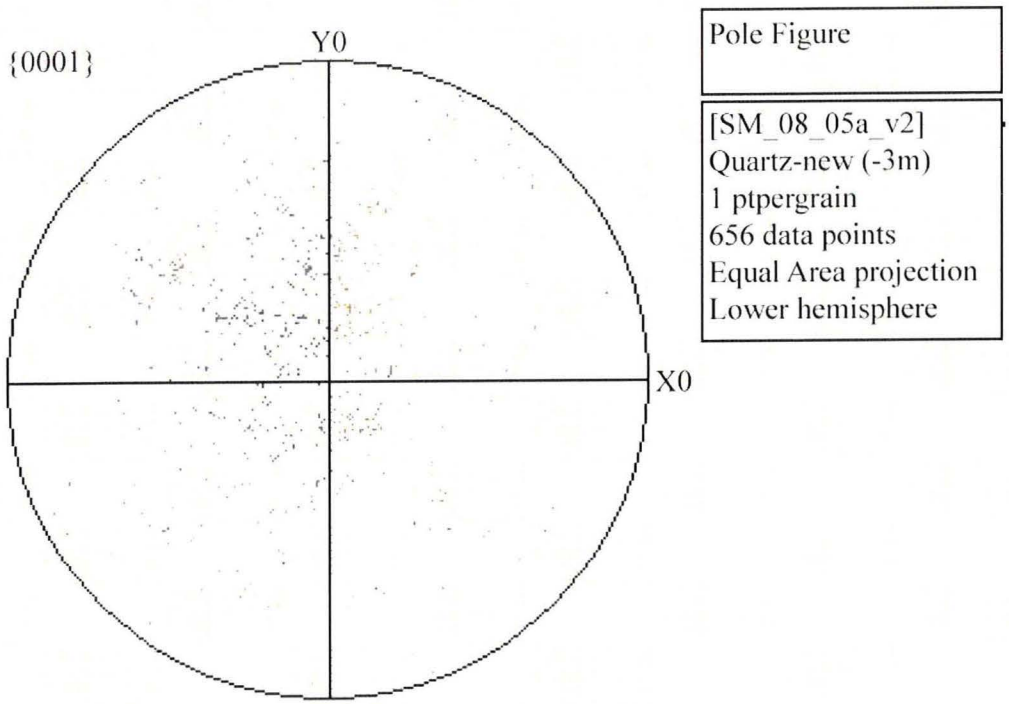

Equal area projection scatter plot pole figure of quartz grain c-axes, with 1 point per grain.

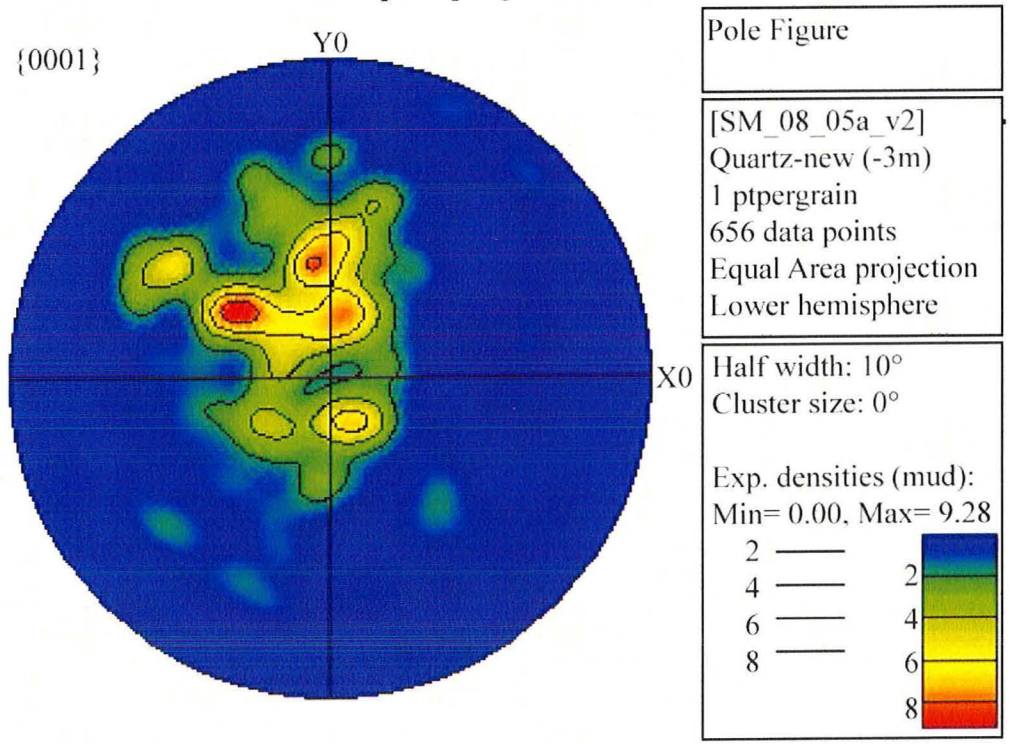

Equal area projection contour pole figure of quartz grain c-axes, with 1 point per grain.

SM-08-06:

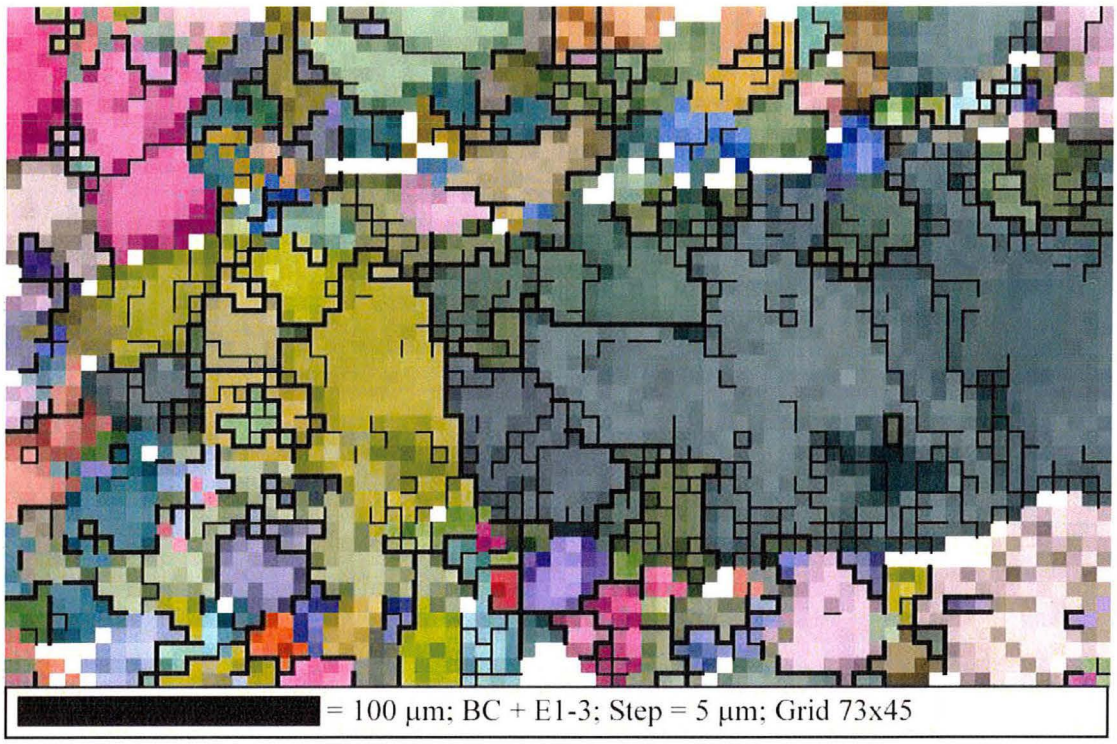

EBSD beam map of SM-08-06-a. Band contrast and Euler angle beam map of quartz, orthoclase, and bytownite. White space is non-indexed minerals. Black lines are grain boundaries. Gray lines are subgrains (> 5°).

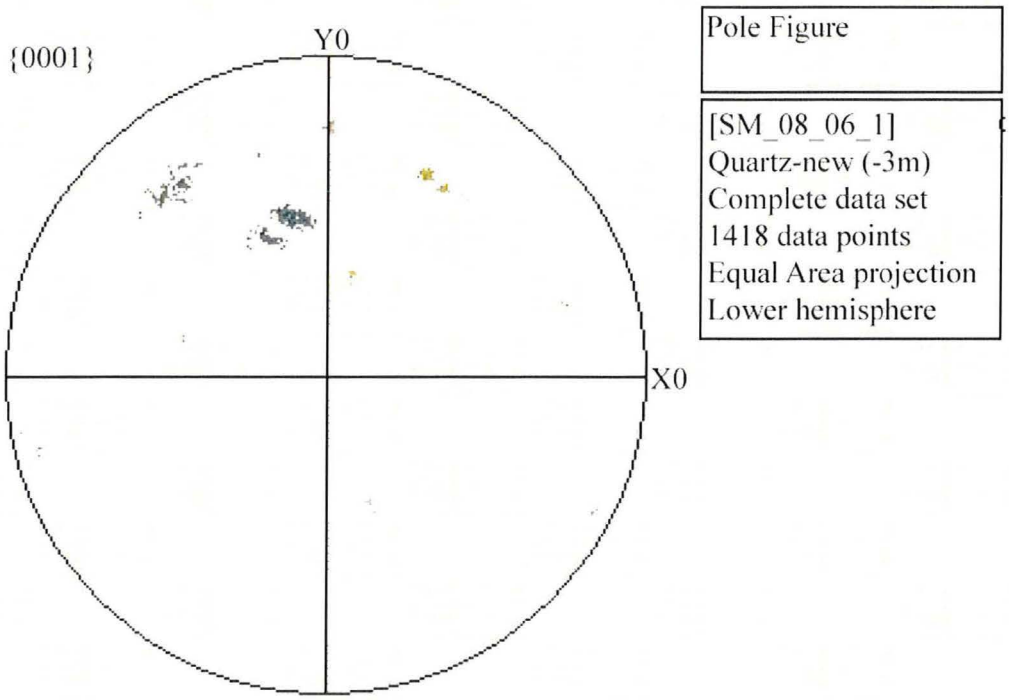

Equal area projection scatter plot pole figure of all quartz c-axes.